



저작자표시-비영리-변경금지 2.0 대한민국

이용자는 아래의 조건을 따르는 경우에 한하여 자유롭게

- 이 저작물을 복제, 배포, 전송, 전시, 공연 및 방송할 수 있습니다.

다음과 같은 조건을 따라야 합니다:



저작자표시. 귀하는 원저작자를 표시하여야 합니다.



비영리. 귀하는 이 저작물을 영리 목적으로 이용할 수 없습니다.



변경금지. 귀하는 이 저작물을 개작, 변형 또는 가공할 수 없습니다.

- 귀하는, 이 저작물의 재이용이나 배포의 경우, 이 저작물에 적용된 이용허락조건을 명확하게 나타내어야 합니다.
- 저작권자로부터 별도의 허가를 받으면 이러한 조건들은 적용되지 않습니다.

저작권법에 따른 이용자의 권리는 위의 내용에 의하여 영향을 받지 않습니다.

이것은 [이용허락규약\(Legal Code\)](#)을 이해하기 쉽게 요약한 것입니다.

[Disclaimer](#)



울산대학교
UNIVERSITY OF ULSAN

Department of Electrical, Electronic and Computer Engineering

Condition-Based Monitoring Techniques for Concrete and Industrial Equipment

Tuan-Khai Nguyen

Doctor of Philosophy

2024

UNIVERSITY OF ULSAN, REPUBLIC OF KOREA

Condition-Based Monitoring Techniques for Concrete and Industrial Equipment



by

Tuan-Khai Nguyen

A thesis submitted in partial fulfillment for the
Degree of Doctor of Philosophy

in the

Department of Electrical, Electronic and Computer Engineering

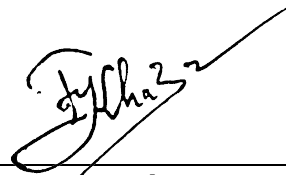
Supervisor: Jong-Myon Kim, Ph.D.

August 2024

DECLARATION OF AUTHORSHIP

I, Tuan-Khai Nguyen, declare that this thesis titled "Condition-Based Monitoring Techniques for Concrete and Industrial Equipment" and the work presented herein are my own. I confirm that:

- This work was done completely while in candidature for a research degree at the University of Ulsan, Republic of Korea.
- Where I have consulted the published work of others, it has always been attributed to its sources, and I have acknowledged all the sources.
- Where I have quoted from the work of others, the source is always mentioned. Except for such quotations, this thesis is entirely my work.
- Each research chapter of this dissertation relates to one or more SCI(E) indexed journal articles, which have been published/accepted.



Tuan-Khai Nguyen

UNIVERSITY OF ULSAN, REPUBLIC OF KOREA

August 2024

TERMS AND CONDITIONS RELATED TO COPYRIGHT

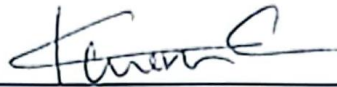


This thesis has been submitted in fulfillment of the requirements for a postgraduate degree (e.g., Ph.D.) at the University of Ulsan, Republic of Korea. Please note the following terms and conditions of use:

- This work is protected by copyright and other intellectual property rights, which are retained by the thesis author, unless otherwise stated.
- A copy can be downloaded for personal non-commercial research or study, without prior permission or charge.
- This thesis cannot be reproduced or quoted extensively without first obtaining permission in writing from the author.
- The content must not be changed in any way or sold commercially in any format or medium without the formal permission of the author.
- When referring to this work, full bibliographic details including the author, title, awarding institution, and date of the thesis must be given.

Condition-Based Monitoring Techniques for Concrete and Industrial Equipment

This certifies that the dissertation of Tuan-Khai Nguyen is approved.



Professor Kwon, Yung-keun
Committer Chair, University of Ulsan



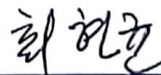
Professor Kim, Jong-myon
Advisor, University of Ulsan



Professor Jo, Dong-sik
Committee Member, University of Ulsan



Professor Im, Ki-chang
Committee Member, Korea Testing & Research Institute



Dr. Choi, Hyun-Kyun
Committee Member, Electronics and Telecommunications Research Institute

Department of Electrical, Electronic and Computer Engineering

UNIVERSITY OF ULSAN, REPUBLIC OF KOREA

August 2024

©2024 – Tuan-Khai Nguyen

All rights reserved.

“There is nothing like a dream to create the future.”

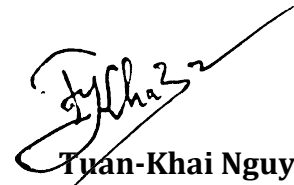
- Victor Hugo -

ACKNOWLEDGEMENTS

First and foremost, I would like to show my gratitude to my family, who have supported me wholeheartedly throughout every stage of my life journey. I am appreciative of their unconditional support, which has provided me with the strength to tread this path.

I would like to sincerely thank my supervisor, Professor Jong-Myon Kim of the Department of Electrical, Electronic, and Computer Engineering, University of Ulsan, South Korea. He has imparted to me many valuable lessons in both technical and non-technical subjects. I am deeply grateful for his generous support, encouragement, and guidance during my PhD.

I am also grateful to my friends and colleagues, specifically Dr. Tra-Viet, Dr. Bach Duong Phi, and Dr. Zahoor Ahmad for their guidance and friendship during my stay in South Korea. My sincere gratitude goes to my thesis committee members for their constructive feedback and valuable suggestions.



Tuan-Khai Nguyen
The University of Ulsan, Republic of Korea
2024

To my loved ones.

Abstract

This thesis presents hybrid techniques that combine signal processing with machine learning for the fault diagnosis and prognosis of concrete structures and industrial equipment. Based on the information collected during the monitoring process, abnormalities in the working conditions can be detected at an early stage. This ensures maintenance can be planned and performed accordingly, thus avoiding irreversible damage to the asset and the surrounding environment at minimal cost. In the third chapter, a scheme for leak localization on a cylinder tank bottom using acoustic emission (AE) is proposed, which utilizes similarity scores to group acoustic emission hits by their sources and analyzes the source locations through a Voronoi Diagram. The results under a one-failed-sensor scenario show a high level of accuracy across multiple test locations. Furthermore, in Chapter 4, an approach to perform leak state detection and size identification for industrial fluid pipelines with an acoustic emission activity intensity index curve (AIIC) using b-value and a random forest (RF) is proposed. This chapter shows that the AIIC outperforms traditional AE features in portraying the pipeline's working states, and along with the classification power of RF, the proposed method also consistently surpasses two state-of-the-art reference methods in the size identification task. Afterwards, Chapter 5 proposes a new technique for the construction of a health indicator for remaining useful life (RUL) prediction of concrete structures based on the Kullback–Leibler Divergence (KLD) and deep learning. The KLD-based indicator is capable of descriptively portraying the concrete structure's fracturing process, and its adaptation to the RUL task shows a high level of accuracy.

Table of Contents

DECLARATION OF AUTHORSHIP	II
TERMS AND CONDITIONS RELATED TO COPYRIGHT	III
ACKNOWLEDGEMENTS	VII
DEDICATION	VIII
ABSTRACT.....	IX
TABLE OF CONTENTS	A
LIST OF FIGURES	D
LIST OF TABLES.....	F
NOMENCLATURE.....	G
CHAPTER 1 INTRODUCTION.....	9
1.1 Motivation.....	9
1.2 Thesis Objective and Contribution	14
1.3 Thesis Organization.....	15
CHAPTER 2 OVERVIEW OF THE EXPERIMENTAL SETUP	17
2.1 Cylinder Tank Setup for Bottom Leakage.....	17
2.2 Pipeline Setup for Leakage Detection and Size Identification	18
2.3 Concrete Setup for RUL Prognosis	18

CHAPTER 3 LEAK LOCALIZATION ON CYLINDER TANK BOTTOM USING ACOUSTIC EMISSION	20
3.1 Introduction.....	20
3.2 Methodology.....	23
3.2.1 AE Hit Detection	24
3.2.2 Similarity Score and Event Grouping	27
3.2.3 Event Localization Using Time Difference of Arrival	28
3.2.4 Voronoi Diagram for Data Density Analysis	28
3.3 Case Study	29
3.3.1 Experimental Setup	29
3.3.2 Result and Discussion	32
3.4 Conclusion.....	35
 CHAPTER 4 LEAK STATE DETECTION AND SIZE IDENTIFICATION FOR FLUID PIPELINES WITH A NOVEL ACOUSTIC EMISSION INTENSITY INDEX AND RANDOM FOREST	 37
4.1 Introduction.....	37
4.1.1 Related Works	38
4.1.2 Overview of the Proposed Method and Contributions.....	40
4.2 Basic Concepts	41
4.2.1 The b-value.....	41
4.2.2 Changepoint Detection.	43
4.2.3 Random Forest.....	44
4.3 Case Study	46
4.3.1 The Proposed Method	46
4.3.2 Experimental Setup and Data Description.	49
4.3.3 Validation of the Proposed Method.	52
4.4 Conclusion.....	57
 CHAPTER 5 A DEEP-LEARNING-BASED HEALTH INDICATOR CONSTRUCTOR USING KULLBACK-LEIBLER DIVERGENCE FOR PREDICTING THE REMAINING USEFUL LIFE OF CONCRETE STRUCTURES	 59
5.1 Introduction.....	60
5.2 The General Health Indicator Construction Framework and Evaluation	63
5.3 The Proposed Health Indicator Construction.	64
5.4 Experimental Setup and Evaluation	67
5.4.1 Experimental Setup	67

5.4.2	Evaluation and Discussion	68
5.5	Conclusions.....	77
CHAPTER 6	CONCLUSION.....	78
6.1	Summary	78
6.2	Future Work	80
REFERENCES	81

List of Figures

Figure 1.1. Thesis graphical abstract	15
Figure 3.1. Overview of the proposed localization scheme	24
Figure 3.2. Simplified average CFAR scheme.	25
Figure 3.3. The significance of choosing the appropriate threshold for the TOA determination.	26
Figure 3.4. Simplified fix-thresholding TOA and end-time determination.	27
Figure 3.5. Example of a Voronoi diagram.	29
Figure 3.6. The cylinder tank under test: (a) vertical dissection schematic and vertical sensor displacement (b) horizontal dissection schematic, sensors, and Hsu-Nielsen test location (c) pictorial depiction of the test setup (d) Hsu-Nielsen test visualization.....	31
Figure 3.7. Hit detection process for a random one-second window: (a) raw AE data (b) cell power versus threshold (c) detected hits.	33
Figure 3.8. TOA and end time determination: (a) CUT containing a hit (b) Detected hit.	33
Figure 3.9. Source localization results in different Hsu-Nielsen test locations: (a) 1 (b) 2 (c) 3 (d) 4 (e) 5 (f) 6 (g) 7 (h) 8 (i) Center.	34
Figure 4.1. Flowchart of the proposed method.	41
Figure 4.2. Visualization of magnitude versus occurrence of different b-values based on GRL.	43
Figure 4.3. A simplified visualization of the classification process in RF.	45
Figure 4.4. Visualization of FAD at pressure level 7 bar with different leak sizes: (a) 0.3 mm, (b) 0.5 mm, and (c) 1 mm.	47
Figure 4.5. Visualization of FAD at pressure level 13 bar with different leak sizes: (a) 0.3 mm, (b) 0.5 mm, and (c) 1 mm.	47
Figure 4.6. Visualization of FAD at pressure level 18 bar with different leak sizes: (a) 0.3 mm, (b) 0.5 mm, and (c) 1 mm.	48
Figure 4.7. Leak detection using BEAST: (a) changepoint occurrence probability; (b) leak detected.	48
Figure 4.8. Experimental setup: (a) an image of the testbed and (b) an illustration of the sensor placements and leak position.....	50
Figure 4.9. A simplified visualization of the Hsu-Nielsen test.	50
Figure 4.10. AIICs for different leak sizes at 7 bar for: (a) channel one, (b) channel two, and (c) channel three.....	53
Figure 4.11. AIICs for different leak sizes at 13 bar for: (a) channel one, (b) channel two, and (c) channel three.....	54
Figure 4.12. AIICs for different leak sizes at 18 bar for: (a) channel one, (b) channel two, and (c) channel three.....	54

Figure 4.13. Comparison between AIIC and traditional indexes, with the blue region indicating normal working state, while the white one indicating leakage: (a) AIIC, (b) mean, (c) RMS, (d) kurtosis, (e) STD, and (f) variance. 56

Figure 4.14. Result of leak size classification with different pressure levels: (a) 7 bar, (b) 13 bar, and (c) 18 bar. 56

Figure 5.1. Flowchart of the HI construction framework and evaluation process. 62

Figure 5.2. Vertical displacement of the specimen and signal difference in two loading stages. 65

Figure 5.3. Experimental setup of the four-point bending test on reinforced concrete beam: (a) pictorial of the specimen under test, (b) schematic of the four-point bending arrangement, and (c) placement of sensors on the specimen. 67

Figure 5.4. Damage sustained by a specimen during the test. 68

Figure 5.5. Visualization of the proposed and other HI-constructing factors (RMS, Kurtosis, Crest Factor, and Skewness) using reinforced concrete beam: (a) α , (b) β , and (c) γ 69

Figure 5.6. RUL prognosis from the three tests 300 time steps before the failure. (a) Reinforced concrete beam α . (b) Reinforced concrete beam β . (c) Reinforced concrete beam γ73

Figure 5.7. RUL prognosis from the three tests 400 time steps before the failure. (a) Reinforced concrete beam α . (b) Reinforced concrete beam β . (c) Reinforced concrete beam γ 74

Figure 5.8. RUL prognosis from the three tests 500 time steps before the failure. (a) Reinforced concrete beam α . (b) Reinforced concrete beam β . (c) Reinforced concrete beam γ 75

List of Tables

Table 3.1. Specifications of the cylinder tank.....	31
Table 3.2. Displacement between the test locations and the results.....	35
Table 4.1. RF hyperparameters.....	49
Table 4.2. Experimental setup description.....	51
Table 4.3. Data description.....	51
Table 4.4. A comparison of leak size identification using the three methods under the pressure of 7 bar.....	57
Table 4.5. A comparison of leak size identification using the three methods under the pressure of 13 bar.....	57
Table 4.6. A comparison of leak size identification using the three methods under the pressure of 18 bar.....	57
Table 5.1. Fitness analysis of the proposed HI-constructing factor and other factors.....	70
Table 5.2. RUL prognosis performance assessment 300 time steps before the failure.....	75
Table 5.3. RUL prognosis performance assessment 400 time steps before the failure.....	76
Table 5.4. RUL prognosis performance assessment 500 time steps before the failure.....	76

Nomenclature

1D-CNN	1-D Convolutional Neural Network
AE	Acoustic Emission
AEE	Acoustic Emission Event
AEH	Acoustic Emission Hit
AHR	Anomalous Hits Removal
AHC	Acoustic Emission Intensity Curve
ANN	Artificial Neural Network
BEAST	Bayesian Estimator of Abrupt Change, Seasonal Change, and Trend
BMA	Bayesian Model Averaging
CFAR	Constant False Alarm Rate
CNN	Convolutional Neural Network
CUT	Cell Under Test
DNN	Deep Neural Network
DT	Decision Tree
EDV	Event Definition Value
FAD	Frequency-Amplitude Distribution
FEM	Finite Element Method
FMECA	Failure Mode, Effects, and Criticality Analysis
GPR	Ground-penetrating Radar
GRL	Gutenberg-Richter Law
HI	Health Indicator
IFT	Infrared Thermography Testing
KLD	Kullback-Leibler Divergence
LDVT	Linear Variable Differential Transformer

LSTM-RNN	Long Short-Term Memory Recurrent Neural Network
NDT	Non-destructive Testing
RCB	Reinforced Concrete Beam
RF	Random Forest
RMS	Root Mean Square
RT	Radiography Testing
RUL	Remaining Useful Lifetime
RVM	Relevance Vector Machine
SAE	Stacked Autoencoder
SHM	Structural Health Monitoring
STD	Standard Deviation
SVM	Support Vector Machine
TD-CNN	Convolutional Neural Network Using Time-Domain Features
TDOA	Time Difference of Arrival
TOA	Time of Arrival
UT	Ultrasonic Testing

Chapter 1

Introduction

The motivations, contributions, and organization of the thesis are presented in this chapter. The following sections of this chapter are arranged as follows: **Section 1.1** discusses the motivation behind this work, **Section 1.2** summarizes the contributions, and **Section 1.3** demonstrates the outline of the rest of the thesis. It should be noted that the materials presented afterward in this thesis have been submitted and published in peer-reviewed journals.

1.1 Motivation

With easy access and high durability, concrete structures have become a ubiquitous sight in recent decades. Along with their everywhere presence, there comes the inevitable need for a maintenance plan to ensure in-service safety and to prolong the lifetime of concrete structures. Numerous studies have been conducted by laboratories, companies, and individuals racing to identify solutions regarding the performance amelioration of structural health monitoring (SHM). By employing an effective monitoring scheme, it is possible to provide the user with more insight into the in-service system/structure, avoid near-future failures, and lessen downtime by a significant amount.

Pipelines play a vital role in civil and industrial settings as one of the major fluid transportation methods. While they can generally provide safe and efficient passage even in long-distance systems, pipelines are not immune to leaking and breaking due to the influence of natural disasters, component corrosion, installation errors, etc. An unattended leak can evolve into a major pipeline burst, which can not only sever the entire transportation system, but potentially lead to human injuries/fatalities, environmental hazards, and huge economic

costs for recovery. Due to the dire consequences of pipeline leaks, the faults must be detected and diagnosed in earlier stages so that maintenance can be performed accordingly.

A cylinder tank is a pressure vessel that is used for liquid, vapor, or gas containment in both industrial and civil settings. In general, pressure vessels are known to provide a long, useful lifetime, even with dangerous substances (e.g., acids), if failures are detected and treated early. However, untreated failures can unleash the contained substance, which does not just cause financial damage, but more importantly, precipitate injuries or even fatalities, and turn the surrounding environment hazardous. An example of how appropriate diagnosis and maintenance can greatly extend service life is shown in a hydrofluoric acid sphere tank test, which was monitored and fixed properly. In the end, it offered a safe service life of 20 years under a continuous corrosive attack. Afterward, the same pressure vessel was decommissioned but could still serve in its new role as a water container for years to come. Leaking on the flat bottom surface is one of the most common problems in a vertical cylinder tank. While in service, it is often not visible or accessible for manual inspection. Diagnostic methods that require tank drainage for inspection are obsolete and can cause unnecessary financial costs while rendering the vessel out of service during the test. Due to this reason, in-service testing has become more favorable in recent years not just for cylinder tanks, but other structures and systems as well. Through this procedure, leak location(s) can be detected early, and maintenance can be performed to prevent further failures and avoid possible environmental contamination.

Currently, non-destructive testing (NDT) has emerged as one of the most popular research topics within the prognosis and health management framework for civil and industrial assets. In addition to its obvious contribution to safety and incident prevention, the other reason behind NDT's relevance is that it allows inspection and evaluation without affecting specimen serviceability, as its name suggests. Multiple techniques have been proposed such as ultrasonic testing (UT), radiography testing (RT), ground-penetrating radar (GPR), infrared thermography testing (IFT), distributed acoustic sensing, active distributed temperature sensing, acoustic emission (AE), etc. Each of these techniques presents various advantages and disadvantages which can best serve different applications. In terms of AE, it studies the elastic waves released upon a discontinuity occurrence. AE offers many upsides, such as non-directionality, no downtime for in-service testing, new damage detection, and outstanding progression monitoring, in which the deterioration process can be captured with only one test. During the monitoring process, AE is sensitive to new damage sustained by the specimen, and to the irregularities of the specimen's working activity due to these damages. Since the foremost purpose of this study is pipeline monitoring, it can benefit from the aforementioned advantages. Thus, AE testing is the NDT method chosen for application in this work.

When a discontinuity happens in the specimen, it releases acoustic waves which can be captured by the AE sensors. In the case of concrete structures, the discontinuities are mainly cracks from both the internal and external of the specimens. Regarding the cylinder tank and fluid pipeline system, the main source of AE activity is not the crack, but rather the disturbances in the fluid flow happening around the leaking region due to the crack. There are, of course, other sources of AE activity interfering with the monitoring process. This can influence the accuracy of the deterioration process portrayal and the estimation of the fault's properties. Chapters 3 to 5 discuss in detail how to harness useful information in different problem sets of cylinder tanks, fluid pipelines, and concrete structures.

Source localization has been one of the most important topics regarding structural and machinery health management frameworks. AE testing can allow localization of an active source, given that an ample amount of data is available through collection from the transducer(s). The most notable approaches concerning an AE source location are zone the location technique, the signal amplitude difference technique, and the timing technique. The zonal approach is one of the more basic techniques for AE localization, which harnesses the idea that the AE source is most likely in the zone of the transducer that returns the highest amplitude, given the assumption of equal transducers' sensitivity. This technique can offer a simple solution when pinpointing the exact source location is not of utmost importance. However, it is found lacking for the more demanding problems. In the case where structural characteristics are known, the signal amplitude difference of the closest transducers (to the source, determined by the highest amplitude with the same assumption of zonal localization) can be measured and then compared with the known attenuation characteristics. Although this method can give a more detailed and accurate answer than zonal localization, obtaining the information for characteristics can be a huge challenge, especially when a structure or machinery is made of more than one material. The timing technique is one of the more favored approaches in recent years, which uses the difference between the time delays of the same event across separate transducers to derive the source location. Methods that follow this approach can obtain results with high accuracy. However, it is necessary to have precise time difference calculations. The time difference can be estimated through different means, including cross-correlation (a time difference measurement based on the cross-correlation of one discrete or continuous wave in accordance with another), grid search (a time difference measurement achieved by searching the grid zone with the least residual between the calculated and the real distance, either spatially or in time), hit detection and event grouping, etc. In the case of hit detection and event grouping, it can be troublesome because AE events usually happen in bursts with multiple hits happening in a short interval. Since this thesis pursues this approach with a time difference of arrival (TDOA) scheme, a constant false alarm rate (CFAR)-based hit detection and an event grouping method are proposed to solve this problem. Moreover, in a real-life leaking situation, AE events are expected to happen not just at the location of the leak, but also in nearby regions due to the turbulent

flow of the stored substance. Therefore, the event location alone does not pinpoint the location at which the leak is located, but it can be found through a density analysis of these points. Assuming that the probability density is identical at every event location due to the lack of statistical information regarding the leak, it can be determined that the leak is most likely to be in the spot where the events are densely located. Thus, a Voronoi diagram is employed here to search for the leak region on the cylinder tank bottom.

Many studies have been conducted that have used AE for pipeline system diagnosis. When a leak occurs in a pipeline system, variations are expected in the AE data. The leak detection process using AE is centered around the differences between the variations that happen in the leak state and the normal state, which have been mostly approached from the view of feature extraction and pattern recognition in recent studies. The studies in this area can be roughly categorized as follows: time domain, frequency domain, and time-frequency domain. Time domain approaches are often the most straightforward out of the three domains; however, they usually require an additional pre-processing step to minimize their susceptibility to interferences. Frequency-domain approaches can be more robust than time-domain ones; however, they are more complicated and often require more expertise regarding system- or fault-specific frequencies. Out of the three domains, time-frequency approaches can provide the most powerful solutions, at the cost of huge computational complexity. As briefly explained in the previous subsection, AE is based on the release of elastic waves upon the occurrence of discontinuity. Such an occurrence, which releases elastic waves, is called an AE event (AEE) and, when an AEE is detected by a sensor, these data can be referred to as an AE hit (AEH). Generally, AEHs can be categorized into two types: burst-type and continuous-type. While the continuous-type is considered noise and contains minimal useful information, the burst-type AEH possesses valuable data that can be used for the determination of the specimen's state. Because of the nature of fluid transportation in pipeline systems, AE events can be recorded from various sources, even under normal working conditions that can involve unstable flow, pressure on joints, pipeline vibration, leaks, and interferences from the environment, etc. The diversity of sources in pipeline systems and their occurrences in a short period introduces a more complex problem (referred to as the multi-source problem of AEEs), in comparison to rigid specimens such as concrete structures and machinery, etc. in which the signal is significantly more transient and there are fewer sources of AEEs (primarily due to discontinuity-related reasons, such as cracks, loose fittings, etc.). Even though AEH features can offer a great description of the AE activity, it is difficult to correctly obtain the data related to these features due to the high AE noise level and the sophisticated AEH detection process. As an alternative, this paper presents AE activity intensity construction, using the b-value for pipeline systems. The b-value was first introduced in the Gutenberg–Richter law (GRL). In brief, it expresses the relationship between the number of earthquakes and their magnitude in a given period and location. Since an AEE can be considered a low-energy seismic event, the b-value was also

adopted for AE applications on concrete structures. As the adopted b-value describes the correlation between the number of AE peaks and the AE amplitude, and there is a proven relationship between the amplitude and the discontinuity size, it is anticipated to provide an accurate description of the AE activity intensity. Based on this intensity index, the pipeline's working condition can be detected and, if a leak is present, the size can be identified.

Health indicator (HI) construction is an essential part of the prognosis to portray the timeline of concrete structure deterioration. HI shows the condition in which the specimen under investigation is. By analyzing the current HI, it is possible to predict future values and their timing, thus allowing the RUL to be estimated. Over the years, numerous studies have proposed different approaches to building a HI, especially in more recent studies, and in summary, this process can be generally divided into two steps: (1) calculation of the HI-constructing factor(s) and (2) HI construction from the calculated factor(s). The calculation of the HI-constructing factor(s) (also known as features) is often performed either in the time, frequency, or time-frequency domain. The time domain approaches generally offer a fast and simple solution that can be widely applicable to systems and fault types. They often include statistical computation and impulse analysis. These methods, however, are susceptible to interferences, which are typically inevitable in real-life applications. Therefore, pre-processing techniques are necessary to minimize performance degradation. Frequency domain solutions explore anomalies in the system with prior information on the fault characteristic frequencies already known. They are often adapted in model-based methods and can offer high efficiency; however, they are not widely applicable. The approaches following the time-frequency domain solution are the most powerful among these three and can be highly robust. Their downside is that such powerful methods often require high computational capability and experience concerning information extraction. Afterward, the second step is to build the HI constructor. As briefed previously, the construction of a HI can be roughly divided into two categories: model-based and data-based. Model-based methods focus on generating a mathematical representation that mimics a real-life process. The development of an HI in these studies requires expertise, and knowledge about the system's behavior, the nature of the faults, and the HI-constructing factors. The aforementioned research and many others have been carried out with expertise in signal processing, and system and fault behavior, which can be troublesome to obtain in more sophisticated scenarios. Moreover, they cannot be adapted to a variation in systems, due to their construction imitating certain real-life processes. Unlike model-based approaches, data-based solutions focus on the nature of the data itself, with less concern for the system or fault nature. Due to their lower complexity and wider application toward different systems and faults, data-based methods have been more favorable in recent years, especially with the rise of artificial intelligence. Notable mentions in this category are statistical projection, deep learning models, evolutionary computation, etc. Different studies following these methods have achieved promising results in HI construction for the RUL prognosis

task. For all the reasons stated above, this thesis discusses a new technique for the construction of a health indicator for concrete structures based on the Kullback–Leibler divergence and deep learning.

1.2 Thesis Objective and Contribution

The objective of this thesis is to build intelligent techniques, using both advanced signal processing and AI, for the fault diagnosis/prognosis of concrete structures and industrial equipment. The abstract of this study is illustrated in Figure 1.1. The contributions of this thesis are as follows:

1. A similarity score is introduced to group AE hits into the same events, whose locations are then used for density analysis using the Voronoi Diagram to find the leak region on the cylinder tank bottom.
2. An AE activity intensity curve (AIIC) based on b-value is introduced as an accurate description of the working state of the industrial fluid pipeline despite the influence of multiple AE sources rather than just the leak. Leak detection and size identification are performed on the AIICs using a Bayesian ensemble estimator and random forest, respectively.
3. This thesis presents the construction of the HI for concrete structures using Kullback-Leibler Divergence, on which the RUL prognosis is performed using LSTM.

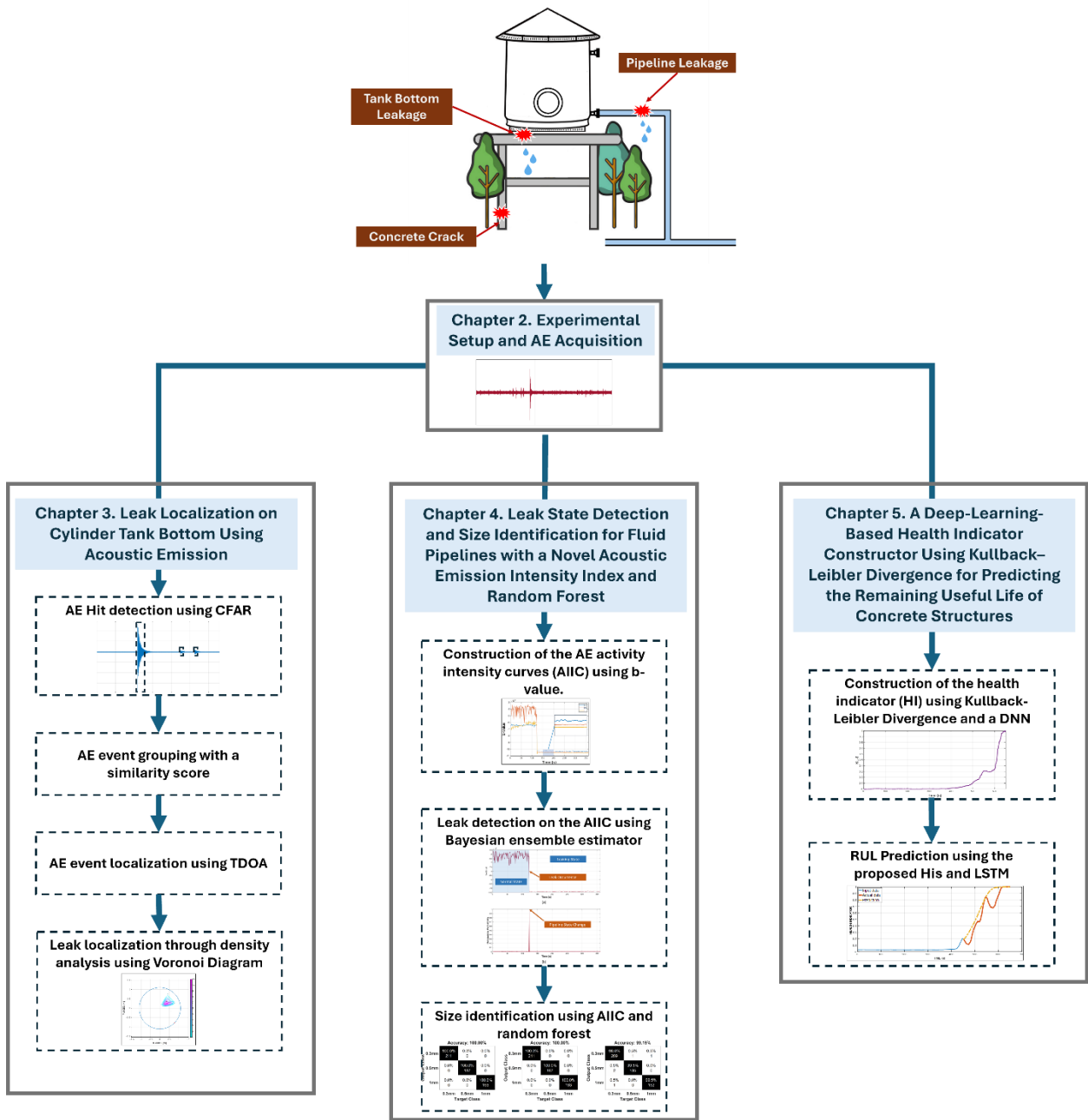


Figure 1.1. Thesis graphical abstract

1.3 Thesis Organization

The following chapters of this thesis are organized as follows:

- **Chapter 2** explains the experimental setups and the data description for concrete structures and industrial equipment.
- **Chapter 3** presents leak localization on the cylinder tank bottom using AE.

- **Chapter 4** presents leak detection and size identification for fluid pipelines with a novel AE intensity index and random forest.
- **Chapter 5** presents a deep-learning-based HI constructor using KLD for predicting the RUL of concrete structures.
- **Chapter 6** concludes the thesis and discusses possible future work.

Chapter 2

Overview of the Experimental Setup

In this chapter, the experimental setup and data description are presented. The data collected from those setups are used to verify the proposed methods for concrete structures and industrial equipment. This chapter includes three different setups: the first one is a cylinder tank with data collected using the Hsu-Nielsen test; the second setup is an industrial standard pipeline system in a normal working condition and a leaking condition; finally, the last setup is a four-point bending, run-to-fail test on multiple reinforced concrete beams (RCB). They provide the data for the studies discussed in chapters III, IV, and V, respectively.

2.1 Cylinder Tank Setup for Bottom Leakage

To verify the proposed method, a Hsu-Nielsen test was employed on a cylinder tank under a one-failed-sensor scenario to imitate a leaking situation. The Hsu-Nielsen test is a test in which a pencil lead of 0.5 mm diameter is broken at a 30° angle against a surface for an AE event generation. The discontinuity upon a lead-breaking occurrence generates an elastic wave that travels along the bottom surface and can be captured by the sensors. For this reason, it is a popular method for an AE event source imitation in multiple experimental setups for different types of machinery or structural failures. In addition, the one-failed-sensor scenario provides a more challenging problem than a conventional setup, in which one of the evenly positioned sensors is considered to be malfunctioning. By doing this, any event that happens in this impaired sensor's neighborhood, which is supposed to be in the coverage of the failed one, would have to be processed from further channels, thus introducing more attenuation and distortion to the available data. A total of six R6I-AST

sensors were attached to the surface of the vertical cylinder tank at a height of 300 mm, and the recordings were taken at a sampling rate of 1 MHz. These sensors from MINTRAS offer high sensitivity, and long-driving cable capability with a built-in 40 dB preamplifier and a filter. Moreover, being enclosed in a metal stainless steel housing can provide resistance to electromagnetic/radio frequency interferences and heat stabilization from -35 to 75 Celsius degrees. The “AST” part in the name shows that this genre also supports the integrated Auto Sensor Test, which allows sensor coupling and performance verification even in service. The detailed specifications and illustrations of the setup are presented later in Chapter 3.

2.2 Pipeline Setup for Leakage Detection and Size Identification

To validate the approach presented in this thesis, data acquisition was conducted using an industrial fluid pipeline system. Three R15I-AST sensors were deployed during this process. The R15I-AST sensor is a highly sensitive product from MITRAS, specifically designed to provide low-noise input, with a built-in auto sensor test and long-cable driving capability without an additional preamplifier requirement. Due to its metal housing, it is less susceptible to radio frequency and electromagnetic interferences. The three sensors were attached to the surface of the pipeline following the application of a coupling medium gel on the contact spots. To ensure that the sensors would not be displaced or fall from the specimen, the tape was utilized. Sensor channels one, two, and three were located at 2500, 1600, and 0 mm (reference position), respectively, along with the leak location at 800 mm. The flow direction was from channel one to channel two, then through the leak position, and finally through channel three. The multiple sensor setup allowed different points of view: channel one offered the view of an upstream flow before the leak; channel two was used for near-leak monitoring, which was expected to have the highest AE activity intensity of all of the channels; channel three offered a view of a downstream flow located after the leak. Though they were recorded from the same test, each of them could be treated as a standalone, which provides more variety to the dataset. The detailed specifications and illustrations of the setup are presented later in Chapter 4.

2.3 Concrete Setup for RUL Prognosis

To evaluate the reliability of the proposed method, data were collected from reinforced concrete beams, which were constructed and installed for the four-point bending test scenario. Each specimen was identically produced with concrete material having a compressive strength of 24 MPa, D16 (SD400) steel rebar, and gridded in 50×50 mm² squares for better visualization of deterioration monitoring. The AE data were acquired at 5 MHz from eight R3I-AST sensors placed around both ends of a specimen. Each specimen was subject to two-point concentrated loading. The loading points were placed 400 mm from the left and right of the specimen’s median, and the stress was applied at a speed of 1 mm/s. In addition, a linear variable differential transformer (LDVT) was set underneath the specimen

Chapter 2: Overview of the Experimental Setup

at its center for vertical displacement measurement. This is an alternate way to track the damage sustained other than the visual monitoring of the specimen's surface fractures. During the test, the specimens were loaded until the damage was high enough that maintenance was not efficient anymore; however, a total collapse was prohibited from happening for the safety of the observers including our team members and construction field specialists.

Chapter 3

Leak Localization on Cylinder Tank Bottom Using Acoustic Emission

In this chapter, a scheme for leak localization on a cylinder tank bottom using acoustic emission (AE) is proposed. This approach provides a means of early failure detection, thus reducing financial damage and hazards to the environment and users. The scheme starts with the hit detection process using a constant false alarm rate (CFAR) and a fixed thresholding method for a time of arrival (TOA) and an end-time determination. The detected hits are then investigated to group those originating from the same AE source together by enforcing an event definition and a similarity score. Afterward, these newly grouped hits are processed by a time difference of arrival (TDOA) to find the locations of the events. Since the locations of the events alone do not pinpoint the leak location, a data density analysis using a Voronoi diagram is employed to find the area with the highest possibility of a leak's existence. The proposed method was validated using the Hsu-Nielsen test on a cylinder tank bottom under a one-failed-sensor scenario, which returned a highly accurate result across multiple test locations.

3.1 Introduction

A cylinder tank is a pressure vessel that is used for liquid, vapor, or gas containment in both industrial and civil settings. In general, pressure vessels are known to provide a long, useful lifetime, even with dangerous substances (e.g., acids), if failures are detected and treated early. However, untreated failures can unleash the contained substance, which does not just cause financial damage, but more importantly, precipitate injuries or even fatalities, and turn the surrounding environment hazardous. An example of how appropriate diagnosis and maintenance can greatly extend service life is shown in a hydrofluoric acid sphere tank test

[1], which was monitored and fixed properly. In the end, it offered a safe service life of 20 years under a continuous corrosive attack. Afterward, the same pressure vessel was decommissioned but could still serve in its new role as a water container for years to come.

Leaking on the flat bottom surface is one of the most common problems in a vertical cylinder tank. While in service, it is often not visible or accessible for manual inspection. Diagnostic methods that require tank drainage for inspection are obsolete and can cause unnecessary financial costs while rendering the vessel out of service during the test. Due to this reason, in-service testing has become more favorable in recent years not just for cylinder tanks, but other structures and systems [1], [2], [3], [4] as well. Through this procedure, leak location(s) can be detected early, and maintenance can be performed to prevent further failures and avoid possible environmental contamination.

AE testing offers a non-destructive and in-service means for diagnosis in general structural and machinery health management frameworks [1], [2]. When a discontinuity occurs within an object, it emits elastic waves, which are most often in the frequency range of 20 kHz to 1 MHz. This phenomenon is known as AE or a low-energy seismic event that can often be observed in nature when a rock fracture occurs. An AE test has several notable attributes, including non-directionality, in-service testing with little to no downtime, progression tracking, and the ability to capture the whole deterioration process with no more than one test. Therefore, it has been widely harnessed for various studies and applications [2], [5], [6], [7], [8], [9], [10], [11], [12], [13], [14] across different structures and systems for both industrial and civil use. However, it should be noted that an inspection must be performed before performing an AE test to obtain a priori knowledge of the specimen condition. AE testing does not show existing failures, but rather the occurrence of new ones with a now-or-never attribute. Otherwise, the specimen is assumed to be in normal working condition at the start of an AE test. In the AE context, the occurrence of a discontinuity that releases elastic waves is referred to as an AE event. When an AE event is recorded by a transducer, it is called an AE hit. Due to the AE being the sole focus of this study, these two terms are henceforth referred to as an event and a hit for convenience.

Source localization has been one of the most important topics regarding structural and machinery health management frameworks. AE testing can allow localization of an active source, given that an ample amount of data is available through collection from the transducer(s). The most notable approaches concerning an AE source location are zone the location technique [1], the signal amplitude difference technique [1], and the timing technique [13], [15], [16], [17], [18], [19], [20]. The zonal approach is one of the more basic techniques for AE localization, which harnesses the idea that the AE source is most likely in the zone of the transducer that returns the highest amplitude, given the assumption of equal transducers' sensitivity. This technique can offer a simple solution when pinpointing the

exact source location is not of utmost importance. However, it is found lacking for the more demanding problems. In the case where structural characteristics are known, the signal amplitude difference of the closest transducers (to the source, determined by the highest amplitude with the same assumption of zonal localization) can be measured and then compared with the known attenuation characteristics. Although this method can give a more detailed and accurate answer than zonal localization, obtaining the information for characteristics can be a huge challenge, especially when a structure or machinery is made of more than one material. The timing technique is one of the more favored approaches in recent years, which uses the difference between the time delays of the same event across separate transducers to derive the source location. Methods that follow this approach can obtain results with high accuracy. However, it is necessary to have precise time difference calculations. The time difference can be estimated through different means, including cross-correlation (a time difference measurement based on the cross-correlation of one discrete or continuous wave in accordance with another) [21], [22], grid search (a time difference measurement achieved by searching the grid zone with the least residual between the calculated and the real distance, either spatially or in time) [23], [24], [25], hit detection and event grouping [13], etc. In the case of hit detection and event grouping, it can be troublesome because AE events usually happen in bursts with multiple hits happening in a short interval. Cross-correlation-related studies such as [21] adopted a wavelet analysis to extract the useful AE data from noise, then applied a cross-correlation method regarding the geometric positioning principle or investigated multiple weighting function options for the generalized cross-correlation algorithm to estimate the delay time, as in [22]. Other studies following grid search, such as [23], performed a deep analysis of the AE source localization for concrete structures or found the location by leveraging the AE waveform's reflection, reverberation patterns, and their dispersive, multimodal characteristics using only one sensor [24]. In addition, the research in [25] investigated the continuous wavelet transform and the fundamental Lamb wave's dispersion curves for localization. For the studies regarding the hit detection and the event grouping approach, the burst phenomenon in the AE signal can be analyzed along with the physical wave-propagation model to achieve a promising result [13]. Since our study pursues this approach with a time difference of arrival (TDOA) scheme, a constant false alarm rate (CFAR)-based hit detection and an event grouping method are proposed to solve this problem.

In a real-life leaking situation, AE events are expected to happen not just at the location of the leak, but also in nearby regions due to the turbulent flow of the stored substance. Therefore, the event location alone does not pinpoint the location at which the leak is located, but it can be found through a density analysis of these points. Assuming that the probability density is identical at every event location due to the lack of statistical information regarding the leak, it can be determined that the leak is most likely to be in the spot where the events

are densely located [26]. Thus, the Voronoi Diagram [27] is employed in this study to search for this region.

In summary, this study proposes the following contributions:

1. A leak localization scheme using AE data, which has not been under investigation, is proposed with a novel event grouping approach, which gathers hits originating from the same event through similarity measurement.
2. The locations of events are further analyzed using a Voronoi diagram to find the area in which the leak is most likely happening.
3. The study is validated through a case study of a one-failed-sensor scenario.

The following parts of this paper are organized as follows: The methodology is presented in Section 3.2, whereas Section 3.3 displays the case study to which the proposed method was applied, and Section 3.4 provides the conclusion along with future research possibilities.

3.2 Methodology

Prior to a detailed discussion of the methodology, an overview of the proposed process is given in Figure 3.1. Initially, raw AE data is processed with a CFAR for hit detection, whose results are further investigated with fixed thresholding to determine the TOA and end time. Afterward, hits from the same origin are grouped using the event definition and similarity score. Using the newly grouped hits, the locations of events can be calculated using TDOA, which are eventually analyzed with a Voronoi diagram to return the final estimated leak location.

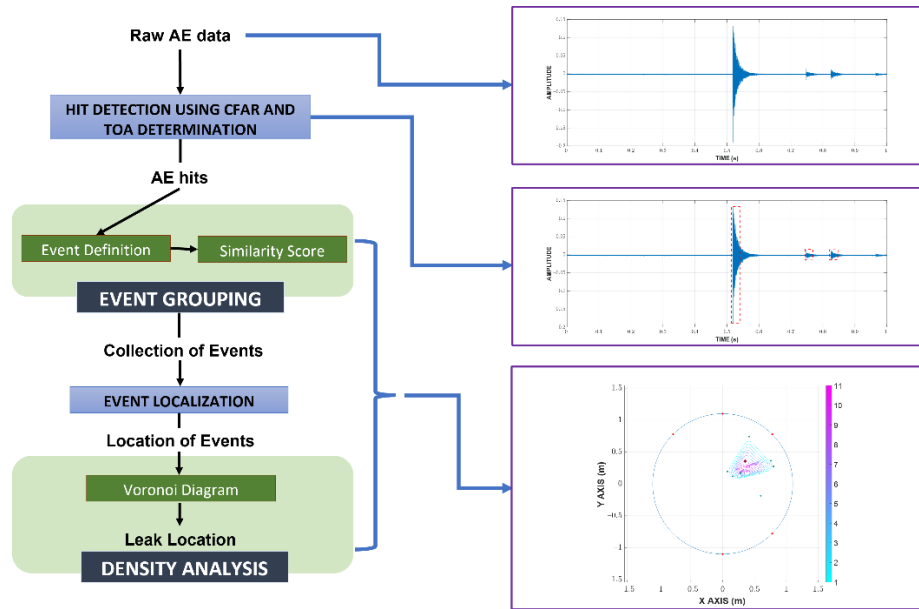


Figure 3.1. Overview of the proposed localization scheme

3.2.1 AE Hit Detection

The CFAR was originally developed in radar systems for target detection [28]. The principle of a CFAR is to set a power threshold, which distinguishes possible real target hits from the rest (i.e., those considered to originate from spurious sources). The calculation of this threshold is governed by a constant false alarm rate (hence the name) as the trade-off metric between true targets and false ones. In real-life problems, due to many factors, the noise can affect the data both temporally and spatially. Therefore, such difficulties render fixed-threshold-based methods ineffective. A CFAR approaches this problem by adaptively adjusting the threshold level regarding the probability of false alarms, thus lowering the susceptibility to real-life noise. Since its first introduction to radar systems, the CFAR has also been harnessed in other fields due to its advantage in the presence of colored noise with unknown variance. For this research, the average CFAR is employed to detect AE hits from the recorded AE sequences. To manage one-dimensional time series such as those investigated in this study, the model displayed in Figure 3.2 can be used.

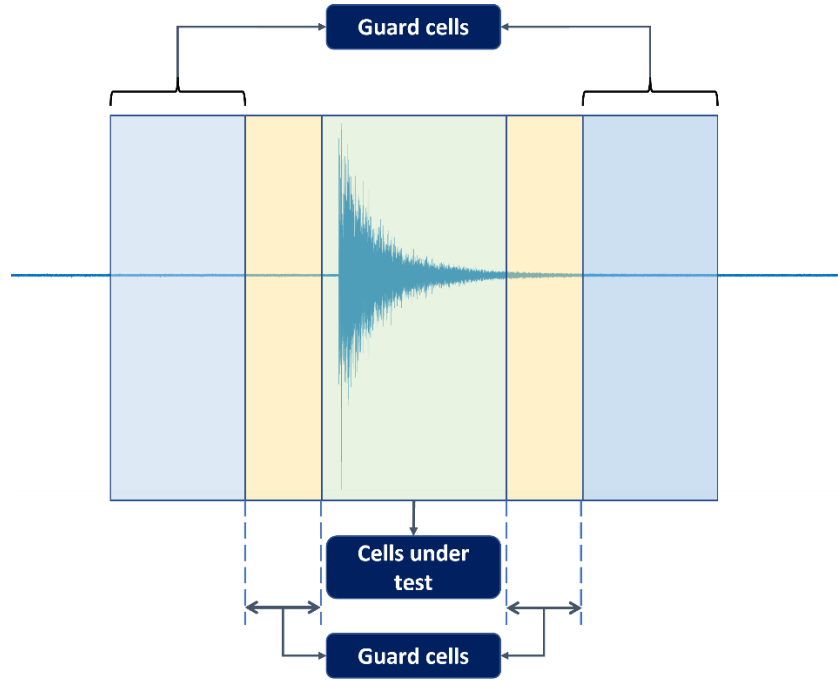


Figure 3.2. Simplified average CFAR scheme.

The algorithm investigates a cell under test (CUT) through its neighboring cells, which are grouped into guarding and training cells on both sides. The CUT is considered to contain a hit upon exceeding the threshold, which can be derived from the noise power as follows:

$$P_{threshold} = \alpha P_{noise} \quad (3.1)$$

Given N training cells with x_i being the sample in the i^{th} training cell and the constant false alarm rate P_{fa} , the threshold factor α and the estimated noise power are obtained as follows:

$$P_{noise} = \sum_{i=1}^N \frac{x_i}{N} \quad (3.2)$$

$$\alpha = \frac{N}{\sqrt[N]{P_{fa}}} - N \quad (3.3)$$

As previously discussed, P_{fa} governs the trade-off between the real and false targets. A lower P_{fa} value allows more real targets to be detected at the expense of increased false targets. A higher P_{fa} eliminates a large number of false targets, but real targets might also be ignored. To ensure that the detected targets are not contaminated by false choices, a value of 1×10^{-4} was found to provide the best performance. The data is processed in one-second segments without overlapping, and each is divided into a collection of 2000 cells. Each CUT is

investigated with 10 guarding cells, and 20 training cells and it is considered to contain a hit if the threshold is surpassed.

Since the localization of events is achieved through TDOA, CFAR can only show whether or not a hit is present in the CUT. The next step is to detect the time of arrival (TOA) of hits. In this study, the duration of a hit, which is marked by the TOA and the end time, is determined with a fixed threshold method [23], [28], [29], which is popular among existing acquisition systems. An appropriate threshold selection is necessary because a low threshold can trigger a premature detection due to noise and a high one can miss the actual TOA by a considerable margin, as can be seen in Figure 3.3. The first and last threshold crossings are registered as the TOA and end time, respectively. The visualization of this process can be found in Figure 3.4.

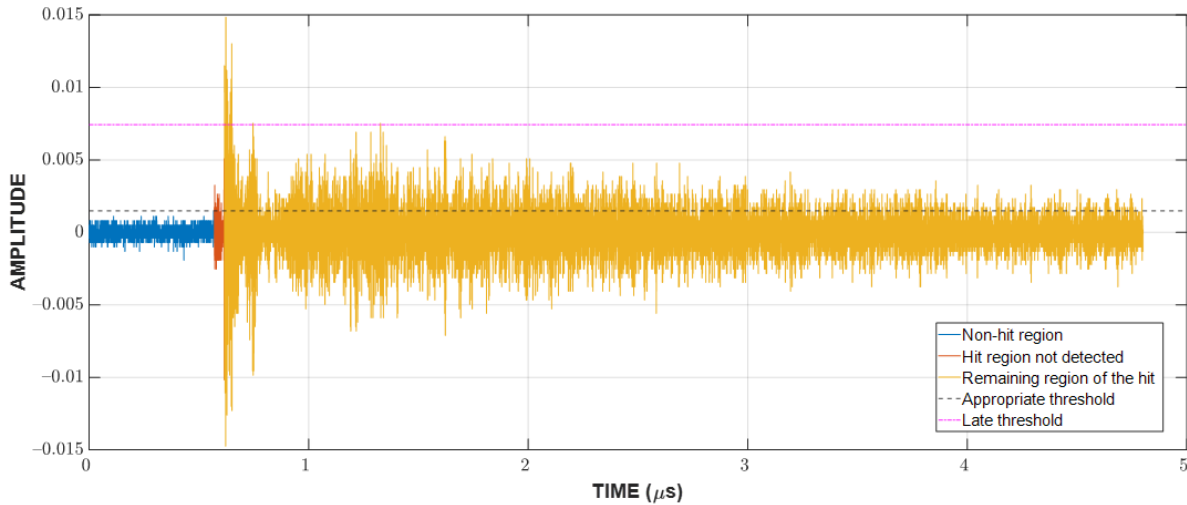


Figure 3.3. The significance of choosing the appropriate threshold for the TOA determination.

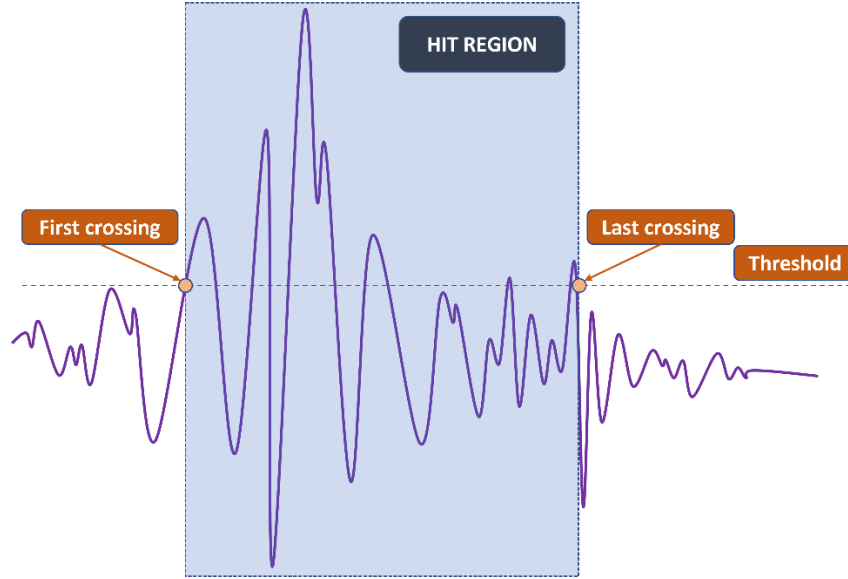


Figure 3.4. Simplified fix-thresholding TOA and end-time determination.

3.2.2 Similarity Score and Event Grouping

Event grouping is often regarded as of lesser importance in comparison to hit detection and event localization in a TDOA-based scheme, even though it is an essential part that directly influences the outcome of localization. In this stage, hits from the same source are grouped so that later their TOAs can be evaluated against each other to pinpoint the event source. The check for event grouping happens between two hits at a time and consists of two stages: the event definition value (EDV) check and the similarity score evaluation.

An EDV is a popular fixed-threshold method for event grouping. It sets the maximum time difference between hits that are from the same event. The formula for the EDV can be found as follows:

$$EDV = \frac{\max(D_{sensors})}{v} \quad (3.4)$$

with D_{sensor} consisting of the distances between each pair of sensors and v being the velocity of the elastic wave. Given that in real-life situations events often occur in bursts with multiple discontinuities happening in quick succession, there could be more than one hit existing within the EDV range of another. Therefore, it would not be sufficient to employ just the EDV for event grouping. Given a reference hit to which others are compared, a list of hits recorded from the next channel and within its EDV range are registered for further evaluation.

Afterward, a similarity score is calculated between the reference hit and each of the hits registered in the list. The authors propose a new similarity score calculation as follows:

$$\text{Similarity Score} = \frac{\max(\text{cross-correlation}(\text{hit}_{ref}, \text{hit}))}{\max(\text{auto-correlation}(\text{hit}_{ref}))} \quad (3.5)$$

The hit that returns the highest similarity score with the reference one is then considered to be sharing the same source. Subsequently, the search continues across other channels. Any hit registered to one event cannot be registered for another and will be removed from the list indefinitely.

3.2.3 Event Localization Using Time Difference of Arrival

Event localization can be computed for each of the event groups found in the previous subsection. The maximum number of hits that can be registered in one group is equal to the number of sensors deployed in the test. However, the required number of hits for localization on a 2-D plane is three. Therefore, only the three earliest hits from the group are used in this study because the later hits come from the far sensors, which could have been distorted and influenced by an AE noise and other hits.

Given the TOAs t_i of the three hits 1–3 and the (x_i, y_i) coordinates from the sensors which recorded them respectively, the source location (x_s, y_s) can be found by solving the following set of equations:

$$\begin{aligned} v * \Delta t_{2,1} &= \sqrt{(x_2 - x_s)^2 + (y_2 - y_s)^2} - \sqrt{(x_1 - x_s)^2 + (y_1 - y_s)^2} \\ v * \Delta t_{3,1} &= \sqrt{(x_3 - x_s)^2 + (y_3 - y_s)^2} - \sqrt{(x_1 - x_s)^2 + (y_1 - y_s)^2} \end{aligned} \quad (3.6)$$

The event location results can be further analyzed to find the possible leak source, as presented in the next subsection.

3.2.4 Voronoi Diagram for Data Density Analysis

The Voronoi diagram's history can be traced back to the 17th century. Throughout the years, it has been known by a few other names, such as Dirichlet tessellation or Thiessen polygons. The core idea of a Voronoi diagram is rather straightforward: given N points in a plane, it tessellates that plane into N convex polygons (also known as regions), each of which is generated from one point (also known as a site), and every point within that region is closer to the generating site than the other ones. The visualization of a Voronoi diagram can be seen in Figure 3.5.

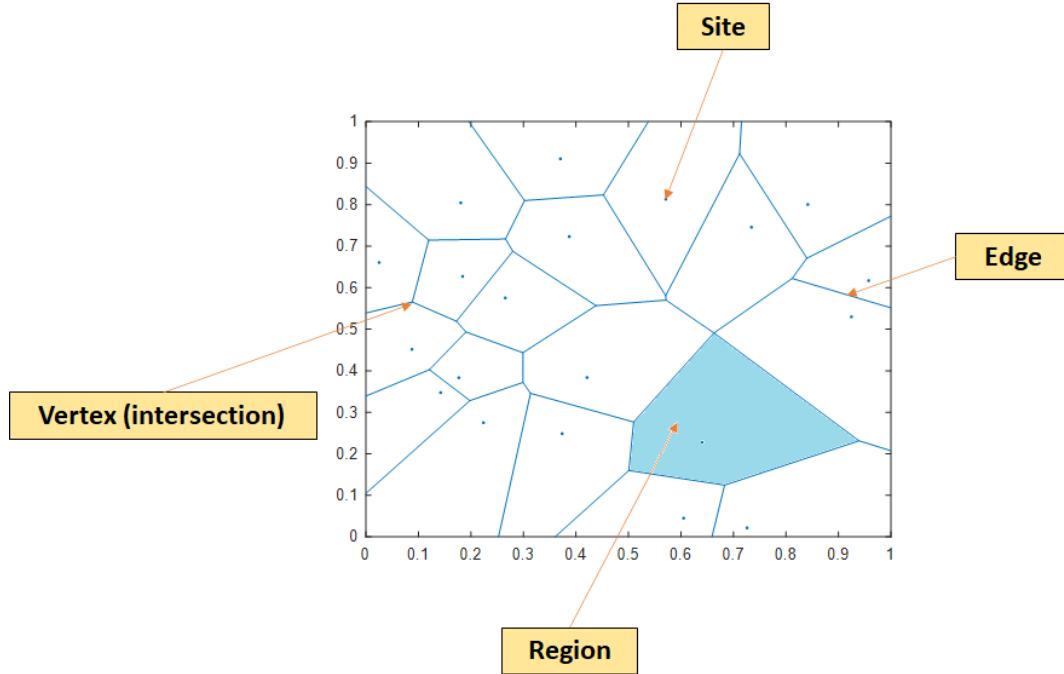


Figure 3.5. Example of a Voronoi diagram.

Each event location is considered a site in a Voronoi diagram, and the tessellation is calculated accordingly. Since in real-life testing, the preceding information concerning the AE sources' probability density function is unavailable, a uniform distribution is assumed to be present. Therefore, the possible leak position can be indicated by the area with the most densely positioned event locations. Since the density of sites is inversely proportional to the regions' area [27], the density around a detected event location is calculated as follows:

$$D(x) = A_x^{-1} \quad (3.7)$$

here A_x is the area of the region around the event location x that is being considered. By grouping regions that belong to the event locations with the highest density, the possible leak location can be estimated.

3.3 Case Study

3.3.1 Experimental Setup

To verify the proposed method, a Hsu-Nielsen test [31] was employed on a cylinder tank under a one-failed-sensor scenario to imitate a leaking situation. The Hsu-Nielsen test is a test in which a pencil lead of 0.5 mm diameter is broken at a 30° angle against a surface for an AE event generation. The discontinuity upon a lead-breaking occurrence generates an elastic wave that travels along the bottom surface and can be captured by the sensors. For this reason, it is a popular method for an AE event source imitation in multiple experimental

setups for different types of machinery or structural failures. In addition, the one-failed-sensor scenario provides a more challenging problem than a conventional setup, in which one of the evenly positioned sensors is considered to be malfunctioning. By doing this, any event that happens in this impaired sensor's neighborhood, which is supposed to be in the coverage of the failed one, would have to be processed from further channels, thus introducing more attenuation and distortion to the available data. A total of six R6I-AST sensors were attached to the surface of the vertical cylinder tank at a height of 300 mm, and the recordings were taken at a sampling rate of 1 MHz. These sensors from MINTRAS offer high sensitivity, and long-driving cable capability with a built-in 40 dB preamplifier and a filter. Moreover, being enclosed in a metal stainless steel housing can provide resistance to electromagnetic/radio frequency interferences and heat stabilization from -35 to 75 Celsius degrees. The "AST" part in the name shows that this genre also supports the integrated Auto Sensor Test, which allows sensor coupling and performance verification even in service.

In this test, the Hsu-Nielsen test was taken multiple times in quick succession at pre-determined locations (1-8 and center). Due to the test specimen being in an outdoor setup, other intentional and unintentional AE activities were also randomly introduced during the test. Detailed information concerning the testbed, sensors, and location of the Hsu-Nielsen test is illustrated in Figure 3.6.

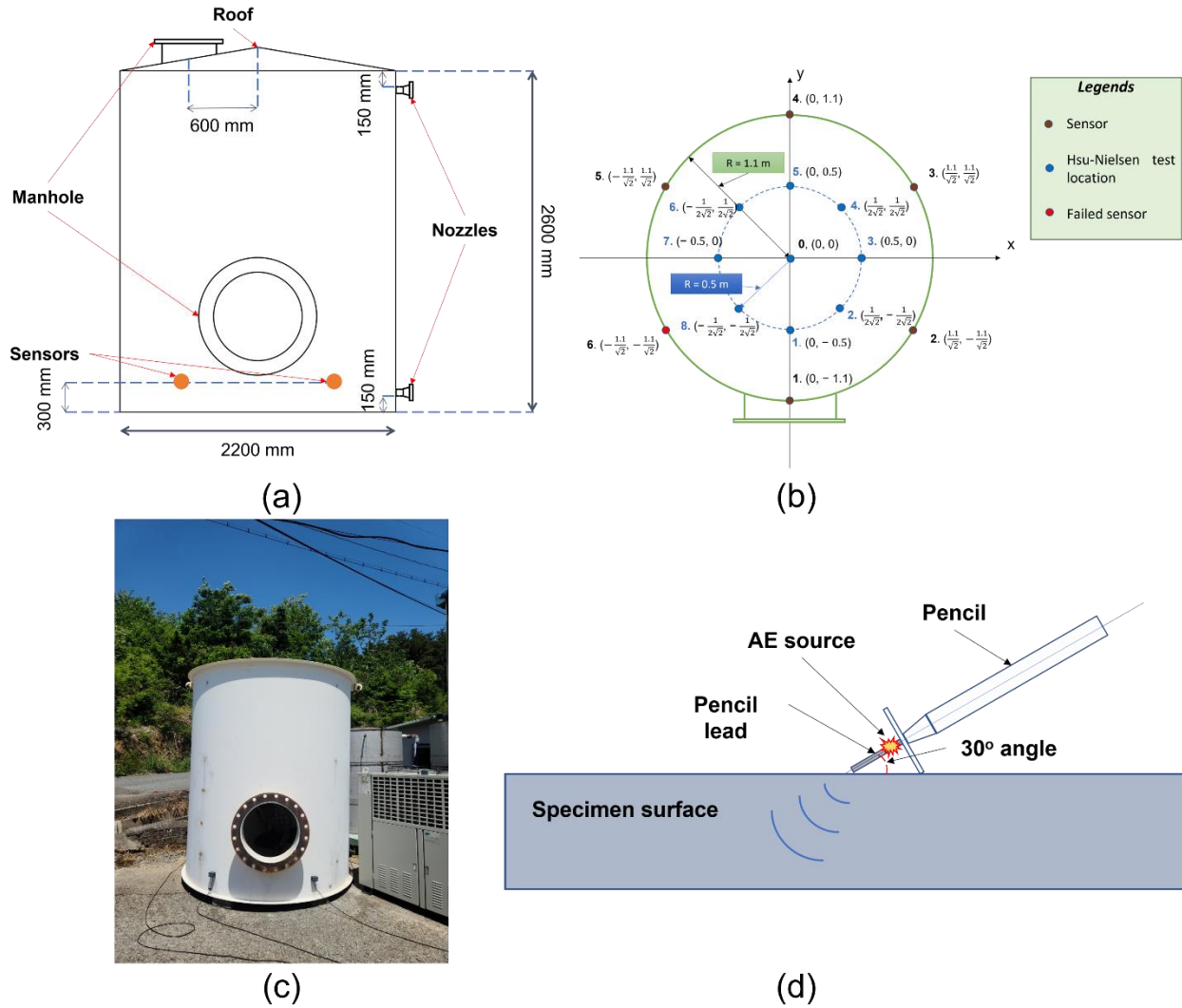


Figure 3.6. The cylinder tank under test: (a) vertical dissection schematic and vertical sensor displacement (b) horizontal dissection schematic, sensors, and Hsu-Nielsen test location (c) pictorial depiction of the test setup (d) Hsu-Nielsen test visualization.

Table 3.1. Specifications of the cylinder tank.

Parameters/Parts	Details
Dimension (without roof)	2.2 × 2.6 m (diameter × height)
Tank capacity	9.85 M ³
Tank empty weight	2.1 tons
Tank operating weight	11.95 tons
Shell/roof/bottom material	SA516-70N carbon steel
Flange material	SA105N carbon steel
Nozzle neck material	SA106-B carbon steel
Earthquake design	Yes

3.3.2 Result and Discussion

An example of the hit detection process and result are shown in Figure 3.7. As previously discussed, a hit is detected when the CUT exceeds the threshold calculated from the neighboring cells. However, this only implies that the CUT contains a hit; it does not show the arrival and end times. A fixed threshold of 10% of the peak value, which is calculated in the current CUT, is chosen to mark these important timestamps of the hit. Since there are a large number of hits, Figure 3.8 shows only the example of a CUT region along with the TOA and end time determination from the respective CUT region. It can be seen that the threshold is capable of detecting the hit's TOA quite similar to how it would be picked manually.

After the hit detection and TOA determination, the results were then processed for event grouping based on event definition and hit similarity. Subsequently, a TDOA is applied to find the location of the events. As discussed above, the locations of events alone do not sufficiently pinpoint the leak's location. Therefore, data density analysis with a Voronoi diagram is employed in the final stage to localize the area with the highest possibility of leak existence. Figure 3.9 shows the real Hsu-Nielsen test's positions previously depicted in Figure 6b: the detected locations of events, and the filtered contours indicating the possible leak region, which are obtained by using the proposed method.

In Figure 3.9, the likeliness of a leak existence in a region is shown by the color of the contour, with the warmer ones indicating a higher probability and the cooler ones indicating a lower possibility. As can be seen, the proposed method provides a very close estimation of the Hsu-Nielsen tests' location across multiple points, even for the ones in the neighborhood of the failed sensor (1, 6, 7, 8). It can also be witnessed that two out of the three real test locations residing outside of the outermost contour are locations 7 and 8 (close to the failed sensor), and even in such cases, the displacement values are insignificant. Some of the abrupt rises in error and large area of possible leak region are due to the introduction of interfering AE activities from the environment and performing Hsu-Nielsen tests.

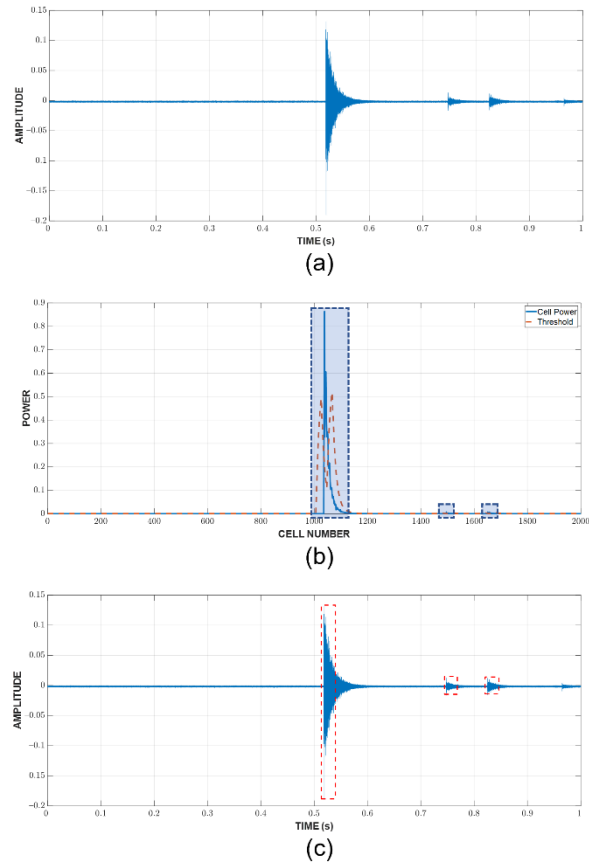


Figure 3.7.Hit detection process for a random one-second window: (a) raw AE data (b) cell power versus threshold (c) detected hits.

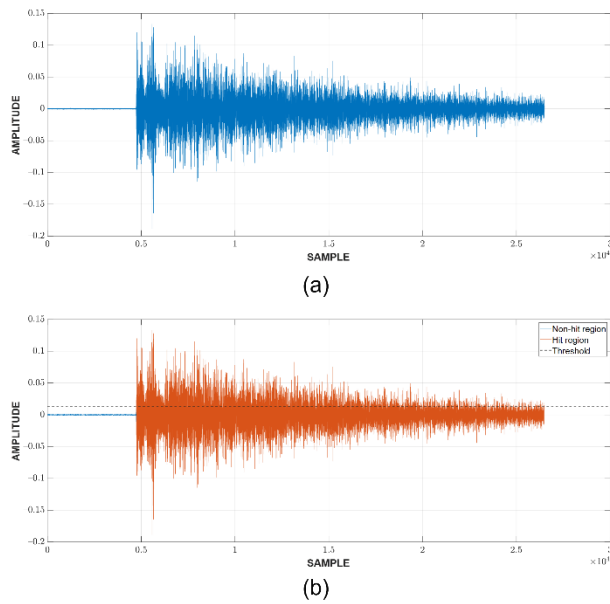


Figure 3.8. TOA and end time determination: (a) CUT containing a hit (b) Detected hit.

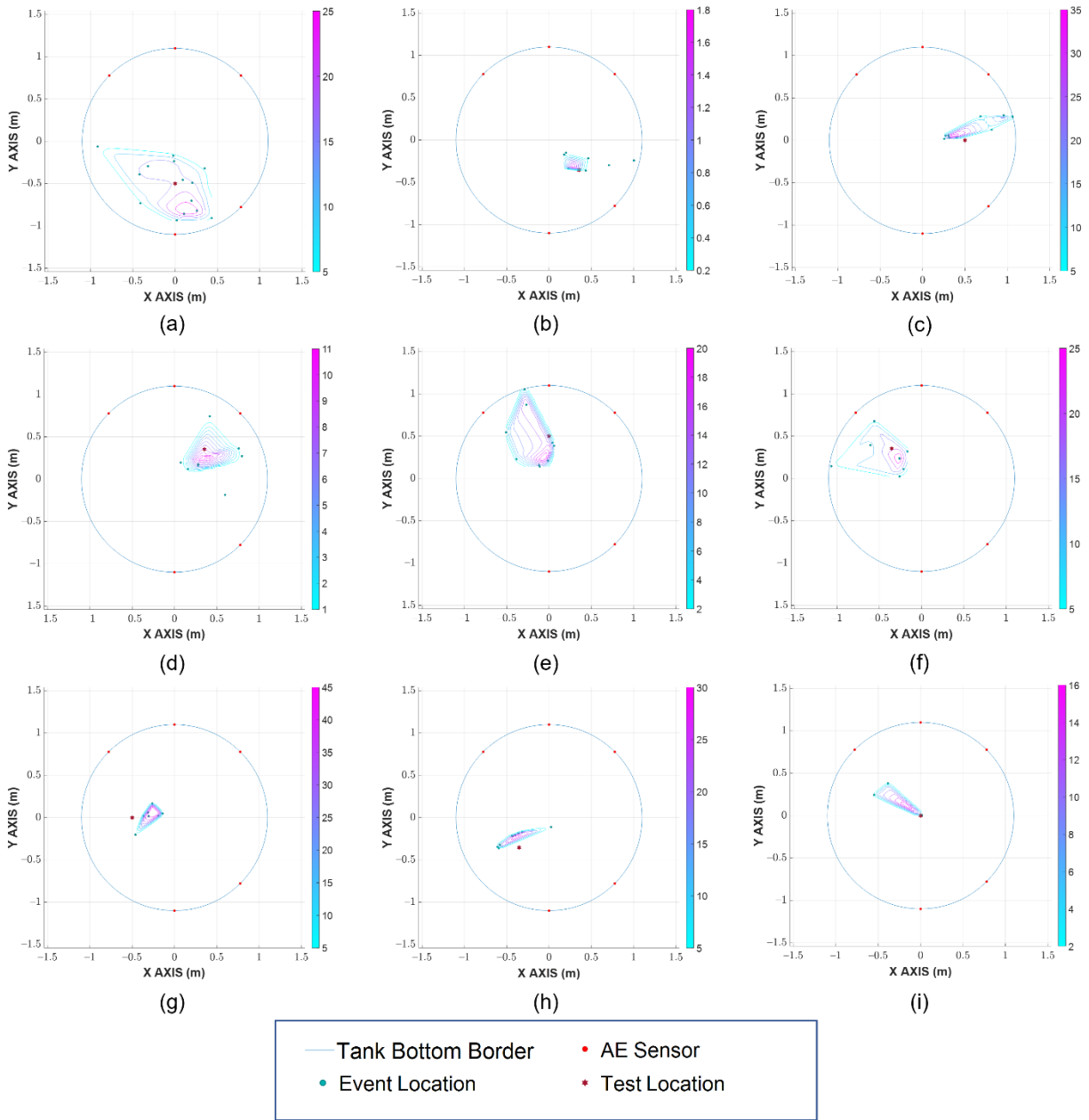


Figure 3.9. Source localization results in different Hsu-Nielsen test locations: (a) 1 (b) 2 (c) 3 (d) 4 (e) 5 (f) 6 (g) 7 (h) 8 (i) Center.

For deeper performance analysis, a comparison was executed between the proposed method and a conventional grid search scheme, which is also a popular approach for industrial applications. The localization scheme using a grid search calculates each grid's residual between the estimated and measured distances to the sensors, then returns the location where this value is minimal. To verify the localization accuracy of the proposed method, the displacement is calculated between the test location and: (1) the innermost region (the one covered by the innermost contour with the warmest color, which has the highest probability

of leak existence); (2) the outermost region (the entire one covered by the outermost contour with the coolest color, which has a smaller probability of leak existence; if the test location is within this region, then displacement is equal to zero). The results presented in Table 3.2 show that the proposed method outperforms the conventional grid search localization scheme by a noticeable margin.

Table 3.2. Displacement between the test locations and the results.

Test Location	Conventional Grid Search Localization	The Proposed Method	
		Estimated Displacement to Innermost Region (m)	Estimated Displacement to the Outermost Region (m)
1	0.31	0.24	0
2	0.18	0.11	0
3	0.27	0.17	0.03
4	0.21	0.15	0
5	0.26	0.22	0
6	0.13	0.09	0
7	0.19	0.19	0.12
8	0.22	0.14	0.07
Center	0	0.12	0
	Mean \approx 0.20/Std \approx 0.09	Mean \approx 0.16/Std \approx 0.05	Mean \approx 0.02/Std \approx 0.04

3.4 Conclusion

In this paper, the authors presented a leak localization scheme for a cylinder tank bottom with acoustic emission (AE) data. By performing this scheme, leak location can be estimated early, thus allowing the appropriate response to be taken to prevent possible injuries, fatalities, and environmental hazards, and minimize the financial damage. The AE data is initially processed with a constant false alarm rate (CFAR) for hit detection, which is then used to find the hits' time of arrival (TOA) and end time using the fixed thresholding method. Following this step hits originating from the same AE source are grouped by applying the event definition and the proposed similarity score. From the obtained results, the sources of AE events were estimated using the time difference of arrival (TDOA). Since AE events can happen in other locations than just the leaking position (due to turbulent flow, etc.), they should be investigated more to derive the estimated leak position. This was analyzed through data density analysis using a Voronoi diagram to obtain the final result.

The proposed scheme was validated in a one-failed-sensor scenario on the cylinder tank bottom with Hsu-Nielsen testing. A total of six sensors were mounted on the tank's surface, one of which was considered to be malfunctioning. Multiple AE sources were generated on the tank bottom in quick succession at nine different locations, along with random interferences. The obtained result using the proposed method showed a highly precise localization. The localization accuracy is evaluated through the displacement between the

real source position and: (1) the innermost region (covered by the innermost contour); and (2) the outermost region (the entire one covered by the outermost contour). The first type of displacement returns an average of 0.16 m along with a standard deviation of 0.05 m, and the second returns an average of 0.02 m along with a standard deviation of 0.04 m, which significantly outperforms the conventional grid search localization scheme in a comparison. For future work, the accuracy can be further enhanced by introducing more complicated TOA estimation methods and event localization approaches.

Chapter 4

Leak State Detection and Size Identification for Fluid Pipelines with a Novel Acoustic Emission Intensity Index and Random Forest

In this chapter, an approach to perform leak state detection and size identification for industrial fluid pipelines with an acoustic emission (AE) activity intensity index curve (AIIC), using b-value and a random forest (RF), is proposed. Initially, the b-value was calculated from pre-processed AE data, which was then utilized to construct AIICs. The AIIC presents a robust description of AE intensity, especially for detecting the leaking state, even with the complication of the multi-source problem of AE events (AEEs), in which there are other sources, rather than just leaking, contributing to the AE activity. In addition, it shows the capability to not just discriminate between normal and leaking states, but also to distinguish different leak sizes. To calculate the probability of a state change from normal condition to leakage, a changepoint detection method, using a Bayesian ensemble, was utilized. After the leak is detected, size identification is performed by feeding the AIIC to the RF. The experimental results were compared with two cutting-edge methods under different scenarios with various pressure levels and leak sizes, and the proposed method outperformed both the earlier algorithms in terms of accuracy.

4.1 Introduction

Pipelines play a vital role in industrial settings as one of the major fluid transportation methods. While they can generally provide safe and efficient passage even in long-distance

systems, pipelines are not immune to leaking and breaking due to the influence of natural disasters, component corrosion, installation errors, etc. An unattended leak can evolve into a major pipeline burst, which can not only sever the entire transportation system, but potentially lead to human injuries/fatalities, environmental hazards, and huge economic costs for recovery. Due to the dire consequences of pipeline leaks, the faults must be detected and diagnosed in earlier stages, so that maintenance can be performed accordingly.

Currently, non-destructive testing (NDT) has emerged as one of the most popular research topics within the prognosis and health management framework for civil and industrial assets [30], [31], [32]. In addition to its obvious contribution to safety and incident prevention, the other reason behind NDT's relevance is that it allows inspection and evaluation without affecting specimen serviceability, as its name suggests. Regarding NDT in pipeline systems, multiple techniques have been proposed such as ultrasonic testing (UT) [33], [34], [35], radiography testing (RT) [36], [37], ground-penetrating radar (GPR) [38], infrared thermography testing (IFT) [39], distributed acoustic sensing [40], active distributed temperature sensing [41], acoustic emission (AE) [1], [2], [9], [42], [43], [44], etc. Each of these techniques presents various advantages and disadvantages which can best serve different applications. In terms of AE, it studies the elastic waves released upon a discontinuity occurrence. AE offers many upsides, such as non-directionality, no downtime for in-service testing, new damage detection, and outstanding progression monitoring, in which the deterioration process can be captured with only one test. During the monitoring process, AE is sensitive to new damage sustained by the specimen, and to the irregularities of the specimen's working activity due to these damages. Since the foremost purpose of this study is pipeline monitoring, it can benefit from the aforementioned advantages. Thus, AE was the NDT method chosen for application in this work.

4.1.1 Related Works

Many studies have been conducted that have used AE for pipeline system diagnosis [45], [46], [47], [48], [49], [50], [51], [52], [53], [54], [55], [56], [57], [58], [59]. When a leak occurs in a pipeline system, variations are expected in the AE data. The leak detection process using AE is centered around the differences between the variations that happen in the leak state and the normal state, which have been mostly approached from the view of feature extraction and pattern recognition in recent studies [46], [47], [51], [52], [53], [54], [55], [56], [57], [58], [59], [60], [61], [62], [63], [64], [65]. The studies in this area can be roughly categorized as follows: time domain [51], [52], [60], [61], frequency domain [62], [66] and time-frequency domain [53], [58], [63], [64], [65].

Time domain approaches are often the most straightforward out of the three domains; however, they usually require an additional pre-processing step to minimize their susceptibility to interferences. Nosedá et al. [51] proposed an approach to transition time

estimation, in combination with the power of a neural network, to devise a propagation classification. AE features, such as AE counts, cumulative AE energy, etc. were investigated and utilized, along with support vector machine (SVM) and relevance vector machine (RVM) in [52], for the identification and localization of a pipeline leak. The authors in [60] presented a solution, using artificial neural networks (ANN) with amplitude data from time domain AEs. As for the study in [61], the authors investigated the leak detection problem by using statistical time domain features, which were selected by principal component analysis and then fed to a support vector data description model for working state classification.

Frequency-domain approaches can be more robust than time-domain ones, however, they are more complicated and often require more expertise regarding system- or fault-specific frequencies. Through the analysis of leak-related frequencies' amplitude, the authors in [66] proposed a solution to leak detection and leak size identification. In addition, the study in [62] presented an approach to leak detection by harnessing AE spectral portraits to obtain encoded spectral envelope features. Because frequency domain analysis is more favorable towards stationary signals, difficulties might arise due to gas/fluid pipeline AE signals being non-stationary [57], [67].

Out of the three domains, time-frequency approaches can provide the most powerful solutions, at the cost of huge computational complexity. The most notable methods in this domain are wavelet transform [58], [63], empirical mode decomposition [53], and variational mode decomposition [65], etc. The features, once extracted by using the previously mentioned methods, are then harnessed by different artificial intelligence techniques for state diagnosis, such as neural network [68], SVM [52], [63], [64], or adversarial network [54], etc.

As briefly explained in the previous subsection, AE is based on the release of elastic waves upon the occurrence of discontinuity. Such an occurrence that releases elastic waves is called an AE event (AEE) and when an AEE is detected by a sensor, these data can be referred to as an AE hit (AEH). Generally, AEHs can be categorized into two types: burst-type and continuous-type [1]. While the continuous-type is considered noise and contains minimal useful information, the burst-type AEH possesses valuable data that can be used for the determination of the specimen state. Because of the nature of fluid transportation in pipeline systems, AE events can be recorded from various sources even under normal working conditions that can involve unstable flow, pressure on joints, pipeline vibration, leaks, and interferences from the environment, etc. The diversity of sources in pipeline systems and their occurrences in a short period introduces a more complex problem (referred to as the multi-source problem of AEEs) in comparison to rigid specimens such as concrete structures, machinery, etc. in which, the signal is significantly more transient and there are fewer sources of AEEs (primarily due to discontinuity-related reasons, such as crack, loose fittings,

etc.). Even though AEH features can offer a great description of the AE activity, it is difficult to correctly obtain the data related to these features due to the high AE noise level and the sophisticated AEH detection process. As an alternative, this paper presents AE activity intensity construction using b-value for pipeline systems. b-value was first introduced in the Gutenberg–Richter law (GRL) [69]. In brief, it expresses the relationship between the number of earthquakes and their magnitude in a given period and location. Since an AEE can be considered a low-energy seismic event [70], the b-value was also adopted for AE applications on concrete structures [71], [72], [73]. As the adopted b-value describes the number of AE peaks - AE amplitude correlation, along with the amplitude being related to discontinuity size [74], [75], it is anticipated to provide an accurate description of the AE activity intensity. Based on this intensity index, the pipeline's working condition can be detected and if a leak is present, the size can be identified. A more detailed walkthrough of the proposed method is presented in the next subsection.

4.1.2 Overview of the Proposed Method and Contributions

The proposed method's simplified flowchart is presented in Figure 4.1. The raw AE data were recorded from the testbed using three AE sensors. Following the collection of raw AE data, a pre-processing step was conducted with a bandpass filter to keep only the desired frequency range. Then, the filtered data were utilized to extract the b-value and construct the AE activity intensity index curves (AIICs). Afterward, the AIICs were harnessed for leak state identification (normal working condition or leakage) using a Bayesian ensemble estimator for changepoint detection, which calculated the probability of the occurrence of a changing event. Once the leakage was confirmed, the AIIC parts that corresponded to the leaking state with multiple leak sizes and pressure levels were separated and fed to a random forest (RF) model for leak size classification training/testing. The proposed method demonstrated high accuracy under various conditions, even in comparison to cutting-edge references.

The summary of this work's contributions is as follows:

1. The AIIC was constructed using the b-value, which provides a robust and descriptive representation of the industrial pipeline's working conditions, addressing the multi-source problem of AEE in pipeline systems.
2. Pipeline leak state detection was implemented using the proposed AIIC, along with changepoint detection using a Bayesian ensemble estimator, and size identification using RF.
3. The validation was performed using AE for industrial fluid pipelines under various leak sizes and pressure levels.

The organization of this paper is as follows:

1. Section 4.1 (Introduction) presents the motivation for and background of this study, along with related works, an overview of the proposed method, and the contributions.
2. Section 4.2 (Basic Concepts) presents the background for the algorithms utilized in this study, including the b-value, changepoint detection using a Bayesian ensemble estimator, and RF.
3. Section 4.3 (Case Study) provides a detailed explanation of the proposed method and its validation, along with a description of the experimental setup and dataset.
4. Section 4.4 (Conclusion) concludes the research and discusses future work.

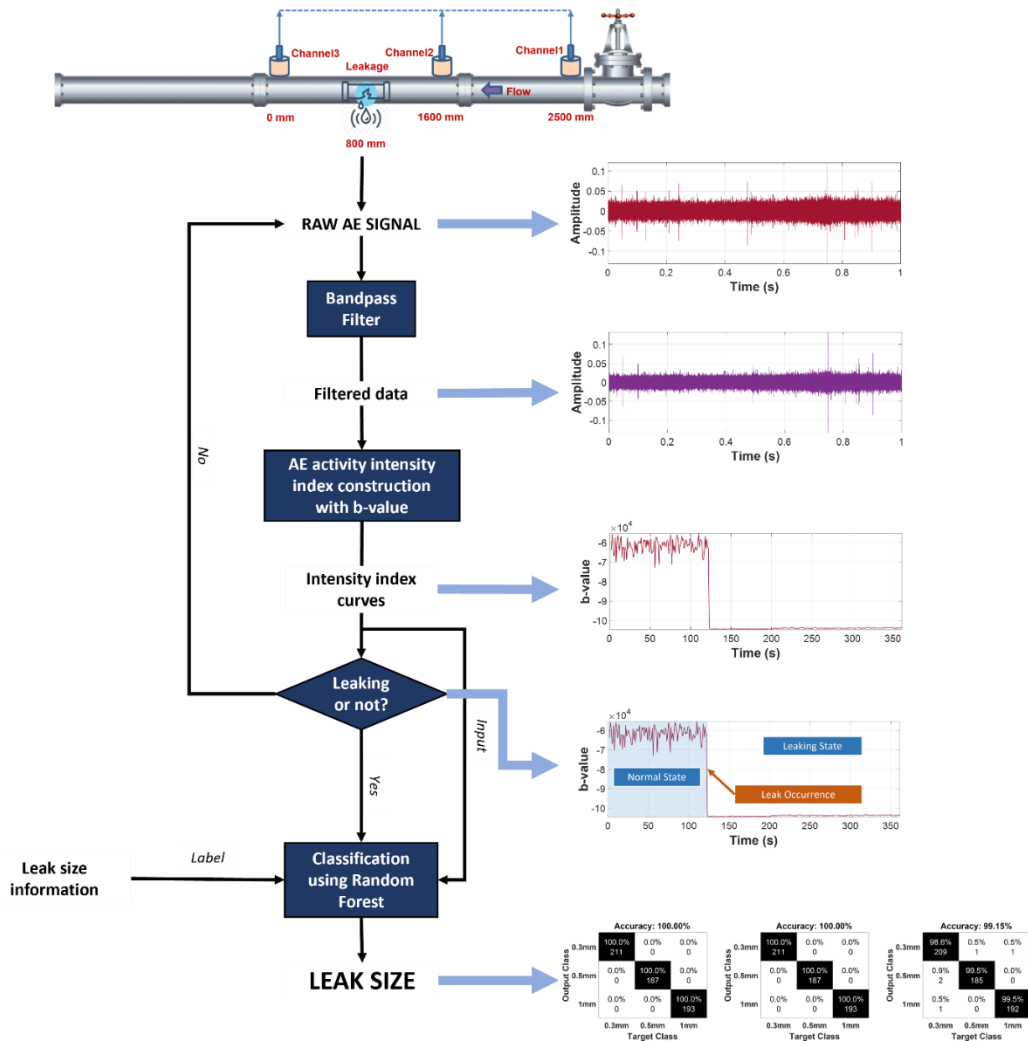


Figure 4.1. Flowchart of the proposed method.

4.2 Basic Concepts

4.2.1 The b-value

The GRL b-value is one of the most important parameters for the probabilistic investigation of seismic hazards. It is the slope of a log-normal distribution of the size of seismic events or

the relationship between the event magnitude and the frequency of occurrence. In a particular region within a specific period, the GRL can be defined as follows:

$$\log_{10} N = a - bM, \quad (4.1)$$

in which a is an empirical constant, b is the b-value, and N is the number of seismic events with a magnitude higher than M . Due to AE being a high-frequency but low-energy seismic activity, the GRL is adaptable to AE analysis with a few modifications, as follows:

$$\log_{10} N(A) = a - b \frac{A}{20} \quad (4.2)$$

with a being an empirical constant (which is set at zero in this study), b being the b-value, and $N(A)$ being the number of AE hits with an amplitude equal to or larger than the amplitude threshold A (dB). A higher b-value indicates that the number of AE peaks with a low amplitude is large, along with the low level of AE activity. These AE activities mostly come from pipeline vibration, unstable flow, or AE noise, etc., from which little useful information can be presumably obtained. In contrast, a lower b-value indicates the presence of multiple AE peaks with high amplitude and a more intense level of AE activity, which can be witnessed in the visualization of the relationship between event magnitude and frequency of occurrence provided in Figure 4.2. In theory, this can be associated with a discontinuity in the fluid pipeline, given that the AE peak amplitude is related to the size of the discontinuity and that the AEEs occurring due to a leak are releasing more energy than those under normal condition [75]. Thus, it is expected that, upon initialization of a leak, a significant decrease in b-value will be recorded and b-value can help discern the difference between leak sizes.

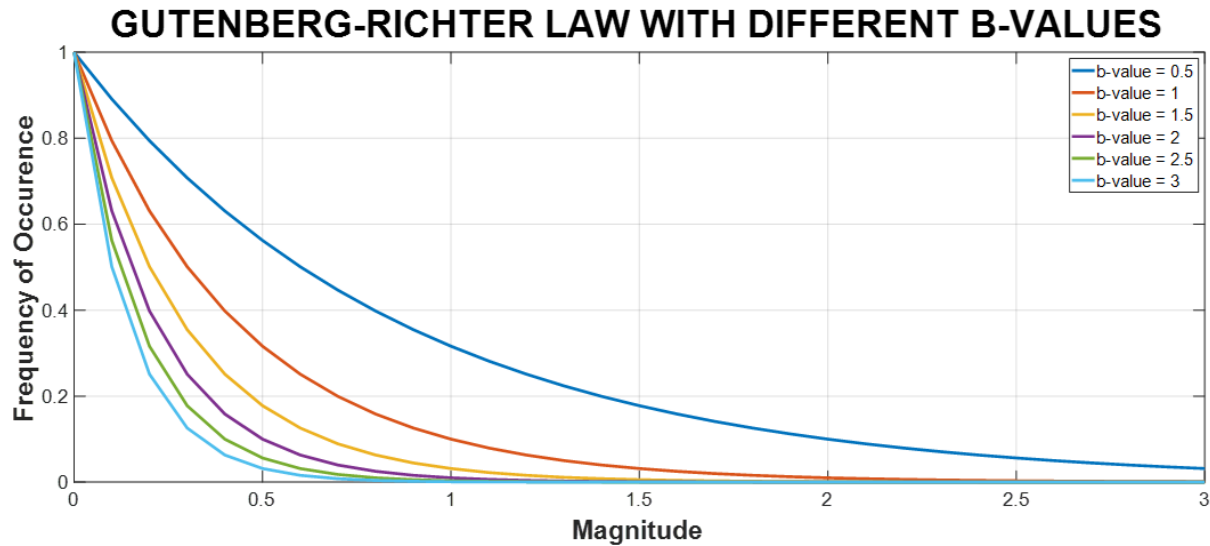


Figure 4.2. Visualization of magnitude versus occurrence of different b-values based on GRL.

The amplitude threshold governs the amount of information the b-value can convey. Given a high threshold with only a minimal number of higher AE peaks or a threshold lower than the majority of AE peaks, the b-value would not be able to capture the change in AE peak amplitude distribution over time. Therefore, it is of paramount importance to obtain a suitable value for the threshold. Variations in the AIICs, which are constructed from the b-value, can be expected in normal conditions due to multiple sources of AEEs and the hard threshold nature of the b-value.

4.2.2 Changepoint Detection.

Trend analysis and changepoint detection can be considered complementary approaches that both target changes in data. Trend analysis detects abrupt changes and nonlinear dynamics in time-series data [76], [77], [78] and has been a dominant research topic, particularly in for geoen지니어ing. One of the most formidable challenges for time-series analysis is the inconsistency in different model findings regarding the same problem during the decomposition of time series. This encouraged the idea of combining multiple models in statistical literature, which can be traced back to Roberts's proposal of a distribution of two models combined (1965). Later, a scheme was designed to evaluate the likelihood of each model in a collection being the best and then use that to average them into a single model, which was later known as Bayesian model averaging (BMA) [79]. In this study, the Bayesian Estimator of Abrupt change, Seasonal change, and Trend (BEAST) by Zhao et al. [77], which was originally developed to handle environmental time-series data, was implemented for leak detection. The idea of this method is to exploit the relative value of decomposition models as individuals by averaging them using BMA. Given a time series $\{t_i, y_i\}_{i=1, \dots, N}$, BEAST decomposes it into different components containing seasonality, trend, and changepoints, along with noise, as follows:

$$y = S(t_i; \theta_S) + T(t_i; \theta_T) + \varepsilon_i, \quad (4.3)$$

in which $S(\cdot)$ and $T(\cdot)$ are seasonal and trend signals, respectively; ε is noise with a Gaussian distribution; and θ_S and θ_T have changepoints (a major changepoint is also referred to as a true abrupt change) implicitly encoded within them. General linear models were applied for $S(\cdot)$ and $T(\cdot)$ parameterization, with $S(\cdot)$ being a piecewise harmonic model and $T(\cdot)$ being a piecewise linear function.

As the pipeline working state changes from normal to leaking, not only will AEEs arise from the discontinuity occurrence on the pipeline surface itself, but flow turbulences are also expected. This further increases the number of high-amplitude AE activities and as such, changes the distribution of the frequency and the amplitude. With the shift of AE activity towards the region with a higher amplitude, a decrease in the b-value should be seen. Since the AIIC can show fluctuations in the pipeline's normal working state as previously mentioned, any sudden drop in value might be misdiagnosed as a changepoint, which would mean a leak initialization transitioning the pipeline from normal conditions into the leaking state. In addition, the underlying processes that change the distribution in fluid pipeline AE signals are nonlinear, rather than being purely linear or piecewise linear. For these reasons, BEAST can perform better than those constructed from either of the previously mentioned views.

4.2.3 Random Forest.

Despite providing good interpretability at a small depth, decision trees (DTs) are susceptible to the overfitting problem and high variance as they get deeper. This hinders DTs from giving good performance with real-world problems, which often go along with huge datasets. Eventually, this shortcoming led to the birth of RF, which was first proposed by Breiman in 2001 [80] inspired by the work of Amit and Geman [81]. The idea of RF is simple: it exploits a DT efficiency with a smaller dataset by training each separately with a bootstrapped dataset and then aggregates these DTs together for a conclusion [82], [83]. The simplified classification process using RF is displayed in Figure 4.3.

Given a real-valued input vector $X = (X_1, \dots, X_p)^T$ and a real-valued response $Y = f(X)$, the goal is to find the prediction function $f(X)$, which is determined by a loss function $L(Y, f(X))$. For classification problems, zero-one loss is often used for L :

$$L(Y, f(X)) = \begin{cases} 1 & \text{if } Y \neq f(X) \\ 0 & \text{otherwise} \end{cases}, \quad (4.4)$$

Then, the problem becomes finding the expected value of the loss $E_{XY}(L(Y, f(X)))$ minimization. Given \bar{Y} as the set contains possible Y values, the minimization problem gives:

$$f(x) = \arg \max P(Y = y | X = x), \quad (4.5)$$

with $y \in \bar{Y}$. This is also known as the Bayes rule. Each of the DTs returns a base learner $(h_1(x), \dots, h_N(x))$ and by majority vote, the ensemble predictor $f(x)$ can be predicted as:

$$f(x) = \arg \max \sum_{i=1}^N I(y = h_i(x)), \quad (4.6)$$

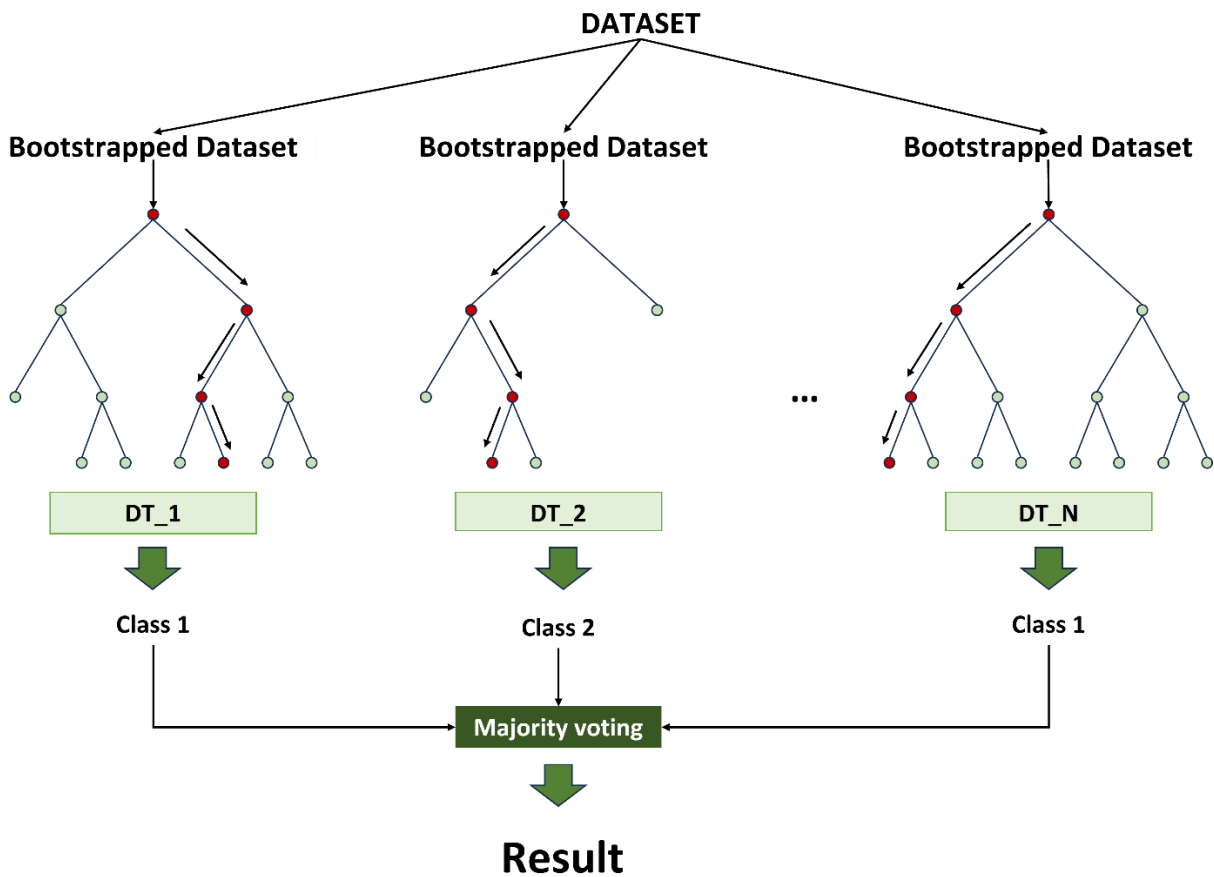


Figure 4.3. A simplified visualization of the classification process in RF.

4.3 Case Study

4.3.1 The Proposed Method

For the overview of the proposed method, the summary can be revisited in Section 4.1.2 and Figure 4.1. The process starts with the preprocessing of raw AE data, collected from the pipeline system. A bandpass filter from 10^5 to 3.5×10^5 Hz was designated for this purpose. This process is necessary to minimize the unwanted frequency bands and to keep only the frequencies in which beneficial leak-related information can be extracted.

Once the filtered data were obtained, b-values were calculated next, using Equation 4.2. For monitoring, this computation cyclically occurs over one second, to construct the AIIC. As previously discussed, choosing the amplitude threshold for b-value calculation is very important. Analysis of the frequency–amplitude distribution (FAD) was conducted to find a suitable value. A visualization of the FAD is demonstrated in Figures 4.4-4.6, for the normal state transitioning into the leaking state under the different pressure levels of 7 bar, 13 bar, and 18 bar, respectively. In each of these scenarios, the pipeline worked under normal condition at the beginning until the 120th cycle, the point at which the leak started, and the pipeline then started working under the leaking condition. More details about the experimental setup with different scenarios are listed in Section 4.3.2. As can be seen across the pressure levels, the FADs were similar under normal working condition, with the majority of AE activity happening in a low-amplitude regime, and only a rather small portion coming from AEEs with a higher amplitude (whose presence is understandable, given that there are sources of AEEs other than leaks). However, when a leak happened, the FAD shifted towards a higher amplitude region, which can be easily spotted as the pressure levels and leak sizes increased. During this period, a noteworthy rise in the number of high-amplitude AE activities was witnessed, which was no mere coincidence as leak-related AE activities were the largest source of these. The differences in FAD for various leak sizes can also be noticed. For the case of low pressure and a micro leak size such as in Figure 4.4a, the rise is still noticeable from 10^{-2} and above, despite it being not as significant as the rest. The FAD analysis showed that the amplitude threshold value at 10^{-2} can best describe the AE activity under different scenarios.

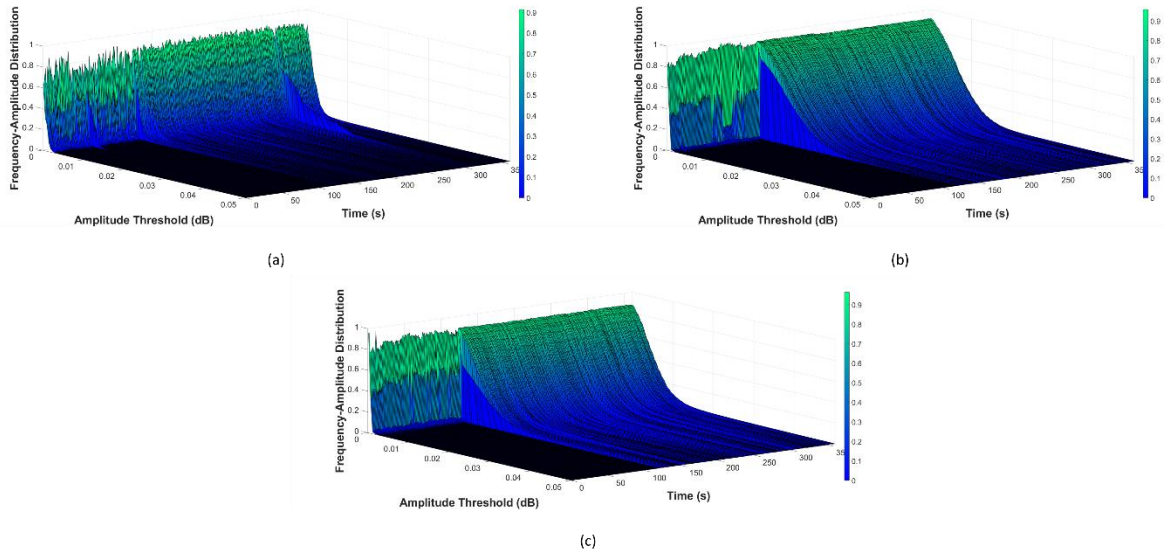


Figure 4.4. Visualization of FAD at pressure level 7 bar with different leak sizes: (a) 0.3 mm, (b) 0.5 mm, and (c) 1 mm.

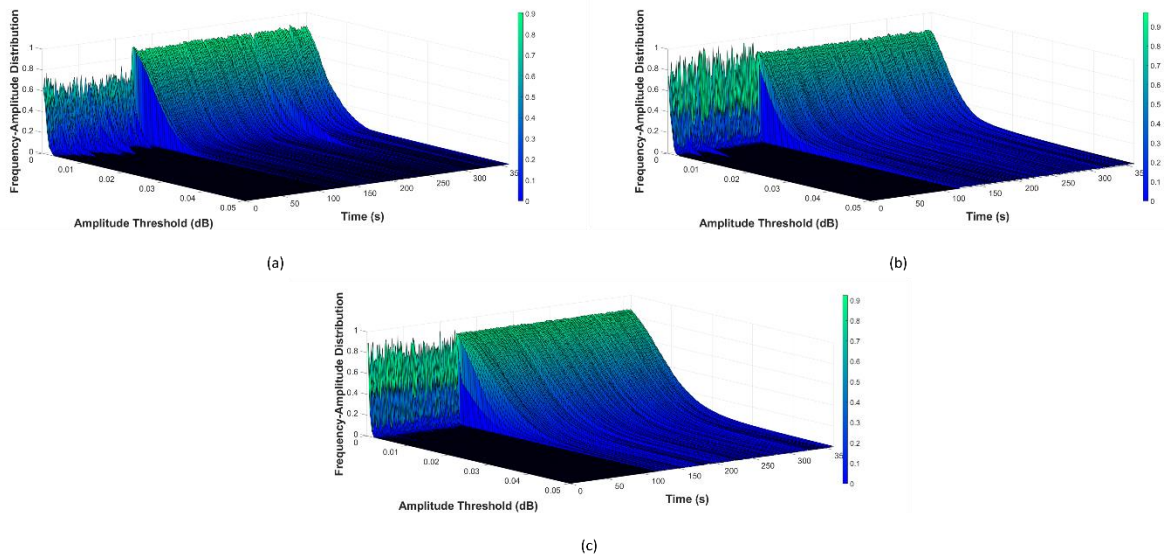


Figure 4.5. Visualization of FAD at pressure level 13 bar with different leak sizes: (a) 0.3 mm, (b) 0.5 mm, and (c) 1 mm.

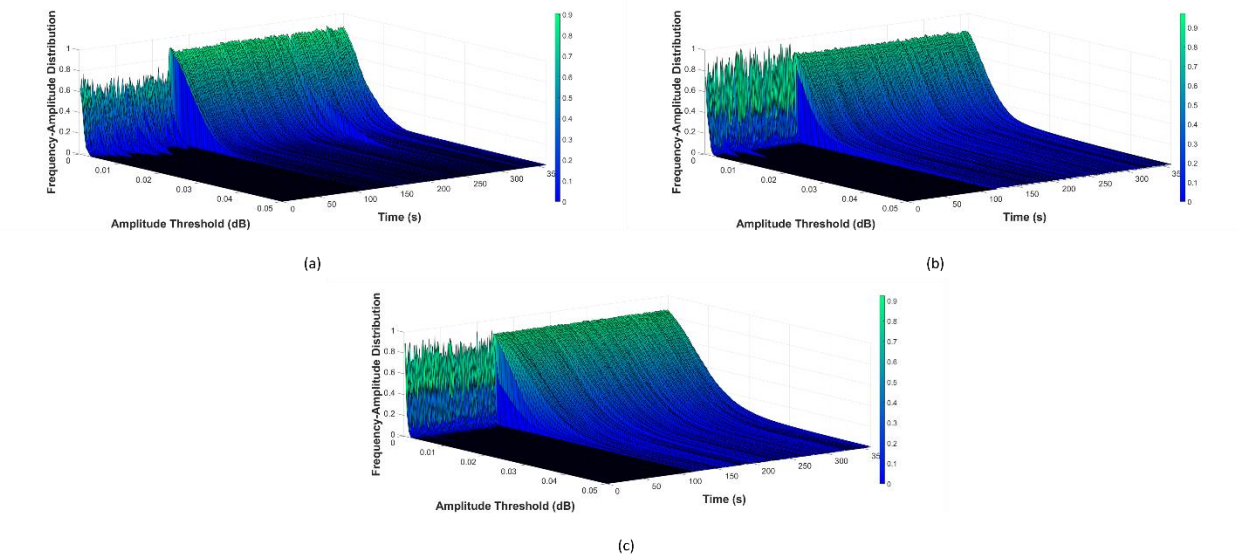


Figure 4.6. Visualization of FAD at pressure level 18 bar with different leak sizes: (a) 0.3 mm, (b) 0.5 mm, and (c) 1 mm.

Following AIIC construction, leakage detection was the next target, for which BEAST was implemented. By analyzing the trend, abrupt changes, and the nonlinear dynamics of the AIIC, it detected the changepoint of the working state (from normal working condition to leakage) by predicting the occurrence probability of a change in the AIIC. The prior probability was obtained following the formulas provided in [77]. A visualization of the detection of leak initialization using BEAST can be found in Figure 4.7.

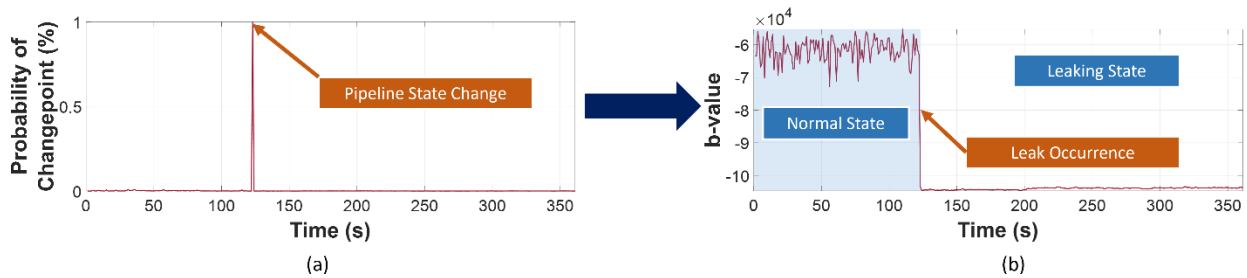


Figure 4.7. Leak detection using BEAST: (a) changepoint occurrence probability; (b) leak detected.

If the pipeline is detected as being in the leaking stage, then the leak size identification process, using RF, begins. The optimal hyperparameters for RF were achieved by using grid search, along with cross-validation, and are displayed in Table 4.1. Finally, a majority voting strategy was utilized to obtain the final size identification result. This can provide a better generalization than a single DT and therefore minimizes the risk of overfitting [84]. A dataset description for training/testing is presented in Section 4.3.2.

Table 4.1. RF hyperparameters.

Hyperparameters	n_estimator	max_depth	min_sample_leaf	min_sample_split	criterion
Value	100	none	1	2	entropy

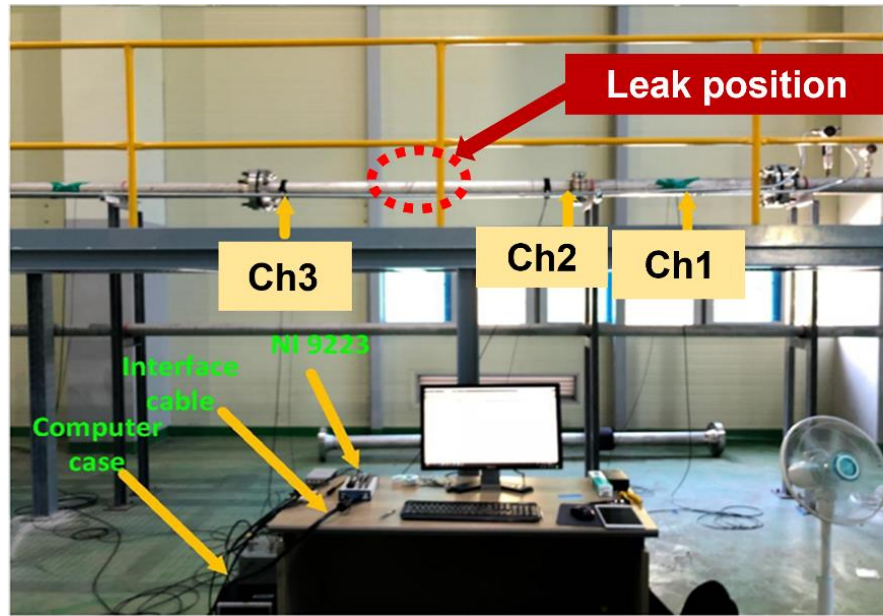
4.3.2 Experimental Setup and Data Description.

To validate the approach presented in this paper, data acquisition was conducted using an industrial fluid pipeline system. Three R15I-AST sensors were deployed during this process. The R15I-AST sensor is a highly sensitive product from MITRAS, specifically designed to provide low-noise input, with a built-in auto sensor test and long-cable driving capability without an additional preamplifier requirement. Due to its metal housing, it is less susceptible to radio frequency and electromagnetic interferences. The three sensors were attached to the surface of the pipeline following the application of a coupling medium gel on the contact spots. To ensure that the sensors would not be displaced or fall from the specimen, tape was utilized. Sensor channels one, two, and three were located at 2500, 1600, and 0 mm (reference position), respectively, along with the leak location at 800 mm. The flow direction was from channel one to channel two, then through the leak position, and finally through channel three. The multiple sensor setup allowed different points of view: channel one offered the view of an upstream flow before the leak; channel two was used for near-leak monitoring, which was expected to have the highest AE activity intensity of all of the channels; channel three offered a view of a downstream flow located after the leak. Though they were recorded from the same test, each of them could be treated as a standalone, which provides more variety to the dataset. An image and schematic of this experimental setup is displayed in Figure 4.8.

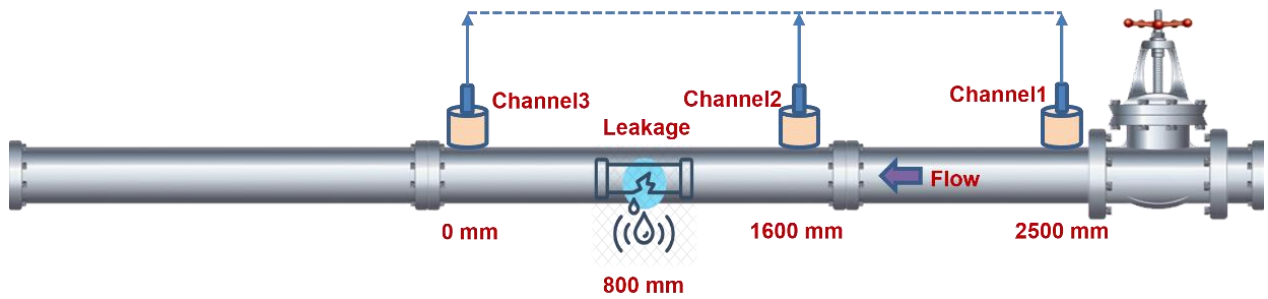
Before the main acquisition, each sensor underwent a sensitivity test and calibration with the Hsu-Nielsen test [85], whose simplified illustration is displayed in Figure 4.9. The Hsu-Nielsen test, also known as the pencil break test, utilizes the breaking of pencil lead, which is positioned on the specimen surface at 30 degrees, to reproduce an AEE. Before AE data acquisition, it is necessary to calculate the attenuation characteristics following the ISO standard 18211:2016, whose computation is as follows:

$$Attenuation_{dB} = 20 \log_{10} \frac{V}{V_{ref}}, \quad (4.7)$$

in which, the attenuation is in decibels (dB); V and V_{ref} refer to the respective measured and reference potentials. It is advised to have an AE sensor surveillance zone within a distance corresponding to 25 dB [1] to avoid severe signal strength loss, which amounts up to 10.9 m for this experimental setup, with R15I-AST sensors and a pipeline system with an outer diameter of 114.3 mm.



(a)



(b)

Figure 4.8. Experimental setup: (a) an image of the testbed and (b) an illustration of the sensor placements and leak position.

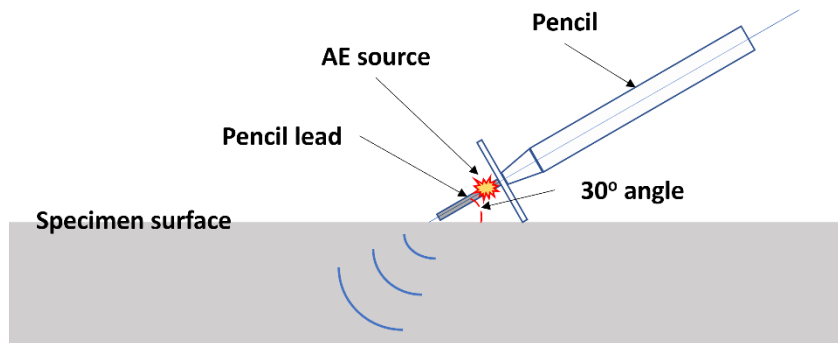


Figure 4.9. A simplified visualization of the Hsu-Nielsen test.

The data collected by AE sensors were first processed by a 16-bit analog-to-digital converter integrated with the National Instruments' NI-9223 module. In combination with software developed specifically for data acquisition by the Ulsan Artificial Intelligence Laboratory, the

whole process was monitored and controlled. A detailed description of the setup can be found in Table 4.2.

Table 4.2. Experimental setup description.

No.	Parameter	Description
1	Pipeline material	304 stainless steels
2	Pipeline thickness	6.02 mm
3	Pipeline outer diameter	114.3 mm
4	Sensor type	R15I-AST
5	Locations of sensors 1, 2, 3	0/1600/2500 mm
6	Leak location	800 mm
7	Total acquisition time	360 s
8	Normal state time/Leaking state time	120 s/240 s
9	Pipeline material	304 stainless steels

A total of nine tests were conducted for this study, including three levels of pressure and three sizes of leak. Each test was initialized under the normal working condition for a period and then switched to the leaking state for the rest of the test with the activation of a simulated leak, whose size and operation status were controlled by a fluid control valve welded on a hole in the pipeline surface. For detailed information, Table 4.3 displays the data descriptions regarding the nine tests conducted for this study. In combination with the three sensors deployed in each test, 27 data streams of the fluid pipeline working under the normal state and then transiting to the leaking state were collected and used for leak detection. After the activation of a leak in the pipeline system, the unstable flow was witnessed for a short time. For this reason, only the parts of data streams from the 126th cycle until the end were utilized for leak size identification. A window size of 10 cycles with a nine-cycle overlap was used to divide the leak-identification dataset into segments, which were then harnessed to train and test RF. For training and testing, the dataset was split with a ratio of 70%/30%. During the training period, the training set was further divided for fivefold cross-validation.

Table 4.3. Data description.

Test Number	Pressure Level	Working Conditions	Acquisition Time (s)	Number of Data Streams
1	7 bar	Normal/0.3 mm leak	120/240	3
2	7 bar	Normal/0.5 mm leak	120/240	3
3	7 bar	Normal/1 mm leak	120/240	3
4	13 bar	Normal/0.3 mm leak	120/240	3
5	13 bar	Normal/0.5 mm leak	120/240	3
6	13 bar	Normal/1 mm leak	120/240	3
7	18 bar	Normal/0.3 mm leak	120/240	3
8	18 bar	Normal/0.5 mm leak	120/240	3
9	18 bar	Normal/1 mm leak	120/240	3

4.3.3 Validation of the Proposed Method.

In this subsection, validation of the proposed method is divided into three different validations: the AIIC constructed from b-value, leak detection using BEAST, and leak size identification using RF.

Firstly, the results of AIIC constructed from the b-value are displayed in Figures 4.10-4.12. The AIIC does not just show a significant gap between normal and leaking conditions, but also the potential to discriminate between different leak sizes. As shown in Figures 4.4-4.6, the FAD for various leak sizes differs, which then translates into the AIIC that was built based on the b-value. In the pipeline's normal working state, fluctuations are witnessed due to the multiple sources with random contributions. However, these variations are witnessed less in the leaking state as the leak becomes the dominant source of all high-amplitude AE activities. With the high-amplitude leak-related AE activities greatly outnumbering other sources, the AIIC becomes less susceptible to the multi-source problem of the AEE. For further validation, a comparison was made between the AIIC and traditional statistical indexes, as shown in Figure 4.13. Among the traditional indexes, mean (Figure 4.13b) and kurtosis (Figure 4.13d) do not distinguish the difference between the two working states; despite root mean Square (RMS, Figure 4.13c), standard deviation (STD, Figure 4.13e), and variance (Figure 4.13f) being able to show a certain level of distinction between normal condition and leakage, wild fluctuations can be witnessed in the later state, in comparison to the AIIC. This type of variation in the indexes, which is minimized using the AIIC, indicates that they are significantly affected by the high noise level, and therefore do not provide a great description of the pipeline's working conditions.

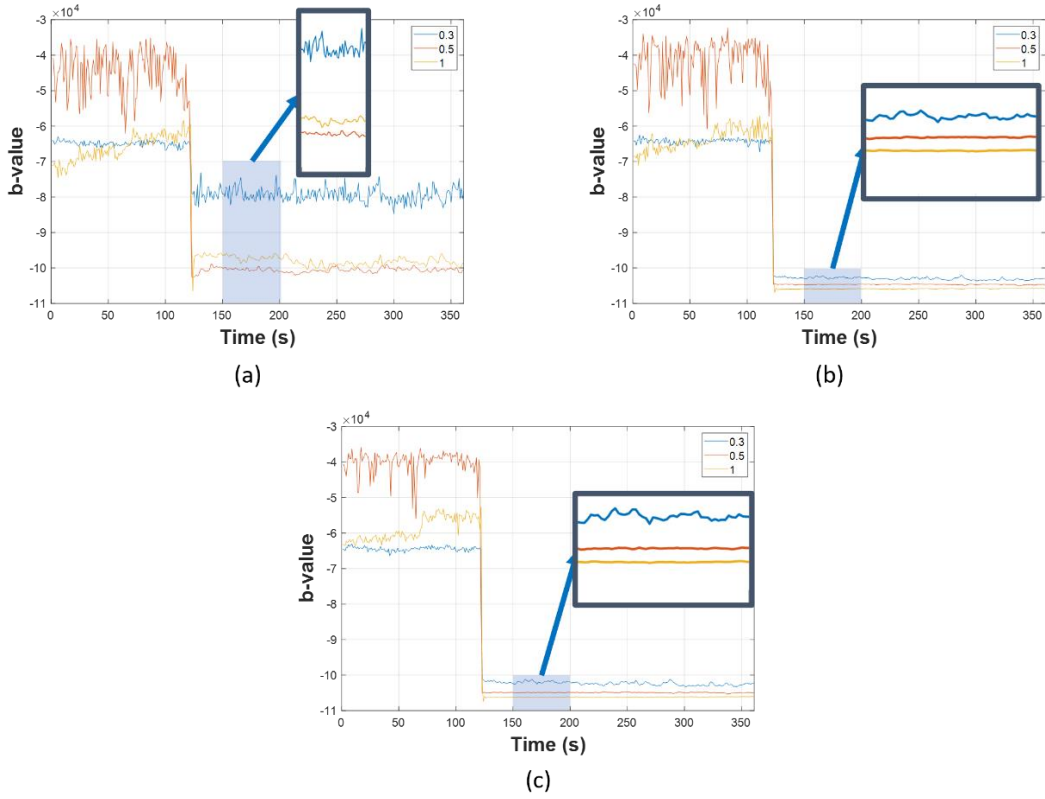


Figure 4.10. AICs for different leak sizes at 7 bar for: (a) channel one, (b) channel two, and (c) channel three.

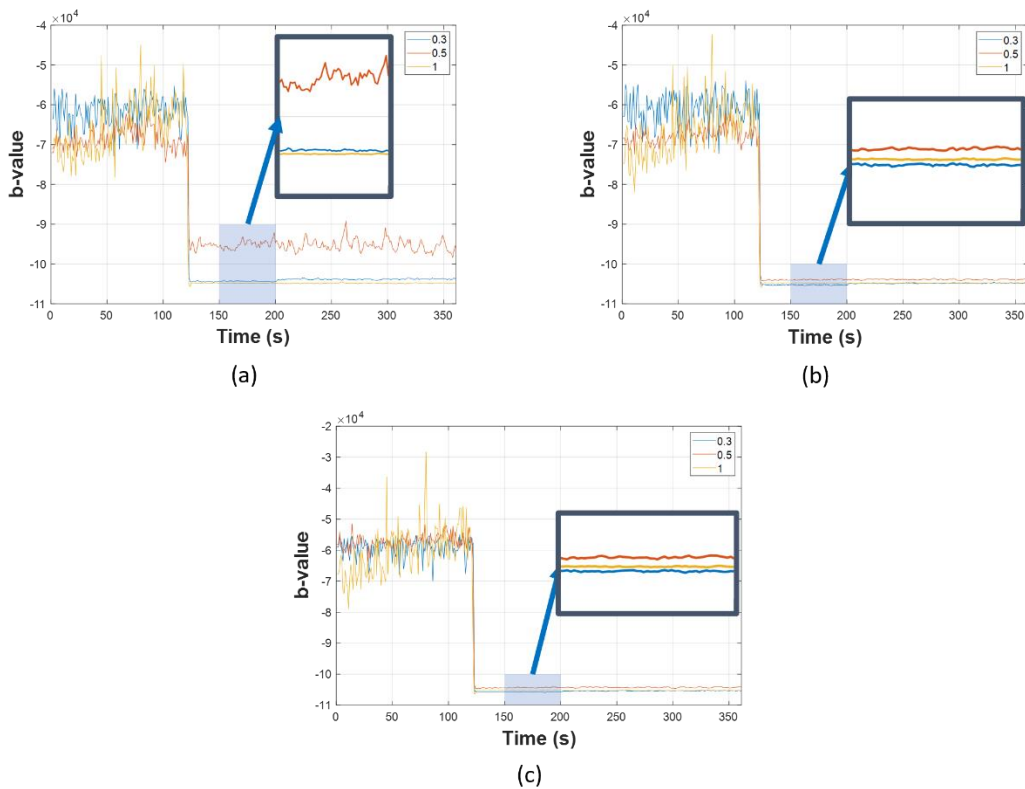


Figure 4.11. AIICs for different leak sizes at 13 bar for: (a) channel one, (b) channel two, and (c) channel three.

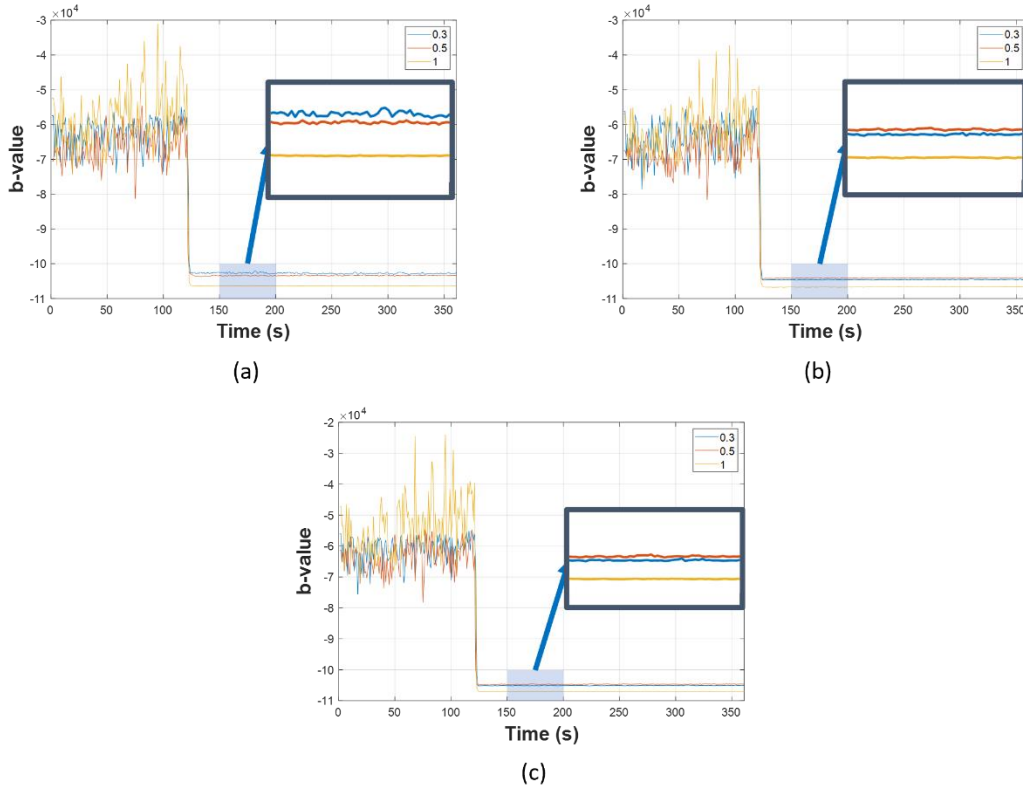


Figure 4.12. AIICs for different leak sizes at 18 bar for: (a) channel one, (b) channel two, and (c) channel three.

For every scenario, a steep drop can be witnessed around the time when the leak would start, as expected and explained in Section 4.3.2. In this method, the cycle error using BEAST is calculated as follows:

$$\text{cycle error} = |t_p - t_r|, \quad (4.8)$$

with t_p being the highest occurrence probability of the changepoint predicted by BEAST and $t_p > 50\%$; and $t_r = 120$ being the real leak activation time. Despite multiple significant decreases in AIIC prior to the leak, the changepoint can still be detected with only an average of a 2.6 cycle error and a standard deviation of 0.5 in all scenarios. This cycle error is impressive because it also consists of the time after leak activation when the fluid flow within the pipeline is unstable, which is often neglected, as the leaking stage is frequently considered to start upon stabilization of the flow.

Finally, leak size identification was conducted once the leakage was confirmed. A ratio of 70%/30% was used for the random train-test split from the dataset. Due to the AIIC's

capability for discrimination and the classification power of RF, it shows a high accuracy of approximately 100% for all levels of pressure. The results obtained from the classification process are shown in Figure 4.14.

For further validation, a comparison was conducted with two cutting-edge methods: 1) a method for size identification using convolutional neural networks (CNN) with time domain AE features (referred to as TD-CNN) and 2) an adaptation of the method proposed by [52] using AEH-based features and a 1D-CNN instead of their proposed SVM-RVM (originally developed for different pressure rates) to classify the leak sizes (referred to as the Banjara et al. adaptation). All three methods, including the proposed one and the two references, were evaluated using the leak identification dataset. This leak identification dataset contained only the leaking state part from the 27 data streams (from the 126th cycle until the end of each stream, as explained in Section 4.3.2). The results for different pressure levels are shown in Tables 4.4-4.6.

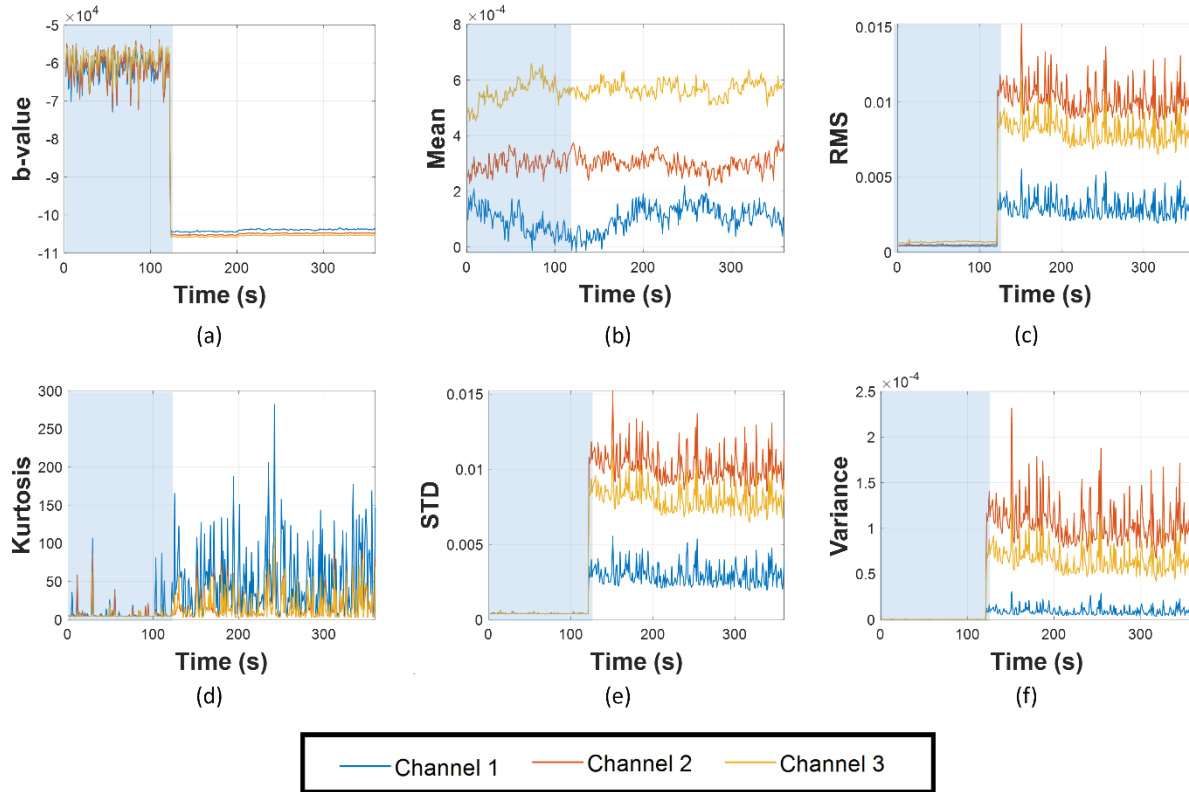


Figure 4.13. Comparison between AIC and traditional indexes, with the blue region indicating normal working state, while the white one indicating leakage: (a) AIC, (b) mean, (c) RMS, (d) kurtosis, (e) STD, and (f) variance.

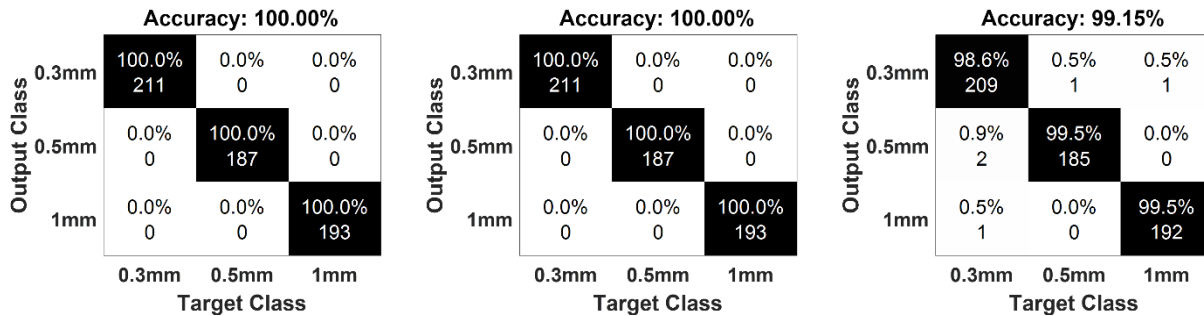


Figure 4.14. Result of leak size classification with different pressure levels: (a) 7 bar, (b) 13 bar, and (c) 18 bar.

The leak size identification results in Tables 4.4-4.6 show that the proposed method outperforms the two state-of-the-art references in terms of the average classification accuracy across different levels of pressure. Concerning the first comparison under a 7 bar pressure, TD-CNN shows a better average accuracy than the Banjara et al. adaptation (88.5% versus 77%); however, it is significantly lower than the 100% accuracy of the proposed method. The second and third comparisons demonstrate a difference because the Banjara et al. adaptation excels in both scenarios (92.2% and 87.0%, respectively) against the TD-CNN (79.6% and 75.9%, respectively). Similar to the first case, the proposed method has the best

result of the three methods. The reference methods show inconsistency with a classification accuracy of up to 100.0% but also as low as 45.0% (Banjara et al.) or 64.4% (TD-CNN). This problem does not exist in the proposed method, which is anticipated because AIIC is more robust against the multi-source problem of AEEs than the other two, and efficiently discriminates leak sizes (Figures 4.10-4.12). The time domain features in the TD-CNN and AEH features in the method of Banjara et al. (despite being capable of providing a great description of AE activity in more transient data) are more likely to be affected by the high level of background noise.

Table 4.4. A comparison of leak size identification using the three methods under the pressure of 7 bar.

Method	Accuracy (%)			Average Accuracy (%)
	0.3 mm	0.5 mm	1 mm	
TD-CNN	86.9	67.0	96.6	88.5
Banjara et al. adaptation	78.8	74.7	77.5	77.0
The proposed method	100.0	100.0	100.0	100.0

Table 4.5. A comparison of leak size identification using the three methods under the pressure of 13 bar.

Method	Accuracy (%)			Average Accuracy (%)
	0.3 mm	0.5 mm	1 mm	
TD-CNN	68.5	75	100.0	79.6
Banjara et al. adaptation	81.6	95.9	100.0	92.2
The proposed method	100.0	100.0	100.0	100.0

Table 4.6. A comparison of leak size identification using the three methods under the pressure of 18 bar.

Method	Accuracy (%)			Average Accuracy (%)
	0.3 mm	0.5 mm	1 mm	
TD-CNN	64.4	67.6	100.0	75.9
Banjara et al. adaptation	97.0	45.0	100.0	87.0
The proposed method	98.6	99.5	99.5	99.2

4.4 Conclusion

Pipelines play an essential role in fluid transportation, and pipeline leakage events can cause great damage to humans, the environment, and assets. Therefore, detection and diagnosis must be continually performed to ensure that maintenance can be planned and performed accordingly to prevent further loss. This study presents a leak state detection and leak size

identification method for an industrial fluid pipeline, using the acoustic emission (AE) activity intensity index curve (AIIC) based on the b-value and random forest (RF). Due to AE being a high-frequency but low-energy seismic activity, the b-value, which is one of the most important parameters for the probabilistic investigation of seismic hazards in seismology, can be adapted to AE applications. Because the adapted b-value characterizes the relationship between the amplitudes and their frequencies of occurrence, along with there being a direct AE activities' amplitude–intensity connection, an AIIC based on the b-value can parameterize the AE activity intensity in any period. A frequency–amplitude distribution (FAD) analysis showed that the majority of high-amplitude AE activities in the leaking state were leak-related, which greatly outnumbered other sources that contributed to the background noise and multi-source problem of AE activities in a fluid pipeline system. The AIIC calculated from the b-value also discriminated between not only normal and leaking operation conditions, but also different leak sizes. In the next step, leak detection was performed using the AIIC through changepoint detection using a Bayesian ensemble, which showed an outstanding average error of only 2.6 s from the moment of leak occurrence. Once a leak was confirmed, the AIICs used for leak detection were again utilized for size identification using RF. The fluid pipeline data, with three pressures and three leak sizes, were used to validate the proposed method. The size identification results were compared with two cutting-edge methods, which showed that the proposed method can outperform the earlier algorithms with significantly higher accuracy. For future work, leak localization can be integrated into this study, along with different scenarios, such as pipelines buried under soil or submerged in water. In addition, the limitation of a hard-threshold b-value can also be further researched to achieve a better description of AE activity.

Chapter 5

A Deep-Learning-Based Health Indicator Constructor Using Kullback–Leibler Divergence for Predicting the Remaining Useful Life of Concrete Structures

This paper proposes a new technique for the construction of a concrete-beam health indicator based on the Kullback–Leibler divergence and deep learning. Health indicator (HI) construction is a vital part of remaining useful lifetime (RUL) approaches for monitoring the health of concrete structures. Through the construction of a HI, the deterioration process can be processed and portrayed so that it can be forwarded to a prediction module for RUL prognosis. The degradation progression and failure can be identified by predicting the RUL based on the situation of the current specimen; as a result, maintenance can be planned to reduce safety risks, reduce financial costs, and prolong the specimen’s useful lifetime. The portrayal of deterioration through HI construction from raw acoustic emission (AE) data is performed using a deep neural network (DNN), whose parameters are obtained by pretraining and fine-tuning using a stacked autoencoder (SAE). Kullback–Leibler Divergence (KLD), which is calculated between a reference normal-conditioned signal and a current unknown signal, was used to represent the deterioration process of concrete structures, which has not been investigated for the concrete beams so far. The DNN-based constructor then learns to generate HI from raw data with KLD values as the training label. The HI construction result was evaluated with run-to-fail test data of concrete specimens with two measurements: fitness analysis of the construction result and RUL prognosis. The results confirm the reliability of KLD in portraying the deterioration process, showing a large improvement in comparison to other methods. In addition, this method requires no adept knowledge of the nature of the AE or the system fault, which is more favorable than model-

based approaches where this level of expertise is compulsory. Furthermore, AE offers in-service monitoring, allowing the RUL prognosis task to be performed without disrupting the specimen's work.

5.1 Introduction

With ease of access and high durability, concrete structures have become a ubiquitous sight in recent decades. Along with their everywhere presence, comes the inevitable need for a maintenance plan to ensure in-service safety and to prolong the lifetime of concrete structures. Numerous studies [5], [73], [86], [87], [88], [89], [90], [91], [92], [93] have been conducted by laboratories, companies, and individuals race to identify solutions regarding performance amelioration of structural health monitoring (SHM). By employing an effective monitoring scheme, it is possible to provide the user with more insight into the in-service system/structure, avoid near-future failures, and lessen downtime by a significant amount.

Among SHM topics, the remaining useful lifetime (RUL) prognosis is one of the most popular problems, in which a solution is provided to predict how long a structure can be used until it is permanently out-of-service because of a failure(s). By predicting the future state of the structure, a user can approximate the time when a failure might occur, thus adjusting the usage and preparing a maintenance plan accordingly in advance. The most recent studies [7], [94], [95], [96], [97], [98] regarding this topic focus on the development of an autonomous system that is capable of extracting feature(s) from data and constructing indicators based on these extracted features. A common scheme for this approach is as follows: initially, sensors are deployed, which are then utilized to collect and send real-time data to the central brain where data processing and health indicator construction occur.

As non-destructive methods for SHM have become dominant in recent years, different methods have been investigated for concrete SHM such as ultrasonic [90], [99], [100], vibration [101], [102], image processing [88], [103], [104], and AE [6], [11], [12], [89], [95], [105], [106], [107], [108], [109], [110], etc. Due to its outstanding properties. Even though ultrasonic testing can detect internal defects and their sizes, it is susceptible to complicated part geometry and certain materials, such as austenitic steel, which can mask defects by causing attenuation. Concerning vibration techniques, they are restricted by their limited band of frequency. In addition, although image processing techniques offer the most facile setup among all the mentioned methods, they are only capable of detecting failures on the surface. In comparison to these non-destructive methods, AE techniques, which study and exploit the release of internal elastic energy by a discontinuity appearance, offer a non-directional mean of monitoring capable of achieving in-service testing without downtime [111]. A single test of AE can allow users to track the specimen's deterioration process dynamically while highlighting the severity of the damage. The drawback of this method is

that AE can only be utilized to detect the occurrence of new discontinuities, not existing ones. However, since the purpose of the AE test is to detect novelties to the current state of the specimen, this drawback can be considered insignificant in comparison to the benefits that it provides. In this study, we focus on employing a technique using AE sensors.

The data collected by AE sensors are then analyzed for health indicator (HI) construction. The approaches of HI construction for RUL prediction, similar to the prognosis and health management framework in general, can be roughly classified as model-based or data-based. The methods following the first category focus on real-life process imitation, which is established via mathematical means. Given the drawback of being increasingly problematic as the model becomes more complex, it is less favorable than the data-based approach, in which the interested patterns are derived from available data even in the absence of knowledge about the nature of the system or the fault. Therefore, the data-based approach is the main priority of this study. Further discussion on HI construction can be found in Section 5.2.

To ensure the reliability of the constructed HI, an evaluation is needed. According to a previous survey [112], the evaluation of HI can be performed by two approaches: one concerning the fitness analysis of the construction result and the other considering the RUL prognosis performance. Further discussion on the HI construction framework for RUL prognosis is continued in Section 5.2.

The HI construction and evaluation is presented in Figure 5.1:

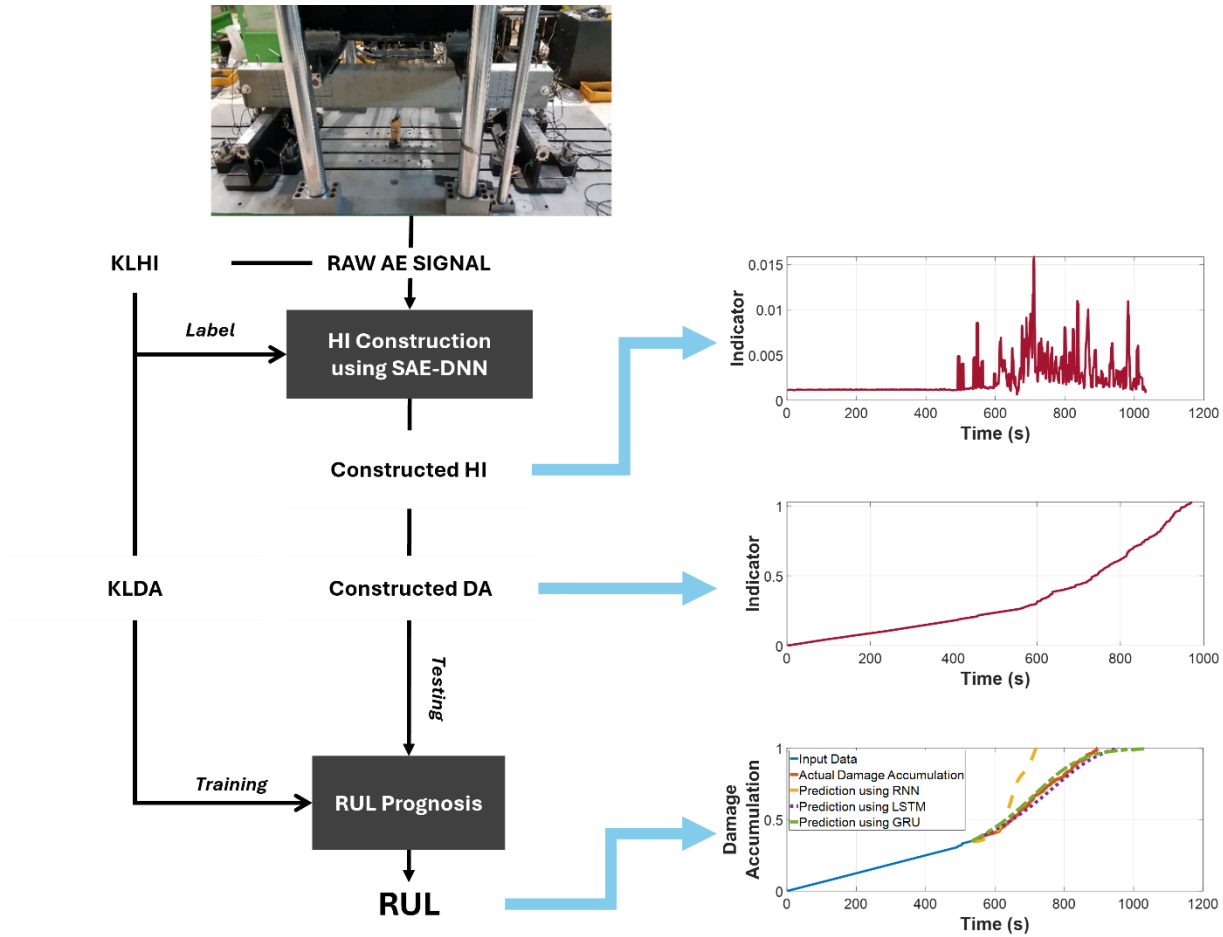


Figure 5.1. Flowchart of the HI construction framework and evaluation process.

Initially, the raw data is collected from the specimen throughout its deterioration process. It is then utilized for the calculation of Kullback–Leibler Divergence (KLD) at each time step of each run-to-fail signal. Afterward, the raw signal is fed to the HI constructor, where its spectrum is computed and used to reduce computation complexity. The stacked auto-encoder (SAE) takes the spectrum as input for the pretraining process, which is subsequently fine-tuned into the deep neural network (DNN) to construct the HI lines with the calculated KLD as the training label. Finally, the evaluation of HI is performed using both intrinsic measures and RUL prediction to test the proposed method’s reliability.

In summary, this study proposes a data-based approach for HI construction based on KLD, for which expertise concerning concrete material and the nature of the fracturing process is not required. The constructed HI, through its ability to accurately describe the deterioration state of concrete structures, can be utilized for RUL prognosis and can allow users to plan maintenance before possible structural failures in the near future. The following contributions are proposed:

1. A novel HI construction process is proposed using KLD to describe the state of the concrete specimen during its lifetime directly from raw AE data, which has not been previously investigated to the extent of the authors' knowledge.
2. Adaption of the proposed indicator for the task of RUL prognosis.

The arrangement of the following sections is as follows: Section 5.2 discusses the general HI construction framework and evaluation; the process of HI construction is provided in detail in Section 5.3; Section 5.4 describes the experimental setup and HI evaluation using the two discussed methods; finally, Section 5.5 provides a conclusion, along with a discussion of future research possibilities.

5.2 The General Health Indicator Construction Framework and Evaluation

HI construction is an essential part of the prognosis to portray the timeline of deterioration. HI shows the condition in which the specimen under investigation is. By analyzing the current HI, it is possible to predict future values and their timing, thus allowing RUL to be estimated. Over the years, numerous studies have proposed different approaches to building HI, especially in more recent studies [113], [114], [115] and in summary, this process can be generally divided into two steps: 1) calculation of the HI-constructing factor(s) and 2) HI construction from the calculated factor(s).

The calculation of the HI-constructing factor(s) (also known as features) is often performed either in time, frequency, or time-frequency domain. The time domain approaches [6], [107], [116], [117] generally offer a fast and simple solution that can be widely applicable to systems and fault types. They often include statistical computation and impulse analysis. These methods, however, are susceptible to interferences, which are typically inevitable in real-life applications. Therefore, pre-processing techniques are necessary to minimize performance degradation. Frequency domain solutions [118], [119] explore anomalies in the system with prior information on the fault characteristic frequencies already known. They are often adapted in model-based methods and can offer high efficiency; however, they are not widely applicable. The approaches following a time-frequency domain solution [120] are the most powerful among these three and can be highly robust. Their downside is that such powerful methods often require high computational capability and experience concerning information extraction.

Afterward, the second step is to build the HI constructor. As previously briefed in the previous section, the construction of HI can be roughly divided into two categories: model-based and data-based. Model-based methods focus on generating a mathematical

representation that mimics a real-life process. The development of HI in these studies requires expertise and knowledge about the system's behavior, the nature of the faults, and the HI-constructing factors. Following this approach, the studies in [94], [106], [119], [120] investigated the faults concerning fault-related frequencies, which indicates that the comprehension of the system and fault nature is necessary. Another study in [121] proposed an effective HI construction method with features manually chosen based on relevance. The aforementioned researches and many others are done with expertise in signal processing, and system and fault behavior, which can be troublesome to obtain in more sophisticated scenarios. Moreover, they cannot be adapted to a variation of systems due to their construction imitating certain real-life processes. Unlike model-based approaches, data-based solutions focus on the nature of the data itself, with less concern for the system or fault nature. Due to their lower complexity and wider application towards different systems and faults, data-based methods have become more favorable in recent years, especially with the rise of artificial intelligence [122]. Notable mentions in this category are statistical projection [118], [123], [124], deep learning models [95], [125], [126], [127], and evolutionary computation [112], [128], etc. Different studies following these methods have achieved promising results in HI construction for the RUL prognosis task.

To verify the constructed HI, the evaluation process must be performed with suitable metrics. Concerning the HI construction for RUL prognosis, the evaluation can be generally divided into two categories: the investigation of the HI's intrinsic nature from the construction result (fitness analysis) and the performance of HI in the RUL prognosis tasks. Fitness analysis is often performed with the following metrics: monotonicity [95], [120] (measurement of the monotonic trend in HI), trendability [95], [120] (the correlation of HI and time), and scale similarity [95], [120], [127] (similarity of HI ranges), etc. The purpose of this type of evaluation is to self-reflect the HI properties via low computational complexity without concern for the prognosis task. Furthermore, the second category evaluates HI by its performance in RUL prognosis. This indirect assessment can be done through mean absolute error, mean square error, mean absolute deviation, etc. In comparison to the first category, it provides more information about the prognosis task as a whole; however, it requires more computational complexity because the whole prognosis block is added. The proposed method is verified in both categories, with monotonicity and trendability in the first and mean absolute error in the second evaluation.

5.3 The Proposed Health Indicator Construction.

KLD is used to construct the HI to investigate how different an unknown signal is from a known normal condition. As the deterioration progresses during the loading test, it can be expected that the difference between the unknown signal to the reference one grows with

the intensity of the AE activity. For that reason, this difference is suitable for the portrayal of the deterioration process from the run-to-failure signals. Figure 5.2 shows a loading test's stages of deterioration and highlights the difference between a reference signal to a signal in which significant AE activities are recorded. The detailed experimental setup and data description are discussed in Section 5.4. As shown in Figure 5.2, the vertical displacement of the specimen grows steadily during the deterioration stage, which indicates continuous damage being sustained; therefore, it is also evident that significant AE activities occur during this period.

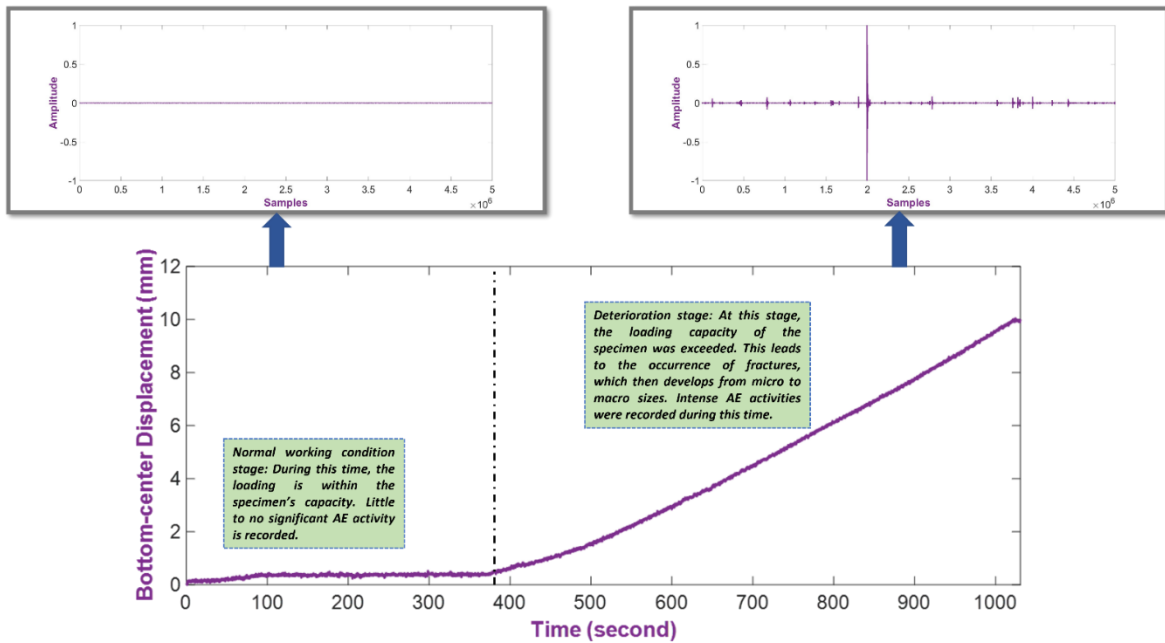


Figure 5.2. Vertical displacement of the specimen and signal difference in two loading stages.

In this study, the signal is segmented into one-second blocks (time steps) for the computations. The HI construction process initiates the calculation of each run-to-fail signal's probability distribution. A signal's values are divided into segments of 10^{-3} width ranging from its minimum value to its maximum, at each of which the probability density function (PDF) of the signal is computed. The result of this computation is later utilized for the KLD calculation.

The divergence of two probability measures was originally defined by Harold Jeffreys [129] in a symmetrized form (directed divergences, also known as the relative entropies in each direction), which is now referred to as the Jeffrey Divergence. Later in the 1950s, Solomon Kullback and Richard Leibler [130] proposed exploring the mean information discrimination between two hypotheses by their according probability measures using relative entropy in an asymmetric manner. This concept later came to be known as the Kullback–Leibler Divergence. Its first context was developed for information theory and later widely adapted

to optimization tasks of machine learning. The value of KLD falls within the range of 0 to 1, which indicates no difference and maximum divergence, respectively. Assuming two probability distributions $P(x_i)$ and $Q(x_i)$ from the reference normal condition and unknown signal, their KLD calculation is as follows:

$$\text{KLD}(P, Q) = \sum_{i=1}^N P(x_i) \log \frac{P(x_i)}{Q(x_i)}, \quad (5.1)$$

It is assumed that all of the run-to-fail signals start at a normal state with little to no significant AE activity recorded during this period. Therefore, a reference normal-conditioned signal can be arbitrarily selected from the very start of the recording.

With the KLD values, the process continues with the establishment of the DNN-based constructor, which outputs HI lines from the input signal spectrum. Initially, the signal spectrum is calculated using the fast Fourier transform and then equally separated into $2e3$ size bands, whose energy can be approximated using the root mean square. By doing such an action, the computation capacity can be reduced for the following operations. Afterward, the pre-training of DNN commences as SAE is fed with the obtained vector of size $2e3$. The SAE consists of an encoder and a decoder, both comprising three dense layers. The encoder processes the data through layers of diminishing sizes (1000-200-10) in the encoder and then layers of increasing size (200-1000-2000) in the decoder. Xavier initialization and an exponential linear unit activation are harnessed for the encoder. In addition, dropout layers of rate 0.1 are appended before the dense layers for the amelioration of the SAE's regularization. The training of SAE is executed with the gradient-descent parameter update, Adam optimization, and a 0.1 fraction of masked zeros, along with an unlabeled signal spectrum as both the input and output. Noise is added to the training data, which forces the reconstruction of the noisy input, thus improving the learned features' robustness.

Once the SAE's training concludes, fine-tuning of the DNN follows as the encoder's layers are utilized as the DNN's hidden layers, on top of which a logistic regression layer is placed. The calculated KLD value, which falls in the range of [0,1], is utilized as the output for the DNN training, along with the input of the signal spectrum. In addition to freezing the reused layers for learning ability preservation, early stopping and checkpoint are also used to achieve better parameters. Similar to the KLD, the constructed HI is also within [0, 1], which indicates the damage the specimen has sustained from the least to the most on the severity scale.

5.4 Experimental Setup and Evaluation

5.4.1 Experimental Setup

To evaluate the reliability of the proposed method, data were collected from reinforced concrete beams, which were constructed and installed for the four-point bending test scenario. Each specimen was identically produced with concrete material having a compressive strength of 24 MPa, D16 (SD400) steel rebar, and gridded in $50 \times 50 \text{ mm}^2$ squares for better visualization of deterioration monitoring. The AE data were acquired at 5 MHz from eight R3I-AST sensors placed around both ends of a specimen. The detailed four-point bending test setup and sensor placement are shown in Figure 5.3.

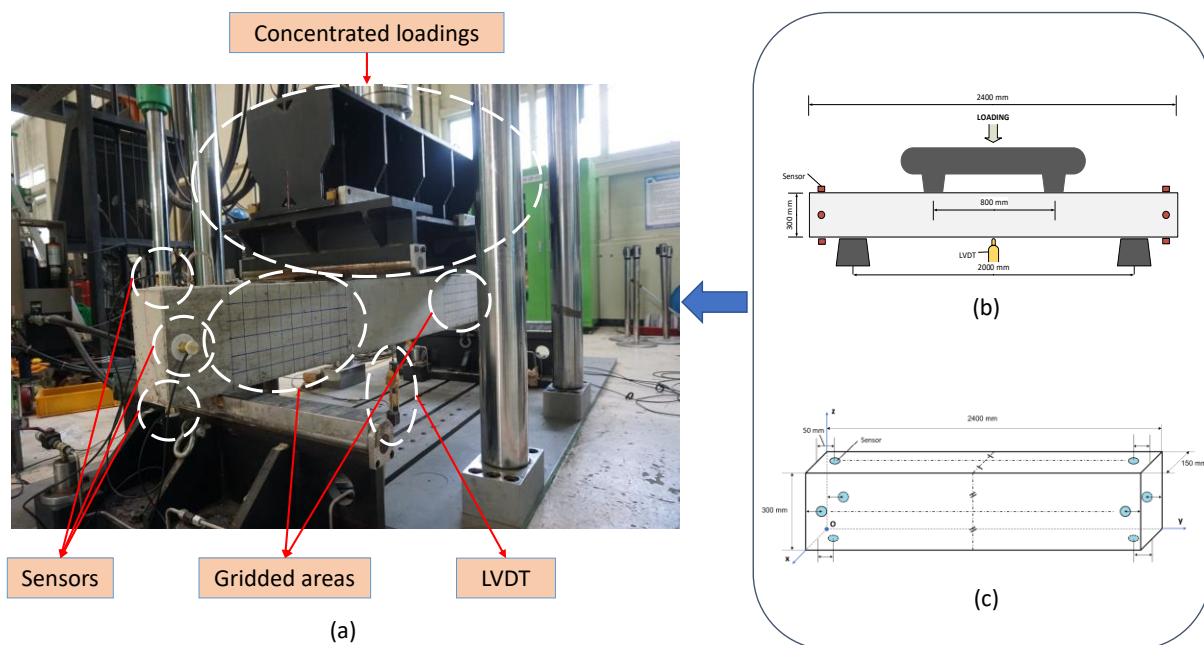


Figure 5.3. Experimental setup of the four-point bending test on reinforced concrete beam: (a) pictorial of the specimen under test, (b) schematic of the four-point bending arrangement, and (c) placement of sensors on the specimen.

Each specimen was subject to two-point concentrated loading. The loading points were placed 400 mm from the left and right of the specimen's median, and the stress was applied at a speed of 1 mm/s. In addition, a linear variable differential transformer (LVDT) was set underneath the specimen at its center for vertical displacement measurement. This is an alternate way to track the damage sustained other than the visual monitoring of the specimen's surface fractures. During the test, the specimens were loaded until the damage was high enough that maintenance was not efficient anymore; however, a total collapse was prohibited from happening for the safety of the observers including our team members and construction field specialists. Figure 5.4 shows the damage sustained by a specimen during the test:

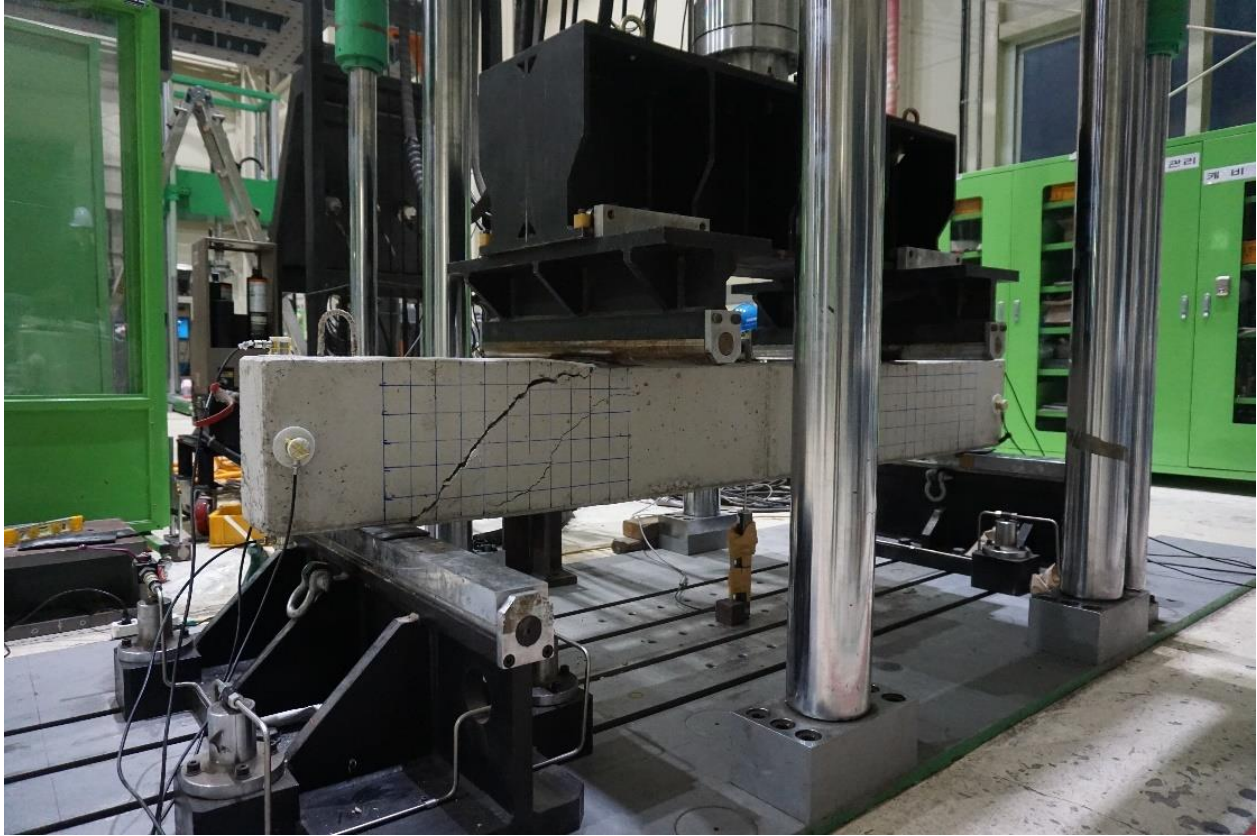


Figure 5.4. Damage sustained by a specimen during the test.

Data from three tests, α , β , and γ , were harnessed for this study. Each test was recorded with eight AE sensors with a total of 24 run-to-fail signals. For each test, signals from one side (recorded from four out of eight sensors) were used for the training processes, and the rest for testing.

5.4.2 Evaluation and Discussion

As aforementioned, the reliability of our proposed method was verified by two evaluations: fitness analysis of the construction result and RUL prognosis performance. In this section, these evaluations are demonstrated in comparison with other methods. The proposed and other HI-constructing factors are visualized in Figure 5.5.

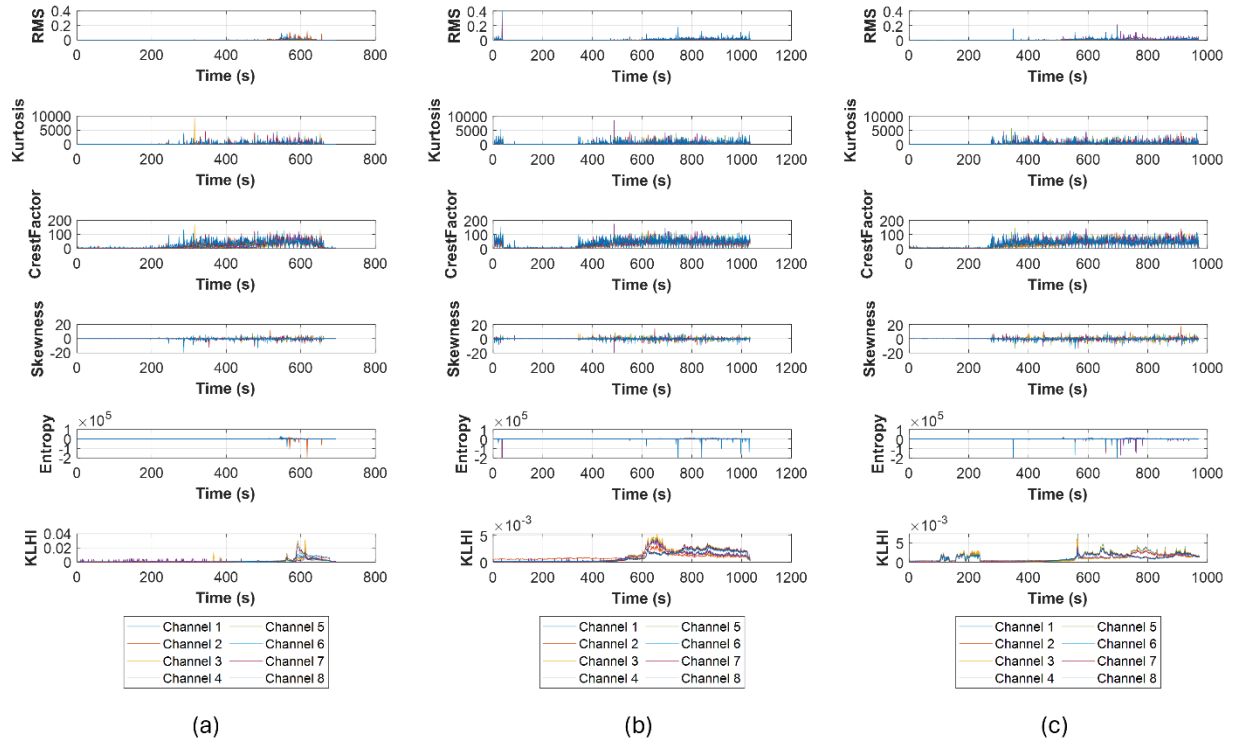


Figure 5.5. Visualization of the proposed and other HI-constructing factors (RMS, Kurtosis, Crest Factor, and Skewness) using reinforced concrete beam: (a) α , (b) β , and (c) γ .

To analyze the HI construction result, trendability and monotonicity were utilized as the evaluation metrics. In the prognosis tasks, trendability can be perceived as the indicator of a feature's variation with regard to time. High trendability can be witnessed in linear functions, whereas a constant function represents the minimum trendability. The resulting line of reliable HI construction is expected to be trendable, especially as the specimen progresses closer to its failure. In our study, this metric is computed as:

$$\text{Trendability} = \frac{N \sum xt - \sum x t}{\sqrt{[N \sum x^2 - (\sum x)^2][N \sum t^2 - (\sum t)^2]}} \quad (5.2)$$

where N is the observation number, and x and t are the feature and time index, respectively.

In addition, monotonicity characterizes the underlying decreasing or increasing trend. Its value is in the range of $[0, 1]$, which indicates a higher level of monotonicity as it rises. A good HI result is expected to not possess a low level of monotonicity. The computation of this metric can be performed as follows:

$$\text{Monotonicity} = \text{absolute} \left(\frac{n_{d/dx>0} - n_{d/dx<0}}{N-1} \right), \quad (5.3)$$

where N is the observation number.

To verify the fitness of the KLD-based HI, a comparison was made with various HI-constructing factors. The results based on the two metrics are shown in Table 5.1.

Table 5.1. Fitness analysis of the proposed HI-constructing factor and other factors.

HI-Constructing Factor	Trendability		Monotonicity	
	Mean	Std	Mean	Std
RMS	0.3404	0.1412	0.5052	0.0112
Kurtosis	0.3547	0.0509	0.4978	0.0091
Crest Factor	0.5755	0.0540	0.4973	0.0090
Skewness	0.0313	0.1209	0.5012	0.0116
Entropy	0.1292	0.1437	0.5080	0.0105
KLD	0.6110	0.1565	0.5073	0.0123

From what can be witnessed in the table, even though the indicators share a comparable level of monotonicity, KLD outperforms the traditional features in trendability by a large margin. While Crest Factor can reach as high as 0.5755, other features such as Skewness is as low as 0.0313. It is known that the traditional AE features are susceptible to high background noise level. In addition, this shows that KLD has a strong correlation with time and it is an implication that the use of KLD is suitable for the portrayal of a concrete structure's deterioration state.

In addition to the fitness analysis of the construction result, the HI was also evaluated by its performance concerning RUL prognosis. Since the HI only shows the instantaneous damage sustained by the specimen during a specific time step, it needs to be transformed into another indicator which can show the accumulated damage. A damage accumulation indicator (DA) can be calculated from the HI as follows:

$$DA(n) = \sum_{k=1}^n HI(k), \quad (5.4)$$

To predict the RUL, a long short-term memory recurrent neural network (LSTM-RNN) [6] was used on the DAs. Because each run-to-fail signal is a sequence of values at the time steps, it can be deemed as a univariate time series. The LSTM-RNN takes in the signals in the form of a 50-sample sliding window, which moves one sample at a time, and predicts the 51st sample. By performing such an action, the model is forced to predict not just the final value, but at each window of the signal. In addition, it also enhances the training speed and stabilization by enabling more error gradients. This model contains an input layer, two hidden size-of-50 LSTM layers, and a dense output layer using a linear activation function. Similar to DNN training, early stopping, and checkpoint techniques are also used here.

The importance of RUL prognosis increases with time. During the normal working stage with no damage sustained yet, it is inessential to make a prediction. From the moment the specimen enters its deterioration stage, the importance of RUL prognosis grows significantly due to the need for maintenance planning. As a result, we chose three major time steps at 300, 400, and 500 time steps before the failure to perform the prediction. Figures 5.6, 5.7, and 5.8 display the RUL prediction from the three tests at these time steps.

To quantify the performance, the useful lifetime expiration is marked at the first occurrence of 0.90 along the DA line; therefore, the RUL can be calculated as follows:

$$RUL = T_{0.90} - T, \quad (5.5)$$

where $T_{0.90}$ is the time step when the HI reaches 0.90 and T is the time step at which the RUL prognosis is being performed. Afterward, an error computation is needed to determine how much the RUL prediction differs from the actual RUL:

$$RUL \text{ error} = \text{absolute}(RUL_{predicted} - RUL_{actual}), \quad (5.6)$$

where $RUL_{predicted}$ is the predicted RUL and RUL_{actual} is the actual RUL. While this measurement is capable of demonstrating the distance between the predicted and actual RUL, it cannot show which of the predicted and the actual useful life expiration comes first. In addition, root mean square error (RMSE) and mean absolute percentage error (MAPE) are also used:

$$RMSE = \sqrt{\frac{\sum_{i=1}^N (actual_i - prediction_i)^2}{N}}, \quad (5.7)$$

$$MAPE = \frac{1}{N} \sum_{i=1}^N |actual_i - prediction_i|, \quad (5.8)$$

The summarized prediction results at the three time steps are shown in Tables 5.2, 5.3 and 5.4. In addition to the plots shown in Figures 5.6, 5.7 and 5.7, it can be seen that the LSTM and GRU predictions can closely follow the underlying trend of the actual HI. This is because LSTM and GRU are capable of capturing the long-time dependencies in the time series, whereas RNN can not. As the result, the RNN's predictions veer off right from the start in every scenario. During the 300- and 400-time-step-before-the-failure predictions, the LSTM and GRU show comparable results in all metrics. However, during the final one, LSTM shows a notable better result in comparison to GRU. The reason is that even though GRU's simpler

architecture offers lower computational load and faster training time, it might limit their ability to model complex relationships within the time-series data. In contrast, LSTM's architecture is more complex with three gates, which allows it to capture sophisticated patterns and temporal dynamics at the cost of higher computational load and slower training.

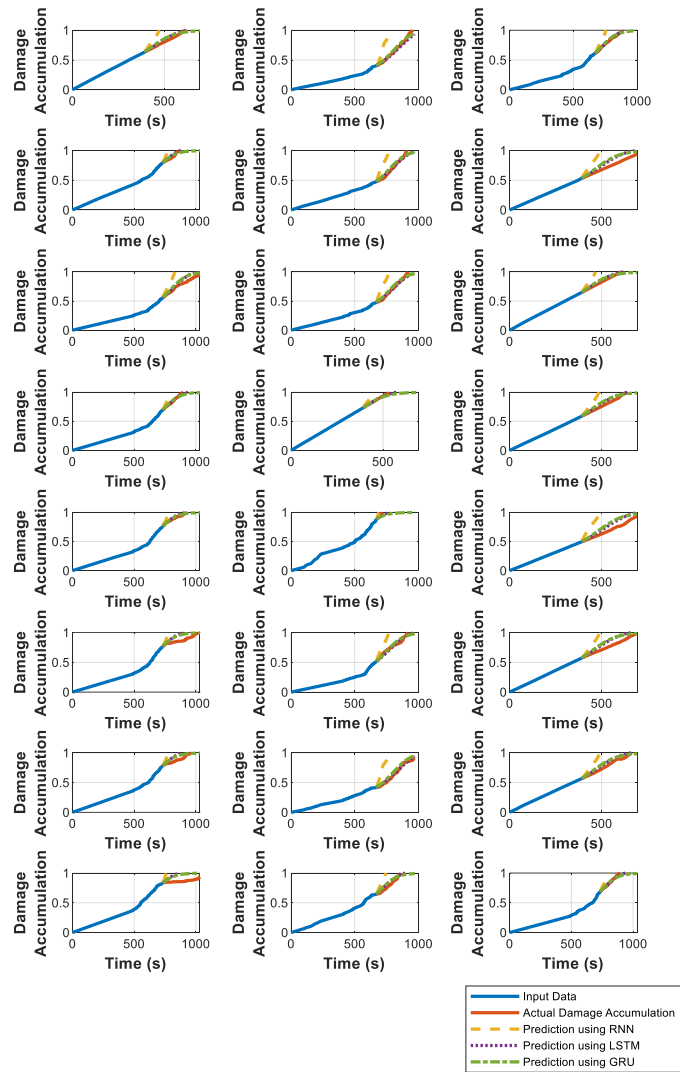


Figure 5.6. RUL prognosis from the three tests 300 time steps before the failure. (a) Reinforced concrete beam α . (b) Reinforced concrete beam β . (c) Reinforced concrete beam γ .

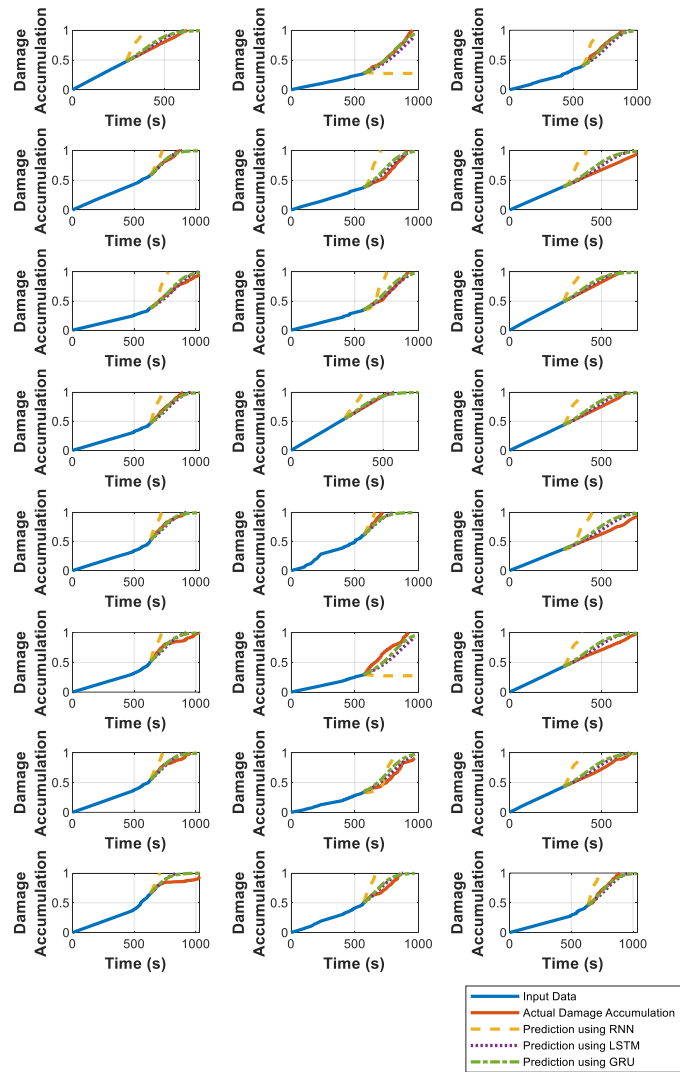


Figure 5.7. RUL prognosis from the three tests 400 time steps before the failure. (a) Reinforced concrete beam α . (b) Reinforced concrete beam β . (c) Reinforced concrete beam γ .

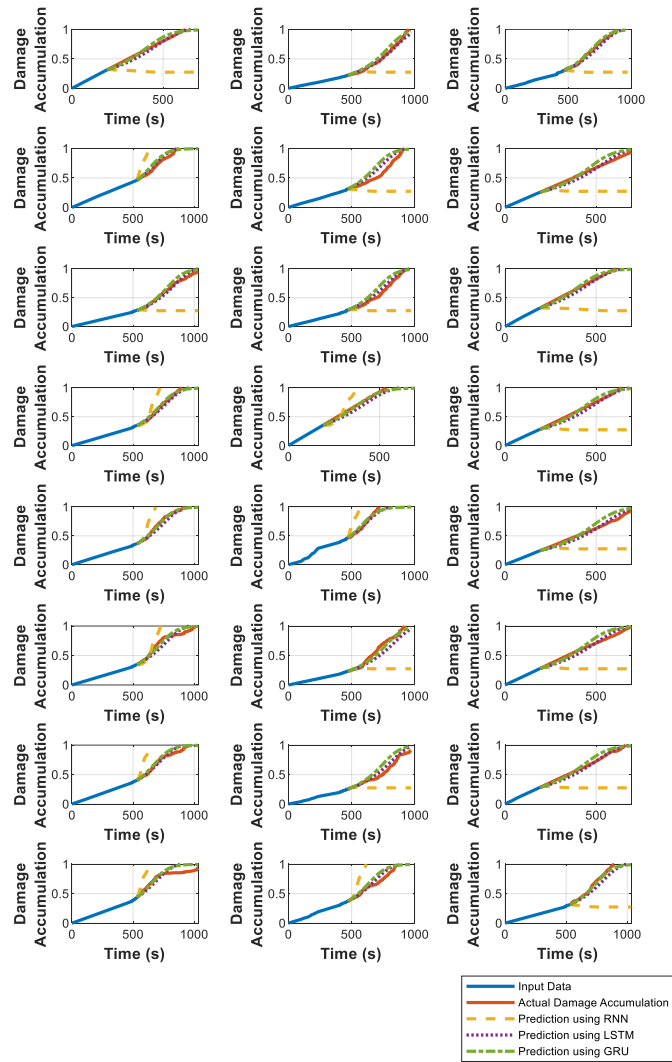


Figure 5.8. RUL prognosis from the three tests 500 time steps before the failure. (a) Reinforced concrete beam α . (b) Reinforced concrete beam β . (c) Reinforced concrete beam γ .

Table 5.2. RUL prognosis performance assessment 300 time steps before the failure.

RCB	Model	RUL error	RMSE	MAPE
1	RNN	74.75	0.26	25.57
	GRU	42.63	0.07	6.50
	LSTM	40.38	0.07	6.49
2	RNN	101.63	0.28	33.99
	GRU	18.00	0.07	6.12

	LSTM	10.00	0.05	4.44
	RNN	110.88	0.29	32.19
3	GRU	48.88	0.08	7.56
	LSTM	39.25	0.06	6.14

Table 5.3. RUL prognosis performance assessment 400 time steps before the failure.

RCB	Model	RUL error	RMSE	MAPE
	RNN	133.50	0.29	33.32
1	GRU	44.00	0.07	5.69
	LSTM	34.75	0.06	5.82
	RNN	-	0.32	37.49
2	GRU	34.50	0.08	9.32
	LSTM	30.50	0.07	8.29
	RNN	187	0.36	45.53
3	GRU	61.75	0.08	8.67
	LSTM	49	0.06	6.56

Table 5.4. RUL prognosis performance assessment 500 time steps before the failure.

RCB	Model	RUL error	RMSE	MAPE
	RNN	-	0.34	39.05
1	GRU	50	0.06	6.00
	LSTM	27.63	0.06	5.97
	RNN	-	0.35	39.13
2	GRU	49.13	0.09	11.42
	LSTM	33.75	0.07	8.32
	RNN	-	0.45	50.93
3	GRU	49.50	0.06	6.36
	LSTM	22.38	0.05	6.67

5.5 Conclusions

This chapter presented an autonomous health indicator (HI) constructor for remaining useful lifetime (RUL) prognosis on concrete structures using Kullback–Leibler Divergence (KLD) with in-service acoustic emission (AE) monitoring. By using a reliable HI for the prognosis task, the user can be warned of future failure and, thus, maintenance can be performed accordingly to minimize safety risks and financial concerns. The process of HI construction was initialized from raw data, which was processed by the Fast Fourier Transform and fed to a constructor to generate the HI. The constructor was a deep neural network (DNN) structure, whose parameters were obtained through pretraining and fine-tuning with a stacked autoencoder (SAE). KLD values of the data were calculated between a reference normal condition and an unknown condition in a one-second window, which was then utilized as the training label for the DNN. The KLD was chosen to portray the deterioration of concrete specimens because of its ability to describe how much a signal is different from another. As the deterioration of the concrete specimens worsens, more significant activities can be expected in the AE signal.

Afterward, an evaluation of the constructed HI was presented to verify its reliability in the prognosis task for concrete specimens. The evaluation was divided into two categories: fitness analysis of the construction result and RUL prognosis using the constructed HI. Trendability and monotonicity were utilized as the metrics for fitness analysis, which showed a significant outperformance by the KLD HI in terms of trendability. This shows that the proposed HI has a strong correlation with time, and it is a promising candidate to capture the run-to-fail process of concrete structures. A comparison was also performed in the RUL prognosis on the proposed HI using LSTM and two state-of-the-art models 300, 400 and 500 time steps before the failure. The result of this comparison shows that even though GRU and LSTM shares comparable level of accuracy in shorter predictions, LSTM is capable of significantly outperforming other models in the longest one.

In future research, the proposed HI construction can be expanded to not just reinforced concrete beams, but also possibly bridges, walls, buildings, etc. It can also be greatly benefitted from covering the concrete crack localization, which provides more information for a preventive maintenance. Other optimization techniques and structures will also be investigated in future work to create a better construction model. We will also aim to approach the HI construction from the system- and fault-specific aspect, to which the finite element method (FEM) simulation shall be implemented along with Failure Mode, Effects, and Criticality Analysis (FMECA).

Chapter 6

Conclusion

This thesis presented condition-based monitoring techniques for concrete structures and industrial equipment. The demonstrated techniques harnessed advanced signal processing and artificial intelligence for early fault detection and prognosis tasks. The following subsections discuss the thesis summarization and future work.

6.1 Summary

Multiple experimental setups were conducted to verify the condition-based monitoring techniques presented in this thesis. This includes a cylinder tank under the Hsu-Nielsen test, an industrial standard pipeline system in a normal working condition and a leaking condition, and a four-point bending, run-to-fail test on multiple reinforced concrete beams. From these setups, acoustic emission (AE) data were collected for verification.

Chapter 3 presented a leak localization scheme for a cylinder tank bottom AE data. By performing this scheme, leak location can be estimated early, thus allowing the appropriate response to be taken to prevent possible injuries, fatalities, and environmental hazards, and minimize the financial damage. The AE data is initially processed with a constant false alarm rate (CFAR) for hit detection, which is then used to find the hits' time of arrival (TOA) and end time using the fixed thresholding method. Following this step hits originating from the same AE source are grouped by applying the event definition and the proposed similarity score. From the obtained results, the sources of AE events were estimated using the time difference of arrival (TDOA). Since AE events can happen in other locations than just the leaking position (due to turbulent flow, etc.), they should be investigated more to derive the

estimated leak position. This was analyzed through data density analysis using a Voronoi diagram to obtain the final result.

Chapter 4 proposed a leak state detection and leak size identification method for an industrial fluid pipeline, using the acoustic emission (AE) activity intensity index curve (AIIC) based on the b-value and random forest (RF). Due to AE being a high-frequency but low-energy seismic activity, the b-value, which is one of the most important parameters for the probabilistic investigation of seismic hazards in seismology, can be adapted to AE applications. Because the adapted b-value characterizes the relationship between the amplitudes and their frequencies of occurrence, along with there being a direct AE activities' amplitude-intensity connection, an AIIC based on the b-value can parameterize the AE activity intensity in any period. A frequency-amplitude distribution (FAD) analysis showed that the majority of high-amplitude AE activities in the leaking state were leak-related, which greatly outnumbered other sources that contributed to the background noise and multi-source problem of AE activities in a fluid pipeline system. The AIIC calculated from the b-value also discriminated between not only normal and leaking operation conditions, but also different leak sizes. In the next step, leak detection was performed using the AIIC through changepoint detection using a Bayesian ensemble, which showed an outstanding average error of only 2.6 s from the moment of leak occurrence. Once a leak was confirmed, the AIICs used for leak detection were again utilized for size identification using RF. The fluid pipeline data, with three pressures and three leak sizes, were used to validate the proposed method. The size identification results were compared with two cutting-edge methods, which showed that the proposed method can outperform the earlier algorithms with significantly higher accuracy.

Chapter 5 proposed an autonomous health indicator (HI) constructor for remaining useful lifetime (RUL) prognosis on concrete structures using Kullback-Leibler Divergence (KLD) with in-service acoustic emission (AE) monitoring. By using a reliable HI for the prognosis task, the user can be warned of future failure and, thus, maintenance can be performed accordingly to minimize safety risks and financial concerns. The process of HI construction was initialized from raw data, which was processed by the Fast Fourier Transform and fed to a constructor to generate the HI. The constructor was a deep neural network (DNN) structure, whose parameters were obtained through pretraining and fine-tuning with a stacked autoencoder (SAE). KLD values of the data were calculated between a reference normal condition and an unknown condition in a one-second window, which was then utilized as the training label for the DNN. The KLD was chosen to portray the deterioration of concrete specimens because of its ability to describe how much a signal is different from another. As the deterioration of the concrete specimens worsens, more significant activities can be expected in the AE signal. Afterward, an evaluation of the constructed HI was presented to verify its reliability in the prognosis task for concrete specimens. The evaluation was divided into two categories: fitness analysis of the construction result and

RUL prognosis using the constructed HI. Trendability and monotonicity were utilized as the metrics for fitness analysis, which showed a significant outperformance by the KLD HI in terms of trendability. This shows that the proposed HI has a strong correlation with time, and it is a promising candidate to capture the run-to-fail process of concrete structures. A comparison was also performed in the RUL prognosis on the proposed HI using LSTM and two state-of-the-art models 300, 400 and 500 time steps before the failure. The result of this comparison shows that even though GRU and LSTM shares comparable level of accuracy in shorter predictions, LSTM is capable of significantly outperforming other models in the longest one.

6.2 Future Work

In the future, the presented study can be further extended as follows:

- Leak localization can be integrated into this study, along with different scenarios, such as pipelines buried under soil or submerged in water. In addition, the limitation of a hard-threshold b -value can also be further researched to achieve a better description of AE activity.
- Multiple faults occurring simultaneously can be investigated for the fluid pipeline system.
- In future research, the proposed HI construction can be expanded to not just reinforced concrete beams, but also possibly bridges, walls, buildings, etc. It can also be greatly benefitted from covering the concrete crack localization, which provides more information for a preventive maintenance. Other optimization techniques and structures will also be investigated in future work to create a better construction model. We will also aim to approach the HI construction from the system- and fault-specific aspect, to which the finite element method (FEM) simulation shall be implemented along with Failure Mode, Effects, and Criticality Analysis (FMECA).

References

- [1] R. K. Miller, E. v. K. Hill, P. O. Moore, and American Society for Nondestructive Testing., *Acoustic emission testing*. American Society for Nondestructive Testing, 2005.
- [2] C. U. Grosse and M. Ohtsu, *Acoustic emission testing: Basics for Research–Applications in Civil Engineering*. Springer Berlin Heidelberg, 2008. doi: 10.1007/978-3-540-69972-9.
- [3] A. Olszewska, “Using the acoustic emission method for testing aboveground vertical storage tank bottoms,” *Applied Acoustics*, vol. 188, Jan. 2022, doi: 10.1016/j.apacoust.2021.108564.
- [4] G. Lackner, P. Ts, and C. Nig, “E WGAE2 0 0 2 ACOUSTIC EMISSION TESTING ON FLAT-BOTTOMED STORAGE TANKS: HOW TO CONDENSE ACQUIRED DATA TO A RELIABLE STATEMENT REGARDING FLOOR CONDITION,” 2002.
- [5] M. Ohtsu, T. Isoda, and Y. Tomoda, “ACOUSTIC EMISSION TECHNIQUES STANDARDIZED FOR CONCRETE STRUCTURES,” vol. 25, pp. 21–32, 2007.
- [6] T.-K. Nguyen, Z. Ahmad, and J. M. Kim, “A Scheme with Acoustic Emission Hit Removal for the Remaining Useful Life Prediction of Concrete Structures,” 2021.
- [7] S. A. Aye and P. S. Heyns, “An integrated Gaussian process regression for prediction of remaining useful life of slow speed bearings based on acoustic emission,” *Mech Syst Signal Process*, vol. 84, pp. 485–498, 2017, doi: 10.1016/j.ymsp.2016.07.039.
- [8] M. Meo, “6 - Acoustic emission sensors for assessing and monitoring civil infrastructures,” in *Sensor Technologies for Civil Infrastructures*, vol. 55, M. L. Wang, J. P. Lynch, and H. Sohn, Eds., in Woodhead Publishing Series in Electronic and Optical Materials, vol. 55. , Woodhead Publishing, 2014, pp. 159–178. doi: <https://doi.org/10.1533/9780857099136.159>.
- [9] J. Q. Huang, “Non-destructive evaluation (NDE) of composites: Acoustic emission (AE),” in *Non-Destructive Evaluation (NDE) of Polymer Matrix Composites*, Elsevier, 2013, pp. 12–32.
- [10] S. Ahmad, Z. Ahmad, C. H. Kim, and J. M. Kim, “A Method for Pipeline Leak Detection Based on Acoustic Imaging and Deep Learning,” *Sensors*, vol. 22, no. 4, Feb. 2022, doi: 10.3390/s22041562.
- [11] Z. Moradian and B. Q. Li, “Hit-based acoustic emission monitoring of rock fractures: Challenges and solutions,” *Springer Proceedings in Physics*, vol. 179, no. May, pp. 357–370, 2017, doi: 10.1007/978-3-319-29052-2_31.
- [12] C. Van Steen, H. Nasser, E. Verstrynge, and M. Wevers, “Acoustic emission source characterisation of chloride-induced corrosion damage in reinforced concrete,” *Struct Health Monit*, vol. 21, no. 3, pp. 1266–1286, 2022, doi: 10.1177/14759217211013324.
- [13] T. B. Quy and J. Kim, “Leak localization in industrial-fluid pipelines based on acoustic emission burst monitoring,” *Measurement*, vol. 151, p. 107150, 2020, doi: 10.1016/j.measurement.2019.107150.
- [14] V. Tra, J. Y. Kim, I. Jeong, and J. M. Kim, “An acoustic emission technique for crack modes classification in concrete structures,” *Sustainability (Switzerland)*, vol. 12, no. 17, pp. 1–12, 2020, doi: 10.3390/SU12176724.

- [15] T. Jia, H. Wang, X. Shen, Z. Jiang, and K. He, "Target localization based on structured total least squares with hybrid TDOA-AOA measurements," *Signal Processing*, vol. 143, pp. 211–221, Feb. 2018, doi: 10.1016/j.sigpro.2017.09.011.
- [16] X. Shang, Y. Wang, and R. Miao, "Acoustic emission source location from P-wave arrival time corrected data and virtual field optimization method," *Mech Syst Signal Process*, vol. 163, Jan. 2022, doi: 10.1016/j.ymssp.2021.108129.
- [17] M. J. Eaton, R. Pullin, and K. M. Holford, "Towards improved damage location using acoustic emission," *Proceedings of the Institution of Mechanical Engineers, Part C: Journal of Mechanical Engineering Science*, vol. 226, no. 9, pp. 2141–2153, Sep. 2012. doi: 10.1177/0954406212449582.
- [18] F. Ciampa and M. Meo, "Acoustic emission localization in complex dissipative anisotropic structures using a one-channel reciprocal time reversal method," *J Acoust Soc Am*, vol. 130, no. 1, pp. 168–175, Jul. 2011, doi: 10.1121/1.3598458.
- [19] P. Mirgal, J. Pal, and S. Banerjee, "Online acoustic emission source localization in concrete structures using iterative and evolutionary algorithms," *Ultrasonics*, vol. 108, Dec. 2020, doi: 10.1016/j.ultras.2020.106211.
- [20] Z. H. Liu, Q. L. Peng, X. Li, C. F. He, and B. Wu, "Acoustic Emission Source Localization with Generalized Regression Neural Network Based on Time Difference Mapping Method," *Exp Mech*, vol. 60, no. 5, pp. 679–694, Jun. 2020, doi: 10.1007/s11340-020-00591-8.
- [21] Y. Li, S. S. Yu, L. Dai, T. F. Luo, and M. Li, "Acoustic emission signal source localization on plywood surface with cross-correlation method," *Journal of Wood Science*, vol. 64, no. 2, pp. 78–84, Apr. 2018, doi: 10.1007/s10086-017-1672-x.
- [22] L. Chen, Y. Liu, F. Kong, and N. He, "Acoustic source localization based on generalized cross-correlation time-delay estimation," in *Procedia Engineering*, 2011, pp. 4912–4919. doi: 10.1016/j.proeng.2011.08.915.
- [23] F. Zhang, L. Pahlavan, and Y. Yang, "Evaluation of acoustic emission source localization accuracy in concrete structures," *Struct Health Monit*, vol. 19, no. 6, pp. 2063–2074, Nov. 2020, doi: 10.1177/1475921720915625.
- [24] A. Ebrahimkhanlou and S. Salamone, "Single-sensor acoustic emission source localization in plate-like structures using deep learning," *Aerospace*, vol. 5, no. 2, Apr. 2018, doi: 10.3390/aerospace5020050.
- [25] A. Ebrahimkhanlou and S. Salamone, "Acoustic emission source localization in thin metallic plates: A single-sensor approach based on multimodal edge reflections," *Ultrasonics*, vol. 78, pp. 134–145, Jul. 2017, doi: 10.1016/j.ultras.2017.03.006.
- [26] W. A. Shewhart *et al.*, "WILEY SERIES IN PROBABILITY AND STATISTICS Editors Emeritus," 1992. [Online]. Available: www.wiley.co.uk
- [27] Q. Du, V. Faber, and M. Gunzburger, "Centroidal Voronoi tessellations: Applications and algorithms," *SIAM Review*, vol. 41, no. 4, pp. 637–676, 1999, doi: 10.1137/S0036144599352836.
- [28] F. Bai, D. Gagar, P. Foote, and Y. Zhao, "Comparison of alternatives to amplitude thresholding for onset detection of acoustic emission signals," *Mech Syst Signal Process*, vol. 84, pp. 717–730, Feb. 2017, doi: 10.1016/j.ymssp.2016.09.004.

- [29] M. Ohtsu *et al.*, “Recommendation of RILEM TC 212-ACD: Acoustic emission and related NDE techniques for crack detection and damage evaluation in concrete: Test method for classification of active cracks in concrete structures by acoustic emission,” *Materials and Structures/Materiaux et Constructions*, vol. 43, no. 9, pp. 1187–1189, Nov. 2010, doi: 10.1617/s11527-010-9640-6.
- [30] E. N. Barkanov, A. Dumitrescu, and I. A. Parinov Editors, “Engineering Materials Non-destructive Testing and Repair of Pipelines.” [Online]. Available: <http://www.springer.com/series/4288>
- [31] M. M. Rosso, A. Aloisio, V. Randazzo, L. Tanzi, G. Cirrincione, and G. C. Marano, “Comparative deep learning studies for indirect tunnel monitoring with and without Fourier pre-processing,” *Integr Comput Aided Eng*, vol. Preprint, pp. 1–20, 2023, doi: 10.3233/ICA-230709.
- [32] J. Melchiorre, A. Manuello Bertetto, M. M. Rosso, and G. C. Marano, “Acoustic Emission and Artificial Intelligence Procedure for Crack Source Localization,” *Sensors*, vol. 23, no. 2, Jan. 2023, doi: 10.3390/s23020693.
- [33] Y. Yan, D. Liu, B. Gao, G. Y. Tian, and Z. C. Cai, “A Deep Learning-Based Ultrasonic Pattern Recognition Method for Inspecting Girth Weld Cracking of Gas Pipeline,” *IEEE Sens J*, vol. 20, no. 14, pp. 7997–8006, Jul. 2020, doi: 10.1109/JSEN.2020.2982680.
- [34] Z.-D. Xu, C. Zhu, and L.-W. Shao, “Damage Identification of Pipeline Based on Ultrasonic Guided Wave and Wavelet Denoising,” *J Pipeline Syst Eng Pract*, vol. 12, no. 4, p. 4021051, 2021, doi: 10.1061/(ASCE)PS.1949-1204.0000600.
- [35] L. Huang, X. Hong, Z. Yang, Y. Liu, and B. Zhang, “CNN-LSTM network-based damage detection approach for copper pipeline using laser ultrasonic scanning,” *Ultrasonics*, vol. 121, p. 106685, 2022, doi: <https://doi.org/10.1016/j.ultras.2022.106685>.
- [36] V. Jamshidi and R. Davarnejad, “Photon backscatter radiography application for the simulation of corrosion detection inside a pipeline: A novel proposal for 360° corrosion consideration in the pipelines,” *Applied Radiation and Isotopes*, vol. 176, Oct. 2021, doi: 10.1016/j.apradiso.2021.109844.
- [37] Y. Yasuda, F. Nabeshima, K. Horiuchi, and H. Nagai, “Visualization of the working fluid in a flat-plate pulsating heat pipe by neutron radiography,” *Int J Heat Mass Transf*, vol. 185, p. 122336, 2022, doi: <https://doi.org/10.1016/j.ijheatmasstransfer.2021.122336>.
- [38] N. Iftimie, A. Savin, R. Steigmann, and G. Dobrescu, “Underground pipeline identification into a non-destructive case study based on ground-penetrating radar imaging,” *Remote Sens (Basel)*, vol. 13, no. 17, Sep. 2021, doi: 10.3390/rs13173494.
- [39] F. Khodayar, S. Sojasi, and X. Maldague, “Infrared thermography and NDT: 2050 horizon,” *Quantitative InfraRed Thermography Journal*, vol. 13, no. 2. Taylor and Francis Ltd., pp. 210–231, Jul. 02, 2016. doi: 10.1080/17686733.2016.1200265.
- [40] Z. Chen *et al.*, “Detecting gas pipeline leaks in sandy soil with fiber-optic distributed acoustic sensing,” *Tunnelling and Underground Space Technology*, vol. 141, p. 105367, Nov. 2023, doi: 10.1016/J.TUST.2023.105367.
- [41] H. J. Li, H. H. Zhu, D. Y. Tan, B. Shi, and J. H. Yin, “Detecting pipeline leakage using active distributed temperature Sensing: Theoretical modeling and experimental verification,” *Tunnelling and Underground Space Technology*, vol. 135, p. 105065, May 2023, doi: 10.1016/J.TUST.2023.105065.
- [42] S. W. Rienstra and A. Hirschberg, “An Introduction to Acoustics,” 2021.

- [43] A. Bobrov and M. Kuten, "Intellectual Innovations in Acoustic Emission Control in the Safety System of Pipeline Transport," in *Transportation Research Procedia*, Elsevier B.V., 2021, pp. 340–345. doi: 10.1016/j.trpro.2021.02.081.
- [44] M. F. Siddique, Z. Ahmad, and J.-M. Kim, "Pipeline leak diagnosis based on leak-augmented scalograms and deep learning," *Engineering Applications of Computational Fluid Mechanics*, vol. 17, no. 1, Dec. 2023, doi: 10.1080/19942060.2023.2225577.
- [45] T. B. Quy and J. M. Kim, "Leak localization in industrial-fluid pipelines based on acoustic emission burst monitoring," *Measurement (Lond)*, vol. 151, Feb. 2020, doi: 10.1016/j.measurement.2019.107150.
- [46] T. B. Quy and J. M. Kim, "Crack detection and localization in a fluid pipeline based on acoustic emission signals," *Mech Syst Signal Process*, vol. 150, Mar. 2021, doi: 10.1016/j.ymsp.2020.107254.
- [47] A. B. Lukonge and X. Cao, "Leak Detection System for Long-Distance Onshore and Offshore Gas Pipeline Using Acoustic Emission Technology. A Review," *Transactions of the Indian Institute of Metals*, vol. 73, no. 7. Springer, pp. 1715–1727, Jul. 01, 2020. doi: 10.1007/s12666-020-02002-x.
- [48] C. Xu, S. Du, P. Gong, Z. Li, G. Chen, and G. Song, "An Improved Method for Pipeline Leakage Localization with a Single Sensor Based on Modal Acoustic Emission and Empirical Mode Decomposition with Hilbert Transform," *IEEE Sens J*, vol. 20, no. 10, pp. 5480–5491, May 2020, doi: 10.1109/JSEN.2020.2971854.
- [49] N. C. Hii, C. K. Tan, S. J. Wilcox, and Z. S. Chong, "An investigation of the generation of Acoustic Emission from the flow of particulate solids in pipelines," *Powder Technol*, vol. 243, pp. 120–129, Jul. 2013, doi: 10.1016/j.powtec.2013.03.038.
- [50] M. G. Droubi, R. L. Reuben, and J. I. Steel, "Flow noise identification using acoustic emission (AE) energy decomposition for sand monitoring in flow pipeline," *Applied Acoustics*, vol. 131, pp. 5–15, Feb. 2018, doi: 10.1016/j.apacoust.2017.10.016.
- [51] F. Nosedá *et al.*, "A Neural Network System for Fault Prediction in Pipelines by Acoustic Emission Techniques," *Research in Nondestructive Evaluation*, vol. 32, no. 3–4, pp. 132–146, 2021, doi: 10.1080/09349847.2021.1930305.
- [52] N. K. Banjara, S. Sasmal, and S. Voggu, "Machine learning supported acoustic emission technique for leakage detection in pipelines," *International Journal of Pressure Vessels and Piping*, vol. 188, Dec. 2020, doi: 10.1016/j.ijpvp.2020.104243.
- [53] C. Xu, S. Du, P. Gong, Z. Li, G. Chen, and G. Song, "An Improved Method for Pipeline Leakage Localization with a Single Sensor Based on Modal Acoustic Emission and Empirical Mode Decomposition with Hilbert Transform," *IEEE Sens J*, vol. 20, no. 10, pp. 5480–5491, May 2020, doi: 10.1109/JSEN.2020.2971854.
- [54] X. Hu, H. Zhang, D. Ma, and R. Wang, "A tnGAN-Based Leak Detection Method for Pipeline Network Considering Incomplete Sensor Data," *IEEE Trans Instrum Meas*, vol. 70, 2021, doi: 10.1109/TIM.2020.3045843.
- [55] H. Fu, L. Yang, H. Liang, S. Wang, and K. Ling, "Diagnosis of the single leakage in the fluid pipeline through experimental study and CFD simulation," *J Pet Sci Eng*, vol. 193, Oct. 2020, doi: 10.1016/j.petrol.2020.107437.
- [56] X. K. Zhu, W. R. Johnson, R. Sindelar, and B. Wiersma, "Artificial neural network models of burst strength for thin-wall pipelines," *Journal of Pipeline Science and Engineering*, vol. 2, no. 4, Dec. 2022, doi: 10.1016/j.jpse.2022.100090.

- [57] N. V. S. Korlapati, F. Khan, Q. Noor, S. Mirza, and S. Vaddiraju, "Review and analysis of pipeline leak detection methods," *Journal of Pipeline Science and Engineering*, vol. 2, no. 4. KeAi Communications Co., Dec. 01, 2022. doi: 10.1016/j.jpse.2022.100074.
- [58] C. Liu, Y. Li, and M. Xu, "An integrated detection and location model for leakages in liquid pipelines," *J Pet Sci Eng*, vol. 175, pp. 852–867, Apr. 2019, doi: 10.1016/j.petrol.2018.12.078.
- [59] D. Zaman, M. K. Tiwari, A. K. Gupta, and D. Sen, "A review of leakage detection strategies for pressurised pipeline in steady-state," *Engineering Failure Analysis*, vol. 109. Elsevier Ltd, Jan. 01, 2020. doi: 10.1016/j.engfailanal.2019.104264.
- [60] W. Wang, X. Mao, H. Liang, D. Yang, J. Zhang, and S. Liu, "Experimental research on in-pipe leaks detection of acoustic signature in gas pipelines based on the artificial neural network," *Measurement (Lond)*, vol. 183, Oct. 2021, doi: 10.1016/j.measurement.2021.109875.
- [61] F. Wang, W. Lin, Z. Liu, S. Wu, and X. Qiu, "Pipeline Leak Detection by Using Time-Domain Statistical Features," *IEEE Sens J*, vol. 17, no. 19, pp. 6431–6442, Oct. 2017, doi: 10.1109/JSEN.2017.2740220.
- [62] T. Bui Quy and J. M. Kim, "Leak detection in a gas pipeline using spectral portrait of acoustic emission signals," *Measurement (Lond)*, vol. 152, Feb. 2020, doi: 10.1016/j.measurement.2019.107403.
- [63] J. Sun, Q. Xiao, J. Wen, and Y. Zhang, "Natural gas pipeline leak aperture identification and location based on local mean decomposition analysis," *Measurement (Lond)*, vol. 79, pp. 147–157, Feb. 2016, doi: 10.1016/j.measurement.2015.10.015.
- [64] S. Pan, Z. Xu, D. Li, and D. Lu, "Research on detection and location of fluid-filled pipeline leakage based on acoustic emission technology," *Sensors (Switzerland)*, vol. 18, no. 11, 2018, doi: 10.3390/s18113628.
- [65] X. Lang and W. Yuan, "Localization Method of Multiple Leaks Based on Time-Frequency Analysis and Improved Differential Evolution," *IEEE Sens J*, vol. 20, no. 23, pp. 14383–14390, Dec. 2020, doi: 10.1109/JSEN.2020.3009091.
- [66] W. Wang, H. Sun, J. Guo, L. Lao, S. Wu, and J. Zhang, "Experimental study on water pipeline leak using In-Pipe acoustic signal analysis and artificial neural network prediction," *Measurement (Lond)*, vol. 186, Dec. 2021, doi: 10.1016/j.measurement.2021.110094.
- [67] A. Keramat and H. F. Duan, "Spectral based pipeline leak detection using a single spatial measurement," *Mech Syst Signal Process*, vol. 161, Dec. 2021, doi: 10.1016/j.ymsp.2021.107940.
- [68] A. A. Carvalho, J. M. A. Rebello, M. P. V. Souza, L. V. S. Sagrilo, and S. D. Soares, "Reliability of non-destructive test techniques in the inspection of pipelines used in the oil industry," *International Journal of Pressure Vessels and Piping*, vol. 85, no. 11. pp. 745–751, Nov. 2008. doi: 10.1016/j.ijpvp.2008.05.001.
- [69] R. R. Heinrich, "Seismicity of the Earth and Associated Phenomena. B. Gutenberg and C. F. Richter. Princeton, N. J.: Princeton Univ. Press, 1949. 273 pp. \$10.00.," *Science (1979)*, vol. 111, no. 2886, p. 437, 1950, doi: 10.1126/science.111.2886.437.a.
- [70] M. Rinne, B. Shen, H.-S. Lee, and L. Jing, "THERMO-MECHANICAL SIMULATIONS OF PILLAR SPALLING IN SKB APSE TEST BY FRACOD."

- [71] D. Jung, W. R. Yu, H. Ahn, and W. Na, "New b-value parameter for quantitatively monitoring the structural health of carbon fiber-reinforced composites," *Mech Syst Signal Process*, vol. 165, Feb. 2022, doi: 10.1016/j.ymssp.2021.108328.
- [72] F. Sagasta, M. E. Zitto, R. Piotrkowski, A. Benavent-Climent, E. Suarez, and A. Gallego, "Acoustic emission energy b-value for local damage evaluation in reinforced concrete structures subjected to seismic loadings," *Mech Syst Signal Process*, vol. 102, pp. 262–277, Mar. 2018, doi: 10.1016/j.ymssp.2017.09.022.
- [73] R. V. Sagar, B. K. R. Prasad, and S. S. Kumar, "An experimental study on cracking evolution in concrete and cement mortar by the b-value analysis of acoustic emission technique," *Cem Concr Res*, vol. 42, no. 8, pp. 1094–1104, 2012, doi: 10.1016/j.cemconres.2012.05.003.
- [74] F. A. Sagasta, "Analysis of Evaluation in R Subjected to Acous." [Online]. Available: <http://creativecommons.org/license>
- [75] D. Jung, W. R. Yu, and W. Na, "Use of acoustic emission b(Ib)-values to quantify damage in composites," *Composites Communications*, vol. 22, Dec. 2020, doi: 10.1016/j.coco.2020.100499.
- [76] I. Batal, D. Fradkin, J. Harrison, F. Moerchen, and M. Hauskrecht, "Mining Recent Temporal Patterns for Event Detection in Multivariate Time Series Data," in *Proceedings of the 18th ACM SIGKDD International Conference on Knowledge Discovery and Data Mining*, in KDD '12. New York, NY, USA: Association for Computing Machinery, 2012, pp. 280–288. doi: 10.1145/2339530.2339578.
- [77] K. Zhao *et al.*, "Detecting change-point, trend, and seasonality in satellite time series data to track abrupt changes and nonlinear dynamics: A Bayesian ensemble algorithm," *Remote Sens Environ*, vol. 232, Oct. 2019, doi: 10.1016/j.rse.2019.04.034.
- [78] M. Mudelsee, "Trend analysis of climate time series: A review of methods," *Earth-Science Reviews*, vol. 190. Elsevier B.V., pp. 310–322, Mar. 01, 2019. doi: 10.1016/j.earscirev.2018.12.005.
- [79] J. A. Hoeting, D. Madigan, A. E. Raftery, and C. T. Volinsky, "Bayesian model averaging: a tutorial (with comments by M. Clyde, David Draper and E. I. George, and a rejoinder by the authors)," *Statistical Science*, vol. 14, no. 4, pp. 382 – 417, 1999, doi: 10.1214/ss/1009212519.
- [80] L. Breiman, "Random Forests," 2001.
- [81] Y. Amit and D. Geman, "Communicated by Shimon Ullman Shape Quantization and Recognition with Randomized Trees," 1997.
- [82] G. Biau and E. Scornet, "A random forest guided tour," *Test*, vol. 25, no. 2, pp. 197–227, Jun. 2016, doi: 10.1007/s11749-016-0481-7.
- [83] *Ensemble Machine Learning*. Springer US, 2012. doi: 10.1007/978-1-4419-9326-7.
- [84] M. M. Rosso, A. Aloisio, J. Parol, G. C. Marano, and G. Quaranta, "Intelligent automatic operational modal analysis," *Mech Syst Signal Process*, vol. 201, p. 110669, Oct. 2023, doi: 10.1016/J.YMSSP.2023.110669.
- [85] N. N. Hsu and B. FR, "Characterization and calibration of acoustic emission sensors," 1981.
- [86] C. Abarkane, F. J. Rescalvo, and Á. Donaire-, "Temporal Acoustic Emission Index for Damage Monitoring of RC Structures Subjected to Bidirectional Seismic Loadings," 2019.

- [87] D. G. Aggelis, A. C. Mpalaskas, and T. E. Matikas, "Investigation of different fracture modes in cement-based materials by acoustic emission," *Cement and Concrete Research*, vol. 48, pp. 1–8, 2013, doi: 10.1016/j.cemconres.2013.02.002.
- [88] M. Flansbjer and J. E. Lindqvist, "Meso Mechanical Study of Cracking Process in Concrete Subjected to Tensile Loading," no. 2, pp. 13–29, 2018, doi: 10.2478/ncr-2018-0012.
- [89] K. Ohno and M. Ohtsu, "Crack classification in concrete based on acoustic emission," *Construction and Building Materials*, vol. 24, no. 12, pp. 2339–2346, 2010, doi: 10.1016/j.conbuildmat.2010.05.004.
- [90] J. Wolf, S. Pirskawetz, and A. Zang, "Detection of crack propagation in concrete with embedded ultrasonic sensors," *Engineering Fracture Mechanics*, vol. 146, pp. 161–171, 2015, doi: 10.1016/j.engfracmech.2015.07.058.
- [91] Q. Han, G. Yang, J. Xu, Z. Fu, G. Lacidogna, and A. Carpinteri, "Acoustic emission data analyses based on crumb rubber concrete beam bending tests," *Engineering Fracture Mechanics*, vol. 210, no. May 2018, pp. 189–202, 2019, doi: 10.1016/j.engfracmech.2018.05.016.
- [92] J. Wang, P. A. M. Basheer, S. V. Nanukuttan, A. E. Long, and Y. Bai, "Influence of service loading and the resulting micro-cracks on chloride resistance of concrete," *Construction and Building Materials*, vol. 108, pp. 56–66, 2016, doi: 10.1016/j.conbuildmat.2016.01.005.
- [93] A. Karimipour and V. Farhangi, "Effect of EBR- and EBROG-GFRP laminate on the structural performance of corroded reinforced concrete columns subjected to a hysteresis load," *Structures*, vol. 34, no. September, pp. 1525–1544, 2021, doi: 10.1016/j.istruc.2021.08.089.
- [94] Y. Wang, Y. Peng, Y. Zi, X. Jin, and K. L. Tsui, "A Two-Stage Data-Driven-Based Prognostic Approach for Bearing Degradation Problem," *IEEE Transactions on Industrial Informatics*, vol. 12, no. 3, pp. 924–932, 2016, doi: 10.1109/TII.2016.2535368.
- [95] V. Tra, T. K. Nguyen, C. H. Kim, and J. M. Kim, "Health indicators construction and remaining useful life estimation for concrete structures using deep neural networks," *Applied Sciences (Switzerland)*, vol. 11, no. 9, 2021, doi: 10.3390/app11094113.
- [96] M. Xia, T. Li, T. Shu, J. Wan, C. W. De Silva, and Z. Wang, "A Two-Stage Approach for the Remaining Useful Life Prediction of Bearings Using Deep Neural Networks," *IEEE Transactions on Industrial Informatics*, vol. 15, no. 6, pp. 3703–3711, 2019, doi: 10.1109/TII.2018.2868687.
- [97] P. R. de O. da Costa, A. Akçay, Y. Zhang, and U. Kaymak, "Remaining useful lifetime prediction via deep domain adaptation," *Reliability Engineering and System Safety*, vol. 195, pp. 1–30, 2020, doi: 10.1016/j.ress.2019.106682.
- [98] T. Tornede, A. Tornede, M. Wever, and E. Hüllermeier, "Coevolution of remaining useful lifetime estimation pipelines for automated predictive maintenance," *GECCO 2021 - Proceedings of the 2021 Genetic and Evolutionary Computation Conference*, pp. 368–376, 2021, doi: 10.1145/3449639.3459395.
- [99] C. Gables, "intensity measurements," pp. 214–220, 1987.
- [100] J. Chakraborty, A. Katunin, P. Klikowicz, and M. Salamak, "Early crack detection of reinforced concrete structure using embedded sensors," *Sensors (Switzerland)*, vol. 19, no. 18, pp. 1–22, 2019, doi: 10.3390/s19183879.

- [101] Q. Zhang and Z. Xiong, "Crack Detection of Reinforced Concrete Structures Based on BOFDA and FBG Sensors," *Shock and Vibration*, vol. 2018, 2018, doi: 10.1155/2018/6563537.
- [102] Z. Ahmad, A. Rai, A. S. Maliuk, and J. M. Kim, "Discriminant feature extraction for centrifugal pump fault diagnosis," *IEEE Access*, vol. 8, pp. 165512–165528, 2020, doi: 10.1109/ACCESS.2020.3022770.
- [103] A. Mohan and S. Poobal, "Crack detection using image processing : A critical review and analysis," *Alexandria Engineering Journal*, vol. 57, no. 2, pp. 787–798, 2018, doi: 10.1016/j.aej.2017.01.020.
- [104] Y. Wang *et al.*, "Research on Crack Detection Algorithm of the Concrete Bridge Based on Image Processing," *Procedia Computer Science*, vol. 154, pp. 610–616, 2018, doi: 10.1016/j.procs.2019.06.096.
- [105] D. G. Aggelis, "Classification of cracking mode in concrete by acoustic emission parameters," *Mechanics Research Communications*, vol. 38, no. 3, pp. 153–157, 2011, doi: 10.1016/j.mechrescom.2011.03.007.
- [106] M. Elforjani and S. Shanbr, "Prognosis of Bearing Acoustic Emission Signals Using Supervised Machine Learning," *IEEE Transactions on Industrial Electronics*, vol. 65, no. 7, pp. 5864–5871, 2018, doi: 10.1109/TIE.2017.2767551.
- [107] F. Pinal Moctezuma, M. Delgado Prieto, and L. Romeral Martinez, "Performance analysis of acoustic emission hit detection methods using time features," *IEEE Access*, vol. 7, no. c, pp. 71119–71130, 2019, doi: 10.1109/ACCESS.2019.2919224.
- [108] Z. Song, T. Frühwirt, and H. Konietzky, "Fatigue characteristics of concrete subjected to indirect cyclic tensile loading: Insights from deformation behavior, acoustic emissions and ultrasonic wave propagation," *Constr Build Mater*, vol. 302, p. 124386, 2021, doi: <https://doi.org/10.1016/j.conbuildmat.2021.124386>.
- [109] H. Xargay, M. Ripani, P. Folino, N. Núñez, and A. Caggiano, "Acoustic emission and damage evolution in steel fiber-reinforced concrete beams under cyclic loading," *Construction and Building Materials*, vol. 274, p. 121831, 2021, doi: <https://doi.org/10.1016/j.conbuildmat.2020.121831>.
- [110] C. Bian, J.-Y. Wang, and J.-Y. Guo, "Damage mechanism of ultra-high performance fibre reinforced concrete at different stages of direct tensile test based on acoustic emission analysis," *Construction and Building Materials*, vol. 267, p. 120927, 2021, doi: <https://doi.org/10.1016/j.conbuildmat.2020.120927>.
- [111] R. K. Miller, E. K. Hill, and P. O. Moore, *Third Edition Technical Editors*.
- [112] K. T. P. Nguyen and K. Medjaher, "An automated health indicator construction methodology for prognostics based on multi-criteria optimization," *ISA Trans*, vol. 113, pp. 81–96, 2021, doi: 10.1016/j.isatra.2020.03.017.
- [113] J. Li, Y. Zi, Y. Wang, and Y. Yang, "Health indicator construction method of bearings based on Wasserstein dual-domain adversarial networks under normal data only," *IEEE Transactions on Industrial Electronics*, p. 1, 2022, doi: 10.1109/TIE.2022.3156148.
- [114] A. González-Muñiz, I. Díaz, A. A. Cuadrado, and D. García-Pérez, "Health indicator for machine condition monitoring built in the latent space of a deep autoencoder," *Reliability Engineering & System Safety*, vol. 224, p. 108482, 2022, doi: <https://doi.org/10.1016/j.ress.2022.108482>.

- [115] P. Wen, S. Zhao, S. Chen, and Y. Li, "A generalized remaining useful life prediction method for complex systems based on composite health indicator," *Reliability Engineering & System Safety*, vol. 205, p. 107241, 2021, doi: <https://doi.org/10.1016/j.ress.2020.107241>.
- [116] S. Shukla, R. N. Yadav, J. Sharma, and S. Khare, "Analysis of statistical features for fault detection in ball bearing," in *2015 IEEE International Conference on Computational Intelligence and Computing Research (ICCIC)*, 2015, pp. 1–7. doi: 10.1109/ICCIC.2015.7435755.
- [117] A. K. Mahamad and T. Hiyama, "Development of artificial neural network based fault diagnosis of induction motor dearing," in *2008 IEEE 2nd International Power and Energy Conference*, 2008, pp. 1387–1392. doi: 10.1109/PECON.2008.4762695.
- [118] J. Yu, "Local and Nonlocal Preserving Projection for Bearing Defect Classification and Performance Assessment," *IEEE Transactions on Industrial Electronics*, vol. 59, no. 5, pp. 2363–2376, 2012, doi: 10.1109/TIE.2011.2167893.
- [119] V. C. M. N. Leite *et al.*, "Detection of Localized Bearing Faults in Induction Machines by Spectral Kurtosis and Envelope Analysis of Stator Current," *IEEE Transactions on Industrial Electronics*, vol. 62, no. 3, pp. 1855–1865, 2015, doi: 10.1109/TIE.2014.2345330.
- [120] B. P. Duong *et al.*, "A Reliable Health Indicator for Fault Prognosis of Bearings," *Sensors*, vol. 18, no. 11, 2018, doi: 10.3390/s18113740.
- [121] K. Liu, N. Z. Gebraeel, and J. Shi, "A Data-Level Fusion Model for Developing Composite Health Indices for Degradation Modeling and Prognostic Analysis," *IEEE Transactions on Automation Science and Engineering*, vol. 10, no. 3, pp. 652–664, 2013, doi: 10.1109/TASE.2013.2250282.
- [122] A. Geron, *Hands-On Machine Learning with Scikit-Learn and TensorFlow 2nd edition*. O'Reilly Media, 2019.
- [123] A. Thieullen, M. Ouladsine, and J. Pinaton, "A Survey of Health Indicators and Data-Driven Prognosis in Semiconductor Manufacturing Process," *IFAC Proceedings Volumes*, vol. 45, no. 20, pp. 19–24, 2012, doi: <https://doi.org/10.3182/20120829-3-MX-2028.00246>.
- [124] A. Mosallam, K. Medjaher, and N. Zerhouni, "Data-driven prognostic method based on Bayesian approaches for direct remaining useful life prediction," *Journal of Intelligent Manufacturing*, vol. 27, no. 5, pp. 1037–1048, 2016, doi: 10.1007/s10845-014-0933-4.
- [125] T. Han, C. Liu, W. Yang, and D. Jiang, "Learning transferable features in deep convolutional neural networks for diagnosing unseen machine conditions," *ISA Transactions*, vol. 93, pp. 341–353, 2019, doi: <https://doi.org/10.1016/j.isatra.2019.03.017>.
- [126] N. Gugulothu, T. R. Vishnu, P. Malhotra, L. Vig, P. Agarwal, and G. M. Shroff, "Predicting Remaining Useful Life using Time Series Embeddings based on Recurrent Neural Networks," *ArXiv*, vol. abs/1709.0, 2017.
- [127] O. Bektas, J. A. Jones, S. Sankararaman, I. Roychoudhury, and K. Goebel, "A neural network filtering approach for similarity-based remaining useful life estimation," *The International Journal of Advanced Manufacturing Technology*, vol. 101, no. 1, pp. 87–103, 2019, doi: 10.1007/s00170-018-2874-0.
- [128] L. Liao, "Discovering Prognostic Features Using Genetic Programming in Remaining Useful Life Prediction," *IEEE Transactions on Industrial Electronics*, vol. 61, no. 5, pp. 2464–2472, 2014, doi: 10.1109/TIE.2013.2270212.

- [129] H. L. S., "Theory of Probability 2nd Ed.," *Journal of the Institute of Actuaries (1886-1994)*, vol. 75, no. 2, pp. 262-264, 1949.
- [130] S. Kullback and R. A. Leibler, "On Information and Sufficiency," *The Annals of Mathematical Statistics*, vol. 22, no. 1, pp. 79-86, 1951, doi: 10.1214/aoms/1177729694.

Tuan-Khai Nguyen

*Graduate Research Assistant
Department of Electric, Electronics & Computer
Engineering, University of Ulsan
Republic of Korea (South Korea)*

Address: 93 Daehak-ro, Nam-Gu, Ulsan, 44610, Korea

Email: ntkhaiwork@gmail.com

Website: <https://khaint.weebly.com/>
<https://www.linkedin.com/in/ntkhai/>
<https://www.researchgate.net/profile/Tuan-Khai-Nguyen>

SHORT BIOGRAPHY

Tuan-Khai Nguyen is an experienced researcher with **6 years of state-of-the-art research in both industrial and academic environments**, including prestigious institutions such as VIETTEL R&D Institute (Vietnam) and University of Ulsan (South Korea). He is currently a PhD candidate in the Ulsan Industrial Artificial Intelligence (UIAI) Laboratory, University of Ulsan (South Korea). During his 6-year period of working and researching, Tuan-Khai Nguyen has authored and co-authored 14 paper journals, 1 book chapter and 2 conference papers. His research expertise is related but not limited to Acoustic Emission, Anomaly Detection, Artificial Intelligence, Deep Learning, Fault Diagnosis and Prognosis, Machine Learning and Signal Processing. He has an expert level of skill for algorithm implementation in Python and MATLAB concerning the previously mentioned topics. During his PhD course, Tuan-Khai Nguyen was awarded with the scholarship from Brain Korea 21 Program.

RESEARCH BACKGROUND AND INTERESTS

Acoustic Emission, Anomaly Detection, Artificial Intelligence, Deep Learning, Fault Detection and Diagnosis, Machine Learning, Signal Processing.

EDUCATION

[Master & PhD.] | [University of Ulsan]
[2020] – [NOW]

- **Major:** Computer Engineering.
- **Research:** Fault Diagnosis & Prognosis for Structures and Industrial Equipment.
- **Advisor:** Jong-Myon Kim, PhD., Professor.
- **Scholarship:** BK21+ Scholarship for Combined Master & PhD. Course under BrainKorea21 Plus (BK21+) project by the Government of South Korea.

[Bachelor] | [University of Engineering and Technology – UET-VNU]
[2014] – [2018]

- **Major:** Electronics & Communication Engineering.

Curriculum Vitae

- **Research:** Signal Processing for wearable-sensor systems.
- **Advisor:** Duc-Tan Tran, PhD., Professor.
- **Award:** 2nd Prize in the UET Research contest on "Development of a Real-time System to Predict and Detect Line-of-duty Firefighter Injuries"
- **Thesis:** "Adaptive step length estimation supporting Indoor Positioning System using Inertial Measurement Units".

[Master & PhD.] | [University of Ulsan]

[2020] – [NOW]

- **Major:** Computer Engineering.
- **Research:** Fault Diagnosis & Prognosis for Structures and Industrial Equipment.
- **Advisor:** Jong-Myon Kim, PhD., Professor.
- **Scholarship:** BK21+ Scholarship for Combined Master & PhD. Course under BrainKorea21 Plus (BK21+) project by the Government of South Korea.

WORK EXPERIENCE

[Researcher] | [Ulsan Industrial AI Lab, University of Ulsan]

[2020] – [Now] Fault Diagnosis/Prognosis Researcher for Structures and Industrial Machineries

[DSP Engineer] | [Technologies Research Center - Information and Electronic Warfare, Viettel High Technology Industries Corporation, VIETTEL Group]

[2018] – [2019] Digital Signal Processing Researcher for Military Devices

SKILLS

- **Research:** Good understanding of concepts related to Acoustic Emission, Anomaly Detection, Artificial Intelligence, Deep Learning, Fault Detection and Diagnosis, Machine Learning and Signal Processing with experience of industrial work, academic research and being a teaching assistant.
- **Languages:**
 - **English:** 7.0 IELTS (7.0 Writing, 7.5 Reading and Listening, 6.0 Speaking); proficient in communication with fluency and coherence; proficient of formal writing and reading.
 - **French:** Intermediate.
 - **Korean:** Beginner.
 - **Vietnamese:** Native.
- **Programming languages:** MATLAB, Python, C, C#.

- **Others**
 - Effective in teamwork and working individually.
 - Experienced with speaking in front of an audience.
 - Efficacious with time management.

RESEARCH TIMELINE

- **2020-Now:** graduate researcher at UIAI laboratory.
 - **2022-Now:** The research mainly focused on **Industrial pipeline leak diagnosis**.
 - **2021-2022:** The research mainly focused on **Leak detection and localization in cylinder tank** and **centrifugal pump fault diagnosis**.
 - **2020-2021:** The research mainly focused on **Reinforced concrete useful lifetime prediction**.
- **2018-2020:** the research mainly focused on **Military Devices, Activity Recognition project, Car Safe, and Boat Safe**.
 - **2018-2019:** Researched **militaries devices**.
 - **2018:** Researched sensors data calibration. Proposed a method for calibration of abnormally abrupt change in barometer data. Also proposed and simulated **Car Safe** project algorithm. Published 2 journal papers for **Boat Safe** and **Car Safe** during this period.
- **2016-2018:** worked as an Assistant-Researcher in projects on **Indoor Positioning System & Injuries of line-of-duty firefighters**.
 - **2017-2018:** Researched and proposed an improvement to achieve a novel adaptive step counting and an adaptive length estimation for **Indoor Positioning System**.
 - **2016-2017:** Researched **line-of-duty firefighter injuries** due to gas poison warning, falling, heart-stroke and more, using sensor fusion.

PUBLICATIONS

Journal Publications

1. Nguyen, D.-T.; **Nguyen, T.-K.**; Ahmad, Z.; Kim, J.-M. A Reliable Pipeline Leak Detection Method Using Acoustic Emission with Time Difference of Arrival and Kolmogorov–Smirnov Test. *Sensors* 2023, 23, 9296. <https://doi.org/10.3390/s23239296>
2. **Nguyen, T.-K.**; Ahmad, Z.; Kim, J.-M. Leak State Detection and Size Identification for Fluid Pipelines with a Novel Acoustic Emission Intensity Index and Random Forest. *Sensors* 2023, 23, 9087. <https://doi.org/10.3390/s23229087>
3. Z. Ahmad, **T. K. Nguyen**, A. Rai, and J. M. Kim, "Industrial fluid pipeline leak detection and localization based on a multiscale Mann-Whitney test and acoustic emission event tracking," *Mech Syst Signal Process*, vol. 189, Apr. 2023, doi: 10.1016/j.ymssp.2022.110067 (**IF=8.934; Rank 1/177 by JCI, Rank 4/137 by JIF; JIF Percentile 97.45%**)
4. Z. Ahmad, **T. K. Nguyen**, and J. M. Kim, "Leak detection and size identification in fluid pipelines using a novel vulnerability index and 1-D convolutional neural network," *Engineering Applications of Computational Fluid Mechanics*, vol. 17, no. 1, 2023, doi: 10.1080/19942060.2023.2165159 (**IF=6.519; Rank 3/177 by JCI, Rank 9/137 by JIF; JIF Percentile 93.8%**)

5. **Nguyen, T.-K.**; Ahmad, Z.; Kim, J.-M. Leak Localization on Cylinder Tank Bottom Using Acoustic Emission. *Sensors* 2023, 23, 27. <https://doi.org/10.3390/s23010027>
6. **Nguyen, T.-K.**; Ahmad, Z.; Kim, J.-M. A Deep-Learning-Based Health Indicator Constructor Using Kullback–Leibler Divergence for Predicting the Remaining Useful Life of Concrete Structures. *Sensors* 2022, 22, 3687. <https://doi.org/10.3390/s22103687>
7. Ahmad, Z.; **Nguyen, T.-K.**; Ahmad, S.; Nguyen, C.D.; Kim, J.-M. Multistage Centrifugal Pump Fault Diagnosis Using Informative Ratio Principal Component Analysis. *Sensors* 2022, 22, 179. <https://doi.org/10.3390/s22010179>
8. **Nguyen, T.-K.**; Ahmad, Z.; Kim, J.-M. A Scheme with Acoustic Emission Hit Removal for the Remaining Useful Life Prediction of Concrete Structures. *Sensors* 2021, 21, 7761. <https://doi.org/10.3390/s21227761>
9. Tra, V.; **Nguyen, T.-K.**; Kim, C.-H.; Kim, J.-M. Health Indicators Construction and Remaining Useful Life Estimation for Concrete Structures Using Deep Neural Networks. *Appl. Sci.* 2021, 11, 4113. <https://doi.org/10.3390/app11094113>
10. N. D. Anh, P. V. Thanh, D. T. Lap, **N. T. Khai**, T. V. An, T. D. Tan, N. H. An and D. N. Dinh, "Efficient Forest Fire Detection using Rule-Based Multi-color Space and Correlation Coefficient for Application in Unmanned Aerial Vehicles," *KSII Transactions on Internet and Information Systems*, vol. 16, no. 2, pp. 381-404, 2022. DOI: 10.3857/tiis.2022.02.002.
11. Quang-Huy, T., **Nguyen, K.**, Doan, P. et al. Interpolated hybrid DBIM approach for enhanced imaging in ultrasound tomography. *Res. Biomed. Eng.* 38, 389–400 (2022). <https://doi.org/10.1007/s42600-021-00192-x>
12. Quang-Huy, T., **Nguyen, T.**, Solanki, V. K., & Tran, D. (2022). An Enhanced Multi-Frequency Distorted Born Iterative Method for Ultrasound Tomography Based on Fundamental Tone and Overtones. *International Journal of Information Retrieval Research (IJRR)*, 12(1), 1-19. <http://doi.org/10.4018/IJRR.289608>
13. **Tuan Nguyen, K.**, Van Pham, T., Nguyen, V. D., Thanh Do, L., Tran, A.-V., & Tran, D.-T. (2020). Development of a Smartphone Application for Safe Car Driving Using Google API and Built-in Sensor. *International Journal of Interactive Mobile Technologies (IJIM)*, 14(02), pp. 178–195. <https://doi.org/10.3991/ijim.v14i02.11118>
14. **Khai, T.N.**, Quang, T.V., Van, D.N., Long, T.D., Duc-Tan, T., 2019. Boat Safe: a smartphone application for safe Inland Waterway Transportation. *Int. J.Simulation: Systems Sci. Technol.* 10, 1–8

Book Chapters and Conference Publications

1. **Nguyen, TK**, Ahmad, Z., Kim, Jm. (2022). Comparison of Health Indicators Construction for Concrete Structure Using Acoustic Emission Hit and Kullback-Leibler Divergence. In: Dang, T.K., Küng, J., Chung, T.M. (eds) Future Data and Security Engineering. Big Data, Security and Privacy, Smart City and Industry 4.0 Applications. FDSE 2022. Communications in Computer and Information Science, vol 1688. Springer, Singapore. https://doi.org/10.1007/978-981-19-8069-5_41
2. V. T. Pham, **T. Khai Nguyen**, D. A. Nguyen, N. Dinh Dang, H. T. Huynh and D. -T. Tran, "Adaptive Step Length Estimation Support Indoor Positioning System using Low-Cost Inertial Measurement Units," 2020 IEEE Eighth International Conference on Communications and Electronics (ICCE), Phu Quoc Island, Vietnam, 2021, pp. 271-275, doi: 10.1109/ICCE48956.2021.9352113.
3. Van Nguyen, D. et al. (2020). Elevator Motion States Recognition Using Barometer Support Indoor Positioning System. In: Van Toi , V., Le, T., Ngo, H., Nguyen, TH. (eds) 7th International Conference on the Development of Biomedical Engineering in Vietnam (BME7). BME 2018. IFMBE Proceedings, vol 69. Springer, Singapore. https://doi.org/10.1007/978-981-13-5859-3_87

CERTIFICATIONS

- Vibration Analysis Category II Certification from AST International

OTHERS

- **Citations/h-index:** 110/6 (per ResearchGate 2024.29.03)
- **Reviewing activities:** Reviewed for Reliability Engineering and System Safety.
- **Teaching Assistant:** IT-Fault Diagnosis
- **Social Activities:** Participated in contests for cultural preservation, environmental conservation and earned prizes
- **Misc:** Technical support and reception at The International Conference on Advanced Technologies for Communications 2016 (ATC)

"We all make choices, but in the end our choices make us."

- Andrew Ryan -

THE END.